The Philosophical Magazine

FIRST PUBLISHED IN 1798

A Journal of Theoretical Experimental and Applied Physics

Vol. 4 March 1959 No. 39
Eighth Series

UNIVERSITY OF HAWAII
LIBRARY
APR 14 '59

£1 5s. 0d., plus postage
Annual Subscription £13 10s. 0d., payable in advance

Printed and Published by
TAYLOR & FRANCIS LTD
RED LION COURT, FLEET STREET, LONDON, E.C.4

THE PHILOSOPHICAL MAGAZINE

Editor

Professor N. F. Mott, M.A., D.Sc., F.R.S.

Editorial Board

Sir Lawrence Bragg, O.B.E., M.C., M.A., D.Sc., F.R.S.
Sir George Thomson, M.A., D.Sc., F.R.S.
Professor A. M. Tyndall, C.B.E., D.Sc., F.R.S.

Authors wishing to submit papers for publication in the Journal should send manuscripts directly to the Publishers.

Manuscripts should be typed in *double* spacing on one side of quarto (8 × 10 in.) paper, and authors are urged to aim at absolute clarity of meaning and an attractive presentation of their texts.

References should be listed at the end in alphabetical order of authors and should be cited in the text in terms of author's name and date. Diagrams should normally be in Indian ink on white card, with lettering in soft pencil, the captions being typed on a separate sheet.

A leaflet giving detailed instructions to authors on the preparation of papers is available on request from the Publishers.

Authors are entitled to receive 25 offprints of a paper in the Journal free of charge, and additional offprints can be obtained from the Publishers.

The *Philosophical Magazine* and its companion journal, *Advances in Physics*, will accept papers for publication in experimental and theoretical physics. The *Philosophical Magazine* publishes contributions describing new results, letters to the editor and book reviews. *Advances in Physics* publishes articles surveying the present state of knowledge in any branch of the science in which recent progress has been made. The editors welcome contributions from overseas as well as from the United Kingdom, and papers may be published in English, French and German.

INTERNATIONAL JOURNAL OF

RADIATION BIOLOGY

and related studies in Physics, Chemistry and Medicine

Editor
W. M. DALE, M.D., D.SC.
Dept. of Biochemistry, Christie Hospital & Holt Radium Institute, Withington, Manchester, 20

Assistant Editor
JOHN WAKEFIELD, B.A., F.Z.S.

Editorial Board
Charlotte Auerbach, *U.K.;* J. H. Baxendale, *U.K.;* D. W. van Bekkum, *Holland;* E. H. Betz, *Belgium;* H. A. S. van den Brenk, *Australia;* A. A. Buzzatti-Traverso, *Italy;* J. Coursaget, *France;* F. Devik, *Norway;* † J. Firket, *Belgium;* M. Haissinsky, *France;* A. Hollaender, *U.S.A.;* B. F. Kaufmann, *U.S.A.;* G. Klein, *Sweden;* H. Langendorff, *Germany;* M. Magat, *France;* † N. Miller, *U.K.;* M. Nakaidzumi, *Japan;* E. Paterson, *U.K.;* H. Ulrich, *Switzerland;* M. Westergaard, *Denmark.*

Contents of January, 1959

The Mechanism of Radiation Protection by Histamine and other Biological Amines. By C. van der Meer and D. W. van Bekkum, Medical Biological Laboratory of the National Defence Research Council T.N.O., Lange Kleiweg 139 Rijswijk (Z.H.), The Netherlands

5-Hydroxytryptamine as a Radiation Protective Substance in Animals. By H. Langendorff, H.-J. Melching and H.-A. Ladner, Radiology Institute, University of Freiburg, Baden, Germany

The DNA Content of the Small Intestine as a Quantitative Measure of Damage and Recovery after Whole Body Irradiation. By R. H. Mole and Diana M. Temple, M.R.C. Radiobiological Research Unit, A.E.R.E., Harwell, Berks.

DNA Synthesis in the Thoracic-Duct Lymphocytes of Rats during Recovery from Sub-Lethal Irradiation. By E. H. Cooper, The Department of Biochemistry, The University of Oxford

Hexokinase, Aldolase and ATP-Creatine Transphosphorylase in X-Irradiated Rats. By M. B. Sahasrabudhe, M. K. Nerurkar and A. J. Baxi, Biology Division, Atomic Energy Establishment, Trombay Indian Cancer Research Centre, Parel, Bombay, India and D. K. Mahajan, Human Variation Unit, Indian Cancer Research Centre, Parel, Bombay, India

On the Relative Role of Mutation and Recombination in Responses to Selection for Polygenic Traits in Irradiated Populations of D. Melanogaster. By R. E. Scossiroli and S. Scossiroli, Istituto di Genetica, Universitá, Pavia, Italy

An Attempt to Assess the Activity of Tumour Cells by the Study of Nucleolar Morphology, Mitotic Index and Phosphorus with ^{32}P. By S. Mitra, P. De, R. Chatterjee, K. Bhattacharya, A. Bose and H. Dutta, Departments of Cell Research and Biophysics, Chittaranjan National Cancer Research Centre, Calcutta

The Inactivation of SH Enzymes by X-Rays. By Rolf Lange, Alexander Pihl and Lorentz Eldjarn, Norsk Hydro's Institute for Cancer Research, The Norwegian Radium Hospital, Oslo, Norway

X-Ray-Induced Abnormal Differentiation of the Epithelium of the Small Intestine in the Mouse. By Richard A. McGrath and C. C. Congdon, Biology Division, Oak Ridge National Laboratory, Oak Ridge, Tennessee

Price per part £1 0s. 0d. plus postage
Subscription per volume (4 issues) £3 15s. 0d. post free, payable in advance

Printed and Published by
TAYLOR & FRANCIS LTD
RED LION COURT, FLEET STREET, LONDON, E.C.4

Orders originating in U.S.A. and Canada should be sent to the
Academic Press Inc., 111 Fifth Avenue, New York 3, N.Y., U.S.A.

A new International Journal

Molecular Physics

Editor: H. C. LONGUET-HIGGINS, F.R.S.
Associate Editor: J. H. VAN DER WAALS

Editorial Board:

J. Bjerrum, *Copenhagen*; G. Careri, *Padua*; C. A. Coulson, *Oxford*; F. H. C. Crick, *Cambridge*; P. J. W. Debye, *Cornell*; D. Hadži, *Ljubljana*; O. Hassel, *Oslo*; W. Heitler, *Zürich*; J. O. Hirschfelder, *Wisconsin*; D. F. Hornig, *Princeton*; J. A. A. Ketelaar, *Amsterdam*; J. G. Kirkwood, *Yale*; R. Kronig, *Delft*; J. W. Linnett, *Oxford*; A. Liquori, *Rome*; Dame Kathleen Lonsdale, *London*; P-O. Löwdin, *Uppsala*; M. Magat, *Paris*; R. S. Mulliken, *Chicago*; A. Münster, *Frankfurt*; L. J. Oosterhoff, *Leiden*; L. E. Orgel, *Cambridge*; J. A. Pople, *Teddington*; I. Prigogine, *Brussels*; R. E. Richards, *Oxford*; J. S. Rowlinson, *Manchester*; G. S. Rushbrooke, *Newcastle upon Tyne*; L. E. Sutton, *Oxford*; H. W. Thompson, *Oxford*; B. Vodar, *Bellevue, Paris.*

Contents of January, 1959

Zur Theorie der generalisierten Gesamtheiten. Von A. Münster, Physikalisch-chemisches Institut der Universität Frankfurt/Main

Pressure-dependent Partition Functions. By R. A. Sack, Department of Theoretical Chemistry, University of Cambridge and British Rayon Research Association, Wythenshawe, Manchester

On Mayer's Ionic Solution Theory. By Harold L. Friedman, Faculté des Sciences, Université Libre de Bruxelles

Rotational Effect on the Thermodynamic Properties of Isotopes. By Agnessa Babloyantz, Faculté des Sciences de l'Université Libre de Bruxelles, Belgique

The Structure of Shock Fronts in Various Gases. By W. H. Andersen and D. F. Hornig, Metcalf Research Laboratory, Brown University, Providence, Rhode Island

Relationship between Proton Shielding Constants and Electric Dipole Moments in the Hydrogen Halides. By H. F. Hameka, Department of Chemistry, Carnegie Institute of Technology, Pittsburgh, Pennsylvania

Chemical Shifts of Thallium Resonance Spectra in Solutions of Thallous Salts. By R. Freeman, R. P. H. Gasser, R. E. Richards and D. H. Wheeler, Physical Chemistry Laboratory, South Parks Road, Oxford

Correlations between the Electronic Spectra of Alternant Hydrocarbon Molecules and their Mono- and Di-valent Ions. I. Benzene, Coronene and Triphenylene. By G. J. Hoijtink, Chemical Laboratory of the Free University, Amsterdam

Absorption Spectra of Actinide Compounds. By Chr. Klixbüll Jørgensen, Chemistry Department A, Technical University of Denmark, Copenhagen, Denmark

Price per part £1 5s. 0d. plus postage
Subscription per volume (4 issues) £4 15s. 0d. post free, payable in advance

Printed and Published by
TAYLOR & FRANCIS LTD
RED LION COURT, FLEET STREET, LONDON, E.C.4

Orders originating in U.S.A. and Canada should be sent to the
Academic Press Inc., 111 Fifth Avenue, New York, 3, N.Y., U.S.A.

Journal of Electronics and Control

A Philosophical Magazine Associated Journal

Editor:
J. Thomson, M.A., D.Sc., M.I.E.E., F.Inst.P.
Consultant Editor:
Professor N. F. Mott, F.R.S.
Editorial Board:
Professor P. Aigrain (France)
Professor H. B. G. Casimir (Holland)
J. F. Coales (U.K.)
Professor K. G. Emeleus (U.K.)
D. W. Fry (U.K.)
Dr. W. Klein (Germany)
Dr. R. Kompfner (U.S.A.)

Contents of January, 1959

Electronics Section

A Three-Frequency Electron Beam Parametric Amplifier and Frequency Converter. By W. H. Louisell, Bell Telephone Laboratories Incorporated, Murray Hill, New Jersey

The Electrical Conductivity and Hall Coefficient of Bismuth Telluride. By B. Yates, Communication from the Staff of the Research Laboratories of The General Electric Company Limited, Wembley, England

The Effect of the Inclination of the Focusing Electrodes on Electron Beam Formation. By R. J. Lomax, Peterhouse, Cambridge

On Space Charge Waves. By D. H. Trevena, Ferranti Ltd., Wythenshawe, Manchester

Discharge Modes using Thermionic Cathodes. By R. B. Cairns and G. C. McCullagh, Physics Department, Queen's University, Belfast

A Comparison of the Theory of Impact Ionization with Measurements on Silicon p–n Junctions. By F. W. G. Rose, Research Laboratory, British Thomson-Houston Co., Ltd., Rugby

Control Section

Magnetization Reversal by Rotation and Wall Motion in Thin Films of Nickel–Iron Alloys. By E. M. Bradley and M. Prutton, Electronics Research Laboratory, British Tabulating Machine Company Ltd., Stevenage, Herts.

Price per part £1 5s. plus postage
Price per volume £7 post free, payable in advance
6 monthly issues per volume

Printed and Published by

TAYLOR & FRANCIS LTD
RED LION COURT, FLEET STREET, LONDON, E.C.4

Orders originating in U.S.A. and Canada should be sent to the
Academic Press Inc., 111 Fifth Avenue, New York, 3, N.Y., U.S.A.

A new International Journal

ERGONOMICS

HUMAN FACTORS IN WORK, MACHINE CONTROL AND EQUIPMENT DESIGN

General Editor
A. T. WELFORD
University of Cambridge, Psychological Laboratory, Downing Place, Cambridge

Associate Editor (Anatomy and Physiology)
W. F. FLOYD

Assistant Editor
Miss H. M. CLAY

Editorial Board

H. Bastenier, *Belgium*; R. B. Bromiley, *Canada*; R. Bonnardel, Bernard Metz, *France*; E. A. Müller, *Germany*; M. G. Bennett, W. E. Hick, Sir Charles Lovatt Evans, L. G. Norman, *Great Britain*; F. H. Bonjer, *Netherlands*; S. P. M. Forssman, *Sweden*; E. Grandjean, *Switzerland*; H. S. Belding, P. M. Fitts, *U.S.A.*

Contents of February, 1959

Symposium on Training

Introductory Address. By P. H. St. J. Wilson, C.B., C.B.E., Chief Industrial Commissioner, Ministry of Labour and National Service
Physiological Bases of Training. By Albert Hemingway, Department of Physiology, School of Medicine, University of Leeds
Training Operatives in Industry. By W. Douglas Seymour, Clent, Worcestershire
The Training of Shoe-Machinists. By W. T. Singleton, The British Boot, Shoe and Allied Trades Research Association, Kettering
A Theory of the Acquisition of Speed-Skill. By E. R. F. W. Crossman, Department of Psychology, Reading University, England
Practice and Knack: Some Comments on Learning and Training in Industry. By Isabel Blain, National Institute of Industrial Psychology
The Operator as a Self-Regulating System: A Factory Experiment. By S. David M. King, Organization & Training (Consultants) Limited, 19 Bolton Street, London, W.1
Note on Current Trends in Literature on Training. By Ezra V. Saul, Institute for Applied Experimental Psychology, Tufts University, Medford, Massachusetts
Circuit Training. By G. T. Adamson, Department of Physical Education, The University, Leeds
The Limitations of a ‘ Procrustean ’ Approach to the Optimization of Man–Machine Systems. By F. V. Taylor and W. D. Garvey, U.S. Naval Research Laboratory, Washington, D.C.
Physical Training in Relation to the Energy Expenditure of Walking and to Factors Controlling Respiration During Exercise. By J. E. Cotes and F. Meade, Medical Research Council, Pheumoconiosis Research Unit, Llandough Hospital, Penarth, Glamorgan, Wales
Problems of Training of the Cardiovascular System. By M. J. Karvonen, Institute of Occupational Health, Helsinki, Finland
Training Muscle Strength. By E. A. Müller, Max-Planck-Institut für Arbeitsphysiologie, Dortmund, Germany
Abstracts of other Papers Delivered at the Symposium

Price £1 5s. 0d. per part plus postage
Subscription price per volume £4 15s. 0d. post free, payable in advance

Printed and Published by
TAYLOR & FRANCIS LTD
RED LION COURT, FLEET STREET, LONDON, E.C.4

Orders originating in U.S.A. and Canada should be sent to the Academic Press Inc., 111 Fifth Avenue, New York, 3, N.Y., U.S.A.

Advances in Physics

A Quarterly Supplement of the Philosophical Magazine

Editor:
PROFESSOR N. F. MOTT, M.A., D.Sc., F.R.S.

Editorial Board:
SIR LAWRENCE BRAGG, O.B.E., M.C., M.A., D.Sc., F.R.S.
SIR GEORGE THOMSON, M.A., D.Sc., F.R.S.
PROFESSOR A. M. TYNDALL, C.B.E., D.Sc., F.R.S.

Contents of January, 1959

The Theory of Superconductivity. By C. G. Kuper, Department of Natural Philosophy, St. Salvator's College, St. Andrews

The Modern Theory of Superconductivity. By I. M. Khalatnikov and A. A. Abrikosov, Institute of Physical Problems, Kaluzhskove Shosse, 32 Moscow, U.S.S.R.

Price per part £1 plus postage

Price per annum £3 15s. post free

Printed and Published by

TAYLOR & FRANCIS LTD

RED LION COURT, FLEET STREET, LONDON, E.C.4

Physics in Medicine and Biology

A Taylor & Francis Journal published in association
with The Hospital Physicists' Association

Editor: J. E. Roberts, D.Sc.
Consultant Editor: Professor N. F. Mott, F.R.S.

Editorial Board

R. Bonet-Maury, *Paris*; J. Dainty, *Edinburgh*; H. E. Johns, *Toronto*; W. A. Langmead. *London*; D. A. McDonald, *London*; J. S. Mitchell, *Cambridge*; G. J. Neary, *Harwell*; B. Rajewsky, *Frankfurt*; J. Rotblat, *London*; S. Rowlands, *London*; H. P. Schwan, *Philadelphia*; R. Sievert, *Stockholm*; F. W. Spiers, *Leeds*; J. F. Tait, *Massachusetts*; A. J. H. Vendrik, *Nijmegen*.

Contents of January, 1959

The Measurement of Exposure Dose for High Energy Radiation with Cavity Ionization Chambers. By T. E. Burlin, B.Sc., Physics Department, Hammersmith Hospital, London, W.12

The Energy Response of a Victoreen Condenser Ionization Chamber. By A. J. D. Szilvasi, Ph.D. and G. N. Whyte, Ph.D., National Research Council, Ottawa, Canada

An Analysis of Clasp Design in Partial Dentures. By J. A. Warr, M.A.(Cantab.), B.Sc. (London), B.D.S.(London), L.D.S.R.C.S.Eng., Department of Prosthetics, The London Hospital Medical College, Turner Street, London, E.1

A Study of the External Gamma-ray Field Arising from a Radioactive Source Situated in Air and in a Scattering Medium. By H. A. B. Simons, M.A., Ph.D. and S. Chomet, M.Sc., Physics Department, The Royal Free Hospital School of Medicine, 8 Hunter Street, London, W.C.1

A Wide Range Direct Reading X-Ray Dosemeter. By S. Stuart, Electronic Instruments Ltd., Richmond, Surrey and S. B. Osborn, B.Sc., A.Inst. P., University College Hospital, London, W.C.1

Pulmonary Diffusion of Oxygen. By B. F. Visser, Ph.D. and A. H. J. Maas, M.Sc., Pulmonary Function Laboratory, State University Hospital, Utrecht, Netherlands

The Influence of the Anomalous Viscosity of Blood upon its Oscillatory Flow. By M. G. Taylor, M.D., Physiology Department, Medical College of St. Bartholomew's Hospital, London

Subscription price per volume £3 10s. post free, payable in advance
4 parts per volume—£1 per part plus postage

Printed and Published by

TAYLOR & FRANCIS, LTD

RED LION COURT, FLEET STREET, LONDON, E.C.4

Orders originating in U.S.A. and Canada should be sent to the
Academic Press Inc., 111 Fifth Avenue, New York, 3, N.Y., U.S.A.

INTERNATIONAL JOURNAL

OPTICA ACTA

European Journal of Optics **Journal Européen d'Optique** **Europäische Zeitschrift für Optik**

English Editor: C. G. Wynne, 13 Elwill Way, Beckenham, Kent, U.K.

Rédacteur Français: A. Maréchal, 3 Boulevard Pasteur, Paris, France

Deutscher Herausgeber: G. Franke, Laufdorfer Weg 2, Wetzlar, Germany

Editorial Board

J. M. Otero y Navascues, *Madrid;* R. W. Ditchburn, *Reading;* A. Arnulf, *Paris;* A. Biot, *Gand;* J. Cabannes, *Paris;* P. Fleury, *Paris;* F. Gabler, *Vienna;* G. Hansen, *Oberkochen;* E. Ingelstam, *Stockholm;* H. Korte, *Braunschweig;* W. S. Stiles, *London;* G. Toraldo di Francia, *Florence;* A. C. S. van Heel, *Delft.*

Contents of January, 1959

N.P.L. Colour-Matching Investigation: Final Report (1958). By W. S. Stiles and J. M. Burch, National Physical Laboratory, Teddington, Middlesex

Optical Constants of Evaporated Films of Zinc Sulphide and Germanium in the Infra-Red. By Lennart Huldt and Torsten Staflin, Institute of Optical Research, Royal Institute of Technology, Stockholm

Das Moiré-Gitter als vielseitiges Testobjekt: Photoelektrische Aberrationsmessung. Von A. Lohmann, z.Zt. Institutet för optisk forskning, Stockholm 70

Matrix Formalism in the Theory of Diffusion of Light. By I. Kuščer, Institute of Physics, University of Ljubljana and M. Ribarič, J. Stefan Institute, Ljubljana, Yugoslavia

Lage und Sichtbarkeit von Keilinterferenzen bei Instrumenteller Beobachtung (Beitrag zur Kohärenztheorie eines Unsymmetrischen Interferenzfalles). Von Rudolf Landwehr, Menden/Sauerland, Deutschland

Essai de Détermination des Très Faibles Diamètres Apparents en Radioastronomie. Par J. Arsac, Observatoire de Meudon

Price per part £1 (1375 fr.), (DM 11.75), ($2.80), plus postage

Subscription price per volume (4 parts) £3 15s. (5155 fr.), (DM 44), ($10.50), post free, payable in advance

Printed and Published by

TAYLOR & FRANCIS LTD

RED LION COURT, FLEET STREET, LONDON, E.C.4

A HISTORY OF MATHEMATICS

from antiquity to the early nineteenth century

by J. F. SCOTT, B.A., D.Sc., Ph.D.
Vice-Principal of St. Mary's College,
Strawberry Hill, Twickenham,
Middlesex

Author of *The Scientific Work of René Descartes* (1596–1650), *Mathematical Work of John Wallis, D.D., F.R.S.* (1616–1703), and other works.

CONTENTS : Mathematics in Antiquity—Greek Mathematics—The Invention of Trigonometry—Decline of Alexandrian Science and the Revival in Europe—Mathematics in the Orient—Progress of Mathematics during the Renaissance—New Methods in Geometry—The Rise of Mechanics—the Invention of Decimal Fractions and of Logarithms—Newton and the Calculus—Taylor and Maclaurin, the Bernoullis and Euler, Related Advances—The Calculus of Variations, Probability, Projective Geometry, Non-Euclidean Geometry—Theory of Numbers—Lagrange, Legendre, Laplace, Gauss.

This volume is intended primarily to help students who desire to have a knowledge of the development of the subject but who have too little leisure to consult original works and documents. The author has availed himself of the facilities afforded by the Royal Society and other learned Societies to reproduce extracts from manuscripts and many scarce works.

9¾ × 6¾ Price 3 guineas

Printed and Published by
TAYLOR & FRANCIS LTD.
RED LION COURT, FLEET STREET,
LONDON, E.C.4

THE SCIENTIFIC WORK OF RENÉ DESCARTES 1596-1650

BY

J. F. SCOTT, B.A., M.SC., PH.D.

With a Foreword by

H. W. TURNBULL, M.A., F.R.S.

This book puts the chief mathematical and physical discoveries of Descartes in an accessible form and fills an outstanding gap upon the shelf devoted to the history of philosophy and science. There is to be found in this volume the considerable contribution that Descartes made to the physical sciences, which involved much accurate work in geometrical optics and its bearing upon the practical problem of fashioning lenses, as also the deeper problems of light and sight and colour. The careful treatment that Dr. Scott has accorded to the work of Descartes is very welcome. The book is well worth reading and will be an asset to all libraries. This publication is recommended and approved by the Publication Fund Committee of the University of London.

212 *pp.* 7 × 10 *amply illustrated*

PRICE £1–0–0 NET

Printed and Published by
TAYLOR & FRANCIS LTD.
RED LION COURT, FLEET STREET,
LONDON, E.C.4

The Heat Capacity of Pure Silicon and Germanium and Properties of their Vibrational Frequency Spectra†

By P. FLUBACHER‡, A. J. LEADBETTER‡
and J. A. MORRISON
Division of Pure Chemistry, National Research Council, Ottawa, Canada

[Received September 30, 1958]

ABSTRACT

Heat capacities of pure silicon and germanium have been measured between 2·5° and 300°K. The estimated accuracies of the measurements are $\pm 0{\cdot}5\%$ for $10° < T < 20°$K and $\pm 0{\cdot}2\%$ for $T > 20°$K. The results for silicon were anomalous in the region $T < 7°$K; it is suggested that this behaviour resulted from adsorption and desorption of exchange gas in the calorimeter vessel. No anomalies were observed in the measurements on germanium; their accuracy at the lowest temperatures is estimated to be $\pm 2\%$. The results for both substances are significantly different from previously published values.

The temperature variation of Θ_D of both silicon and germanium below about $T = \Theta_D/3$ is consistent with general harmonic theory, but at high temperatures Θ_D decreases with increasing temperature. This appears to be a clearly marked anharmonic effect of a type that cannot be explained by change of volume alone. The results for $T < \Theta_D/3$ are therefore extrapolated to high temperatures to give a heat capacity consistent with harmonic theory at all temperatures. From this, properties of an effective harmonic spectrum are derived; these include the low frequency expansion and a number of positive and negative moments. The apparent anharmonic contribution $\Delta C_v = [C_v - C_v \text{ (harmonic)}]$ is found for both elements to be approximately a linear function of the temperature in the region between $\Theta_D/3$ and room temperature. The possible significance of this result is discussed in the light of anharmonic theory.

The results are compared where possible with vibrational properties determined from other experiments and the agreement is very satisfactory.

§ 1. INTRODUCTION

THE diamond structure elements (diamond, silicon, germanium and grey tin) present attractive features for an investigation of lattice vibrations. Their lattices have a simple crystal structure and their interatomic forces should not be very complex. It might be hoped therefore that appropriate models for the crystals could be devised and tested adequately with different measured vibrational properties. A model for diamond based on short-range forces has been proposed (Smith 1948) but it does not seem to give thermodynamic properties in agreement with experiment (Desnoyers and Morrison 1958). The same model applied to silicon and germanium (Hsieh 1954) shows an even wider disagreement. Recently Lax (1958) has suggested that longer range interactions of a special type may need to be considered.

---

† Communicated by the Authors.
‡ National Research Council Postdoctorate Fellow.

Although at present a satisfactory model has not been developed there is now the possibility of correlating all measurements of vibrational properties of silicon and germanium without specific reference to a model. Recent work on neutron scattering by germanium (Brockhouse and Iyengar 1957, 1958, Pelah *et al.* 1957) has yielded among other things frequency-wave number relations for lattice waves in certain directions in the crystal. These have been compared (Brockhouse and Iyengar 1957, 1958) with measured elastic properties (McSkimin 1953) and infra-red absorption (Collins and Fan 1954, MacFarlane *et al.* 1957) and the agreement is found to be excellent. As a further development Phillips (1959) has deduced a lattice frequency spectrum for germanium by a moment-singularity method using the dispersion relations found by neutron spectrometry. The way is therefore clear to include thermodynamic properties in the comparision of vibrational properties since, in the harmonic approximation, they depend only upon the frequency spectrum.

Existing values of the heat capacity of silicon (Pearlman and Keesom 1952) and of germanium (Esterman and Weertman 1952, Hill and Parkinson 1952, Keesom and Pearlman 1953) cover only limited temperature regions and where the measurements have been duplicated the agreement is hardly satisfactory. Hence it has seemed valuable to obtain new results for as wide a temperature range as possible. In the present paper we report measurements for both substances in the temperature region 2·5° to 300°K. The specimens used were of such purity that electronic contributions to the heat capacity were entirely negligible below 300°K.

Since it is the heat capacity at constant volume which is directly related to the lattice frequency spectrum, this quantity must be computed from the experimentally measured heat capacity at constant pressure. For both silicon and germanium the difference can be determined accurately because both the thermal expansion and the compressibility of the lattices are well known for a wide temperature range below room temperature. There is, however, an additional factor to be considered which introduces unavoidable uncertainty; this concerns possible effects of anharmonicity in the lattices. In the present examples of silicon and germanium we shall see that Θ_D decreases with increasing temperature at higher temperatures. This behaviour cannot be accounted for by harmonic lattice theory. A heat capacity compatible at high temperatures with harmonic theory can be obtained by extrapolation of the results from lower temperatures ($T < \Theta_D/3$); such a procedure was used previously in the analysis of heat capacity results for ionic crystals (Barron *et al.* 1957, 1959).

The heat capacity is taken to correspond to the effective harmonic spectrum of the lattice and the good agreement of the derived properties with those obtained from other work suggests that this is a fruitful concept. The detailed interpretation of the anharmonic effect is not simple but a general discussion is given in § 4.2.

§ 2. EXPERIMENTAL

2.1. *Calorimetric Specimens*

The silicon (du Pont Hyperpure grade) was obtained in the form of eleven single crystal slabs whose average resistivity at room temperature was approximately 100 ohm cm. This corresponds to a carrier concentration of not more than 10^{15} cm ^{3}. The germanium (supplier: Société des Mines et Fonderies de Zinc de la Vieille Montagne, S.A., Belgium) was received in the form of rods and was stated to have a minimum resistivity of 50 ohm cm. The resistivities of the particular rods used for the calorimetric work were determined by G. Fischer of the Division of Pure Physics and found to be 59 ohm cm at room temperature. Low temperature resistivity meaurements indicated a carrier concentration of not more than 10^{14} cm^{-3}. For both the silicon and germanium specimens the electronic contribution to the heat capacity was negligible down to the lowest temperatures.

The specimens were broken into pieces of about 3 mm in size for filling the calorimeter vessels. The filled vessels for both calorimeter assemblies used were evacuated to a pressure of 10^{-6} mm of mercury and then sealed with a small amount of helium exchange gas inside. The amounts of the specimens and exchange gas are given in table 1.

Table 1. Calorimeter Fillings

	Calorimeter I		Calorimeter II	
	Specimen (g atom)	Helium (10^{-6} g atom)	Specimen (g atom)	Helium (10^{-6} g atom)
Silicon	6·0318	2·5	5·1658	4·8
Germanium	2·8698	2·7	2·8729	4·7

2.2. *Calorimetry*

The higher temperature calorimeter (calorimeter II) was used exactly as in previous experiments (Berg and Morrison 1957) and no further description of it is necessary here.

The essential features of the lower temperature calorimeter (calorimeter I) have been described previously (Morrison *et al.* 1955). We shall, however, discuss briefly the establishment of the temperature scale for the measurements with this calorimeter in the temperature range 2° to 20°K. The working thermometer, a carbon resistor (Allen Bradley 10 ohms ½ watt) attached to the calorimeter vessel, was calibrated for each set of experiments by comparing it against a normal hydrogen vapour pressure thermometer at five temperatures and a helium vapour pressure thermometer at at least one temperature. The same vapour pressure thermometer bulb, attached to the adiabatic shield, was used for both sets of measurements. The heating of the shield was so adjusted that the temperature of the calorimeter vessel did not change significantly during a comparison. Three of the fixed points (at about 4°, 14° and 20°K) were used to determine constants of an interpolation formula (Clement and Quinnell 1952) which gave a working temperature scale; the rest of the fixed points served as checks. Liquid hydrogen temperatures were calculated from the vapour pressure equation of normal hydrogen (Woolley *et al.* 1948) and liquid helium temperatures from vapour pressure data for the T_{L55} scale (van Dijk and Durieux 1955).

It remained to relate the working-temperature scale to the thermodynamic scale; this was accomplished by attaching a gas thermometer bulb to the calorimeter vessel and by comparing the gas thermometer with the carbon thermometer at about twenty points between 2·5° and 20°K. Below 2·5°K the gas thermometer was turned into a vapour pressure thermometer. At the same time the two thermometers were compared where possible with the vapour pressure thermometer on the shield. In this way small temperature differences due to thermal gradients and to vibrational energy appearing in the calorimeter vessel were automatically taken into account. Although the resistance of the carbon thermometer at a given temperature generally changed each time the thermometer was cooled from room temperature, the sensitivity did not alter significantly. In principle, therefore, one series of gas thermometer comparisons would have sufficed. Actually three sets of comparisons were made during the course of the heat capacity measurements. Their consistency suggests that the final temperature scale used agreed with the thermodynamic scale to within ±0·02° from 2° to 20°K. The slope of the scale is estimated to be correct within ±1% at the lowest temperature and ±0·5% for $T > 10$°K.

§ 3. RESULTS

3.1. *The Heat Capacity Measurements*

The primary experimental results (the heat capacity at constant pressure) are tabulated in the Appendix. The temperature intervals used in the measurements were 0·5° ($2° < T < 7$°K), 1° ($7° < T < 20$°K) and 3° ($T > 20$°K). Curvature corrections were applied where necessary. The thermochemical calorie (4·1840 abs. joule) is used throughout. Results for silicon for $T < 7·7$°K are not given in the table because in this region anomalous effects appeared which can be attributed to adsorption of exchange gas in the calorimeter vessel. The details are discussed in § 3.3.2.

The internal consistency of the results may be judged from figs. 1 and 2 where the apparent Debye characteristic temperatures (Θ_D) corresponding to the experimental heat capacities of silicon and germanium are plotted as a function of temperature. The sensitivity of the graphs are indicated.

The values of Θ_D were obtained from C_v which was deduced from C_p by means of the usual thermodynamic formula

$$C_p - C_v = \frac{\alpha^2 T V}{\chi}, \qquad (3.1)$$

where α is the cubical coefficient of thermal expansion, V the molar volume and χ the isothermal compressibility. Thermal expansion data obtained by Gibbons (1958) for silicon and germanium were used; their estimated accuracy is 1%. The compressibilities were calculated from measured elastic constants (McSkimin 1953) and are probably reliable to at least 3%. Hence the values of $C_p - C_v$ would seem to be accurate to 5%.

Fig. 1

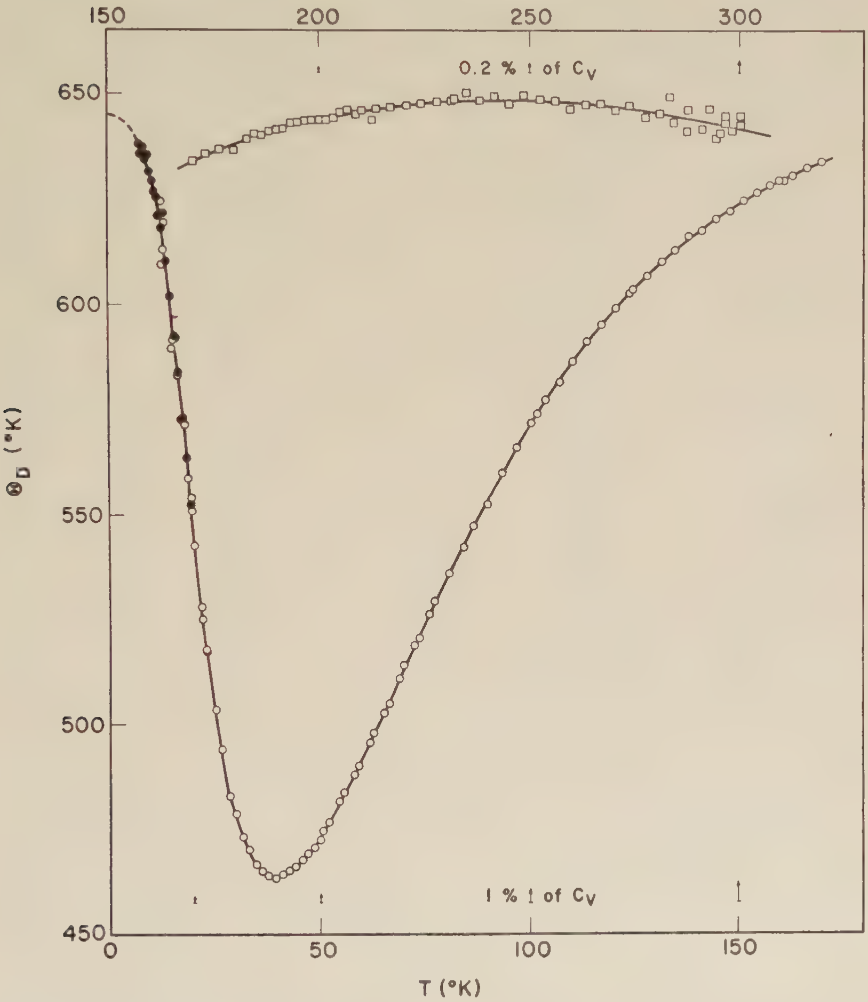

The apparent Debye characteristic temperature of silicon as a function of the absolute temperature.

- ● Calorimeter I.
- ○ Calorimeter II ($12° < T < 170°$K).
- □ Calorimeter II ($170°$K $< T < 300°$K).

Fig. 2

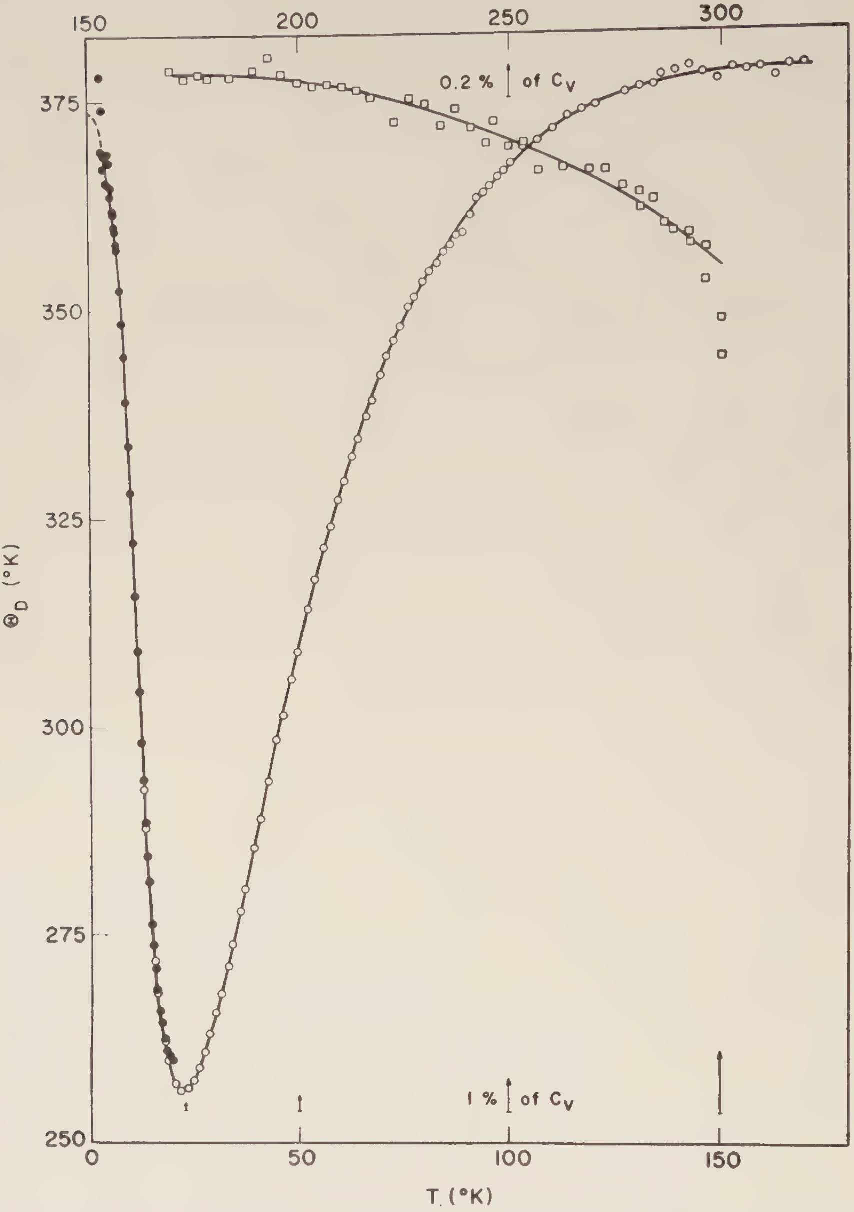

The apparent Debye characteristic temperature of germanium as a function of the absolute temperature.

- ● Calorimeter I.
- ○ Calorimeter II ($12° < T < 170°$K).
- ☐ Calorimeter II ($170° < T < 300°$K).

Smoothed values of C_p and of $C_p - C_v$ for both silicon and germanium are given in table 2. Since the actual values of $C_p - C_v$ are so small, their uncertainty does not affect C_v significantly.

Table 2. C_p and $C_p - C_v$ at Rounded Values of the Temperatures
[Units — cal/g atom deg]

T (°K)	Silicon		Germanium	
	C_p	$C_p - C_v$	C_p	$C_p - C_v$
2·5	(0·0000271)		0·0001413	
5	(0·000219)		0·001199	
10	0·001845		0·01394	
15	0·007300		0·07672	
20	0·02265		0·2174	
25	0·05702		0·4140	
30	0·1149		0·6316	
35	0·1962		0·8531	
40	0·2957		1·067	
50	0·5272		1·479	
60	0·7725		1·879	
70	1·019		2·269	
80	1·261		2·640	
90	1·502		2·989	0·001
100	1·739		3·302	0·001
120	2·205		3·838	0·003
140	2·650		4·261	0·005
160	3·057		4·587	0·007
180	3·420	0·001	4·837	0·009
200	3·735	0·001	5·033	0·011
220	4·009	0·001	5·190	0·013
240	4·246	0·002	5·318	0·015
260	4·455	0·002	5·423	0·017
280	4·638	0·003	5·511	0·020
300	4·796	0·004	5·590	0·023

The accuracy of the measurements is therefore determined primarily by uncertainties in the temperature scales. The estimates for these for calorimeter I suggest that the heat capacity results are accurate to $\pm 2\%$ at the lowest temperatures and $\pm 0{\cdot}5\%$ in the region $10^\circ < T < 20^\circ$K. Previous work with calorimeter II (Berg and Morrison 1957, Morrison and Patterson 1956) indicates its accuracy to be $\pm 0{\cdot}5\%$ for $12^\circ < T < 20^\circ$K and $\pm 0{\cdot}2\%$ for $T > 20^\circ$K. The results for the two calorimeters agree to better than $\pm 0{\cdot}5\%$ between 12° and 20°K.

3.2. *Comparison with Other Measurements*

There are several previous reports of heat capacity measurements on silicon and germanium for more limited temperature ranges than have been covered in the present work. Except for low temperature results

Fig. 3

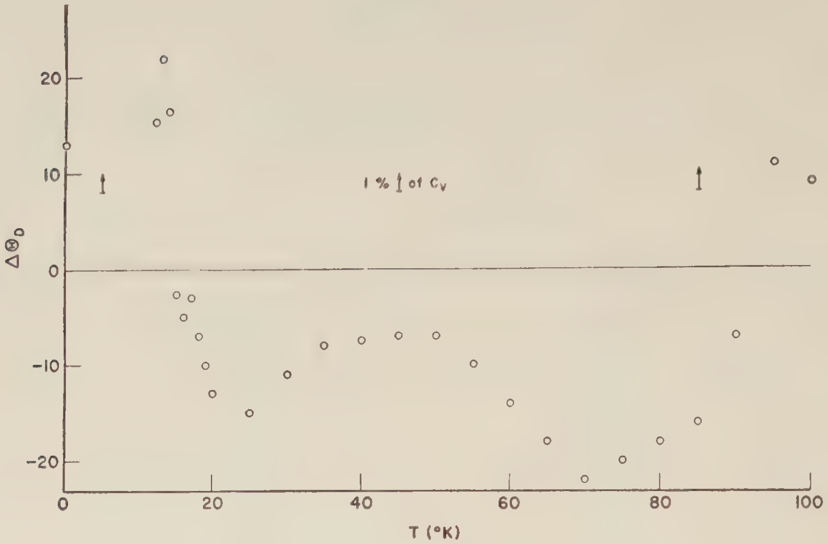

A comparison of smoothed Θ_D values for silicon.

$\Delta\Theta_D = [\Theta_D$ (Pearlman and Keesom 1952) $- \Theta_D$ (present results)].

Fig. 4

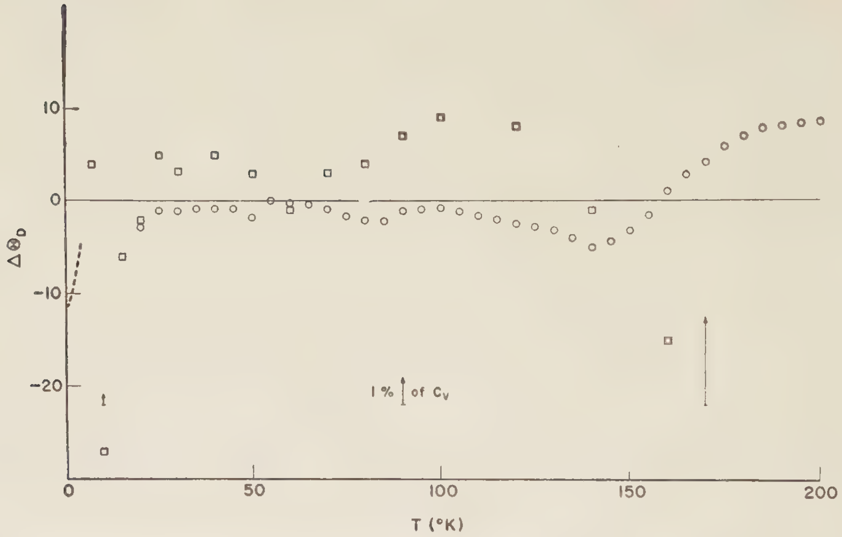

A comparison of the present results for germanium with previously published values. The graph gives differences between smoothed Θ_D values.

----- Keesom and Pearlman (1953).
□ Hill and Parkinson (1952).
○ Esterman and Weertman (1952).

for germanium (Keesom and Pearlman 1953) only smoothed values of the heat capacity are given. We have therefore chosen to compare the available results through difference graphs using as references smoothed Θ_D–T relations which reproduce the present results to well within their estimated accuracies. A comparison with the results of Pearlman and Keesom (1952) for silicon is shown in fig. 3, and it is evident that the deviations are large. It should be pointed out, however, that the specimens used by Pearlman and Keesom contained appreciable amounts of electronically active impurities.

The results for germanium are shown in fig. 4. Here, the values obtained by Hill and Parkinson (1952) and by Esterman and Weertman (1952) deviate for the most part in opposite directions. Over the major portion of the temperature region covered the agreement between the present results and those of Esterman and Weertman is close to what one might expect for totally independent calorimetric measurements. The results of Keesom and Pearlman (1953) for the temperature range 1° to 4°K were fitted to the T^3 law. The present results, however, show that Θ_0 is not constant in this region.

Additional heat capacity results for germanium in the temperature range 12 to 270°K have recently been obtained by Clusius and Piesbergen (1958)†. Between 20° and 270°K they agree with the present values within about 1%. Below 20°K the difference increases, becoming about 10% at 12°K.

3.3. *Analysis of the Experimental Results*

3.3.1. *General remarks*

The type of analysis to be outlined in the next section has been fully described previously (Barron *et al.* 1957, 1959). Its object is to deduce properties of the vibrational frequency spectrum from measured heat capacities. An essential factor is the recognition of and correction for anharmonic effects.

In approximate general shape the Θ_D curves for silicon and germanium (figs. 1 and 2) are of the form of Θ_D curves found for potassium halides (Berg and Morrison 1957). Starting from the lowest temperatures Θ_D first decreases to a minimum, then increases to a flat maximum and finally decreases slowly. The decrease at high temperatures cannot be accounted for by harmonic lattice theory which requires that Θ_D should increase asymptotically to a constant value. We propose to adopt the view taken previously that the decrease in Θ_D is to be associated with an anharmonic effect of a type which cannot be explained by change of volume alone; we shall further assume that below $T = \Theta_D/3$ the only anharmonic effect due to thermal energy which needs to be considered is thermal expansion.

---

† We should like to thank Professor Clusius for sending us these results.

3.3.2. *Properties of the vibrational spectra*

The extrapolation of the results for intermediate temperatures to infinite temperature is illustrated in fig. 5. The solid curves represent the fitting of the results to the Thirring expansion which has the form

$$\Theta_D{}^2=\Theta_\infty{}^2\left[1-A\left(\frac{\Theta_\infty}{T}\right)^2+B\left(\frac{\Theta_\infty}{T}\right)^4\ldots\right]. \qquad (3.2)$$

The values of Θ_D used here have all been reduced to a fixed volume, namely, the volume of the crystal at 0°K. The intercepts of the solid curves at $1/T^2=0$ give values of Θ_∞ and hence values of the second moments, μ_2. The dashed curves represent estimates of limits on the extrapolations. The most probable values of Θ_∞ are 674 ± 4°K for silicon and 395 ± 3°K for germanium.

Fig. 5

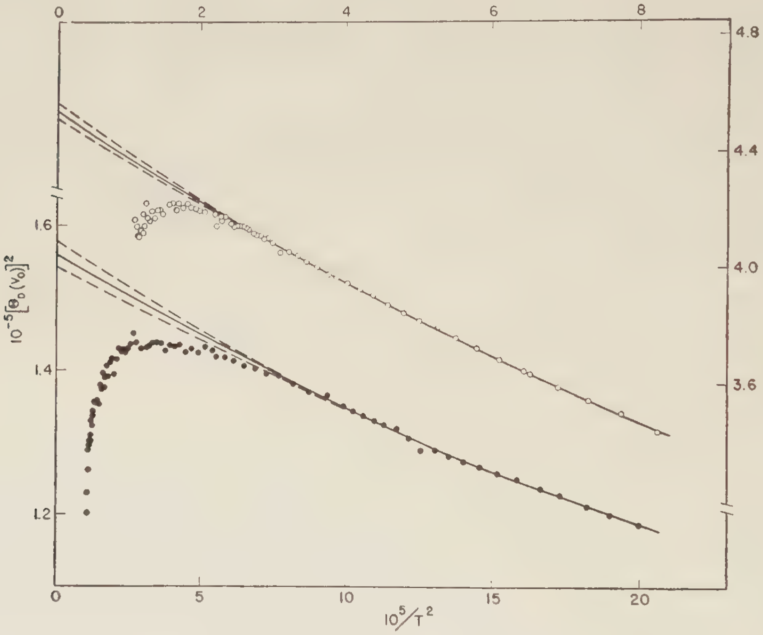

The estimation of Θ_∞.

○ Silicon.
● Germanium.

The coefficients A and B in eqn. (3.2) are related to μ_4 and μ_6 (see Barron *et al.* 1957); their values have been estimated graphically, but the details are not given here.

The results obtained for very low temperatures have been used to determine the coefficients of the low frequency expansions of the spectra of silicon and germanium:

$$G(\nu)=\mathcal{N}(\alpha\nu^2+\beta\nu^4+\gamma\nu^6+\ldots). \qquad (3.3)$$

Fig. 6

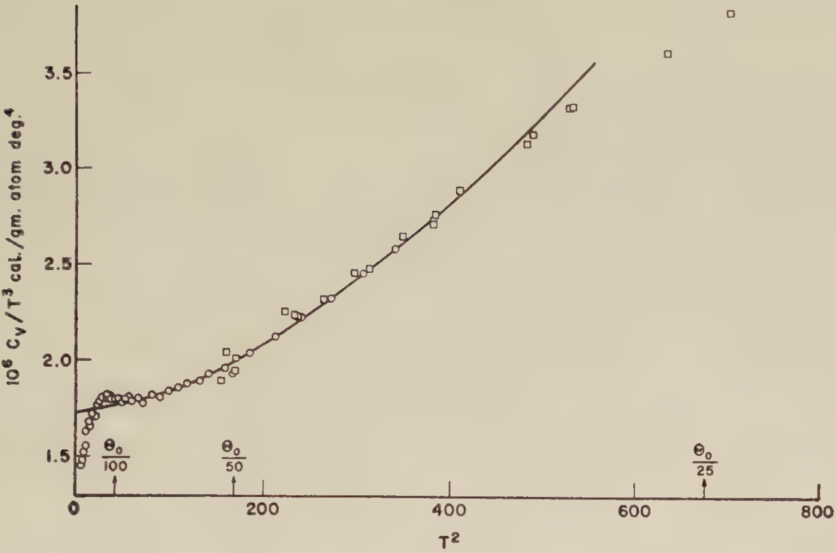

A graph of C_v/T^3 against T^2 for silicon.

○ Calorimeter I.
□ Calorimeter II.

Fig. 7

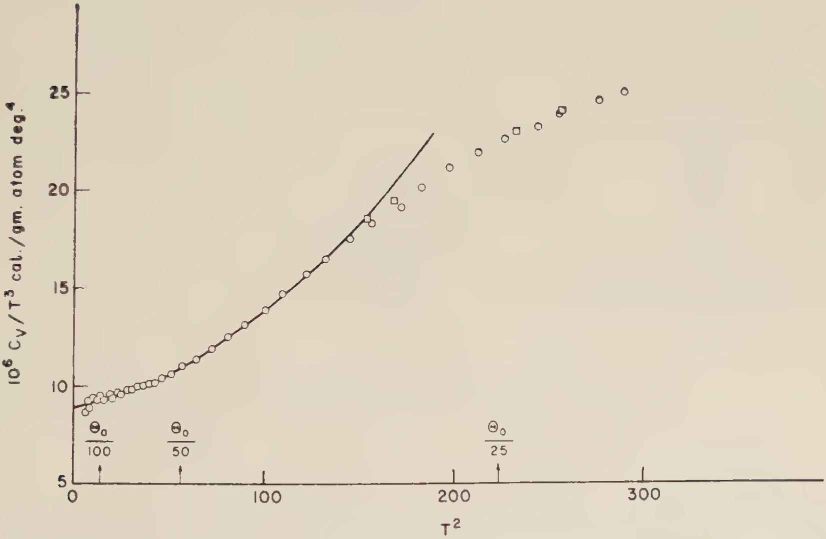

A graph of C_v/T^3 against T^2 for germanium.

○ Calorimeter I.
□ Calorimeter II.

The corresponding expansion for the heat capacity is

$$C_v = aT^3 + bT^5 + cT^7 + \ldots; \qquad (3.4)$$

the determination of the coefficients a, b and c is illustrated in figs. 6 and 7. The fitting of experimental results to eqn. (3.4) has been discussed elsewhere (Barron and Morrison 1957). All of the experimental results for silicon are included in fig. 6 and those for $T < 7$°K show an unexpected behaviour. In the experiments with silicon between 2° and 4°K it was observed that the equilibrium time after the heating of the calorimeter vessel was very long, which indicated that the helium exchange gas was all adsorbed because normally the observed equilibrium time was a few seconds. If thermal equilibrium was not being attained, the apparent heat capactiy would be too small as was found. Desorption of helium would be expected to produce too large apparent heat capacities over a limited temperature range and it is significant that the observed heat capacities lead to a maximum in C_v/T^3 at about 6°K (fig. 6). No anomalies were observed in the experiments with germanium (fig. 7) where the surface area of the specimen was much smaller (less than half) and the total heat capacity of the system was some six times larger. It therefore seems probable that the anomalous results for silicon are to be accounted for by effects of adsorption and desorption of the exchange gas. Hence, it is justifiable to represent the true heat capacity of silicon for the region $T < 7$°K by the extrapolated portion of the solid curve shown in fig. 6.

Table 3. The Coefficients in Eqns. (3.3) and (3.4), Θ_0 and Θ(elastic)

	Silicon	Germanium
a (cal g atom^{-1} deg^{-4})	$1{\cdot}73 \pm 0{\cdot}04 \times 10^{-6}$	$8{\cdot}90 \pm 0{\cdot}16 \times 10^{-6}$
b (cal g atom^{-1} deg^{-6})	$5 \pm 5 \times 10^{-10}$	$2{\cdot}0 \pm 0{\cdot}7 \times 10^{-8}$
c (cal g atom^{-1} deg^{-8})	$6{\cdot}0 \pm 1{\cdot}4 \times 10^{-12}$	$3{\cdot}0 \pm 0{\cdot}5 \times 10^{-10}$
α (sec^3)	$3{\cdot}71 \pm 0{\cdot}08 \times 10^{-39}$	$1{\cdot}91 \pm 0{\cdot}03 \times 10^{-38}$
β (sec^5)	$9 \pm 9 \times 10^{-65}$	$3{\cdot}6 \pm 1{\cdot}2 \times 10^{-63}$
γ (sec^7)	$4{\cdot}4 \pm 1{\cdot}0 \times 10^{-89}$	$2{\cdot}2 \pm 0{\cdot}4 \times 10^{-87}$
Θ_0 (previous work)	658° †	362 ± 6° ‡
Θ_0 (present work)	645 ± 5°	374 ± 2°
Θ(elastic) §	647·8°	374·0°

† Pearlman and Keesom (1952).
‡ Keesom and Pearlman (1953).
§ de Launay (1956).

The values of the coefficients occurring in eqns. (3.3) and (3.4) are given in table 3. Also shown are values of Θ_0 based on the present and on earlier results and Θ(elastic) as calculated by de Launay (1956). For both silicon and germanium Θ_0 from the present heat capacity measurement and Θ(elastic) agree within the probable errors assigned to Θ_0.

Other moments of the frequency spectra, in addition to the even positive moments derived from the Thirring expansion, have been calculated from expansions involving integrals of the form

$$\int_0^T \frac{C_v}{T^n}\,dT$$

(for details, see Barron *et al.* 1957). All of the computed moments, together with their estimated accuracies, are given in table 4. They are also illustrated by graphs of the function

$$\nu_{\mathrm{D}}(n) = \left(\frac{n+3}{3}\mu_n\right)^{1/n}$$

in fig. 8. This function would be a constant for a Debye spectrum; its primary usefulness is to serve as a check for internal consistency in the calculations.

Table 4. Derived Moments of the Frequency Spectra

	Silicon	Germanium
$\mu_{-2\cdot5}$ (sec$^{5/2}$)	$1\cdot355 \pm 0\cdot004 \times 10^{-32}$	$5\cdot73 \pm 0\cdot03 \times 10^{-32}$
μ_{-2} (sec^{2})	$2\cdot450 \pm 0\cdot006 \times 10^{-26}$	$7\cdot82 \pm 0\cdot02 \times 10^{-26}$
$\mu_{-1\cdot5}$ (sec$^{3/2}$)	$5\cdot361 \pm 0\cdot011 \times 10^{-20}$	$1\cdot277 \pm 0\cdot003 \times 10^{-19}$
μ_{-1} (sec)	$1\cdot304 \pm 0\cdot002 \times 10^{-13}$	$2\cdot314 \pm 0\cdot004 \times 10^{-13}$
ν (sec^{-1})	$8\cdot93 \pm 0\cdot02 \times 10^{12}$	$5\cdot110 \pm 0\cdot015 \times 10^{12}$
μ_{1} (sec^{-1})	$1\cdot003 \pm 0\cdot004 \times 10^{13}$	$5\cdot82 \pm 0\cdot02 \times 10^{12}$
μ_{2} (sec^{-2})	$1\cdot182 \pm 0\cdot014 \times 10^{26}$	$4\cdot06 \pm 0\cdot06 \times 10^{25}$
μ_{4} (sec^{-4})	$2\cdot03 \pm 0\cdot13 \times 10^{52}$	$2\cdot50 \pm 0\cdot15 \times 10^{51}$
μ_{6} (sec^{-6})	$3\cdot9 \pm 0\cdot6 \times 10^{78}$	$1\cdot75 \pm 0\cdot21 \times 10^{77}$

Table 5. The Entropy and Zero Point Energy

	$S°$ at $298\cdot15$°K (cal/g atom deg)	Zero point energy (cal/g atom)
Silicon	$4\cdot497 \pm 0\cdot009$	1435 ± 5
Germanium	$7\cdot432 \pm 0\cdot015$	833 ± 3

The moment μ_1 is related to the internal energy of the lattice and ν_g, the geometric mean frequency, to the entropy. μ_1 gives the zero point energy directly (Barron *et al.* 1957) and numerical values of this quantity for silicon and germanium are given in table 5. Also shown are values of the entropies at $298\cdot15$°K, which have been calculated from C_p.

Fig. 8

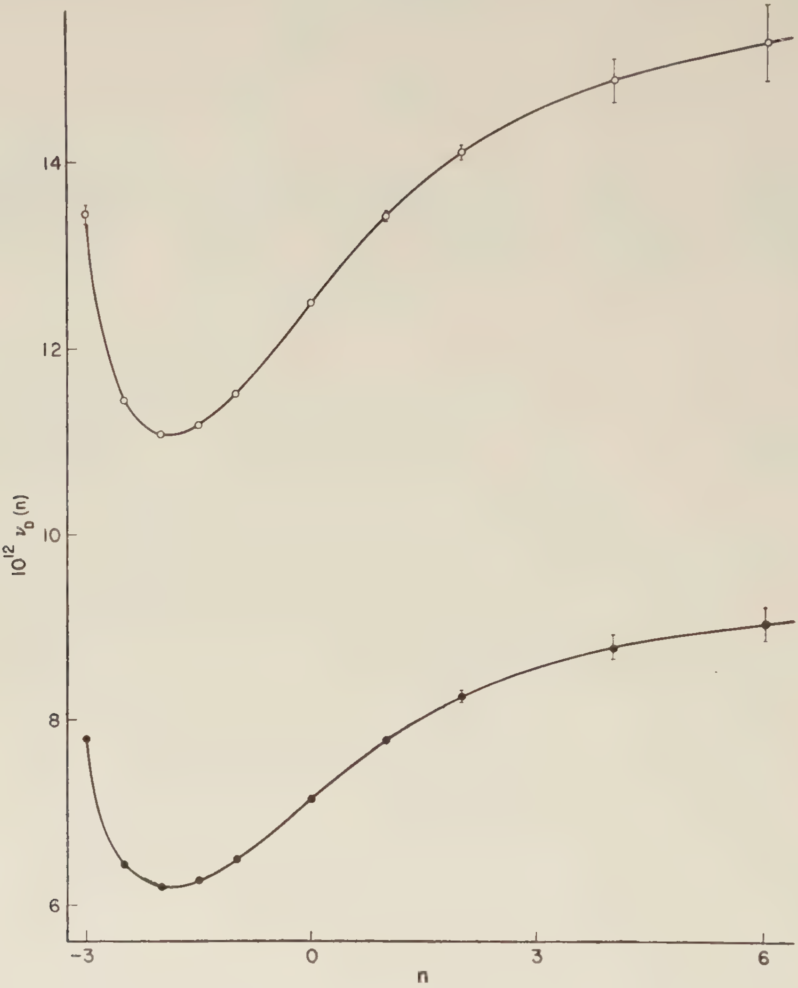

The function $\nu_D(n) = \left(\frac{n+3}{3}\mu_n\right)^{1/n}$ for silicon and germanium.

○ Silicon.
● Germanium.

The heights of the vertical bars indicate the estimated uncertainties. Where no bar is shown, the uncertainty is less than the diameter of the plotted circles.

§ 4. Discussion

4.1. *Correlation of Vibrational Properties*

It is appropriate now to see if the harmonic vibrational properties deduced from the heat capacity results are consistent with the results of other measurements. A difficulty here is that neutron scattering and some optical absorption measurements have only been made at room temperature where anharmonic effects appear in the heat capacity. Care must be taken, therefore, in making direct comparisons. On the other hand, measurements of elastic properties (McSkimin 1953) have been carried down to low temperatures and a direct comparison of elastic and thermal properties is possible through Θ(elastic) and Θ_0. As we have seen (table 3), the agreement between these two quantities is excellent for both silicon and germanium.

Brockhouse and Iyengar (1958) have compared their frequency-wave number relations for germanium with elastic properties corresponding to room temperature and with infra-red absorption results and have shown that all of the data are mutually consistent. They have also included existing heat capacity results in the comparisons but only to a limited extent and without specific consideration of anharmonicity. Concurrently with the present work, Phillips (1959) has determined a vibrational frequency spectrum for germanium and this allows a better comparison to be made with the heat capacity. Phillips used the experimental data of Brockhouse and Iyengar to determine critical points occurring in the spectrum and constructed the remaining parts of the spectrum by his interpolation method (Phillips 1956). The resulting spectrum gave Θ_D values some 3% larger than those calculated from the experimental heat capacities for the temperature range 15° to 125°K (Phillips 1959). By reducing all of the neutron frequencies by an amount within their probable error, Phillips has constructed a second spectrum for which the Θ_D values are within 1% of those derived from our experiments.

It is satisfying that Phillips's spectrum, which has been derived assuming harmonic vibrations, fits the heat capacity results rather well in the temperature region where we have supposed the behaviour of the lattice vibrations to be harmonic. The limiting high temperature behaviour is also similar; Phillips's modified spectrum gives $\Theta_\infty = 392$°K compared with $\Theta_\infty = 395 \pm 3$°K obtained by extrapolation of the heat capacity results from the region $T < \Theta_D/3$.

Marcus and Kennedy (1959)† have used the neutron results of Brockhouse and Iyengar (1958) to deduce other features of the vibrational frequency spectrum of germanium. In particular, they have been concerned with the dispersion of the lattice waves of low frequency and have estimated the coefficient β of eqn. (3.3). Their result agrees with that given in table 3 within the uncertainty assigned to the latter quantity.

Rather less can be said about results for silicon because the frequency-wave number relations for it have yet to be measured. As is apparent from the discussion of the germanium results, these relations contain the most important information about vibrational properties. However, certain deductions about the frequency spectrum for silicon can be made. Brockhouse (1958) has suggested that to a useful degree of approximation the spectra of germanium and silicon are related by a constant factor. This may be seen from a reduced plot of Θ_D against T (fig. 9), but it is also evident that there must be small differences between the two spectra. Phillips (1959) has shown that apart from the change of scale only small changes in the positions of peaks need to be made to obtain a spectrum for silicon which is in good agreement with the measured heat capacity.

---

† We appreciate Dr. Marcus's courtesy in sending us a preprint.

Fig. 9

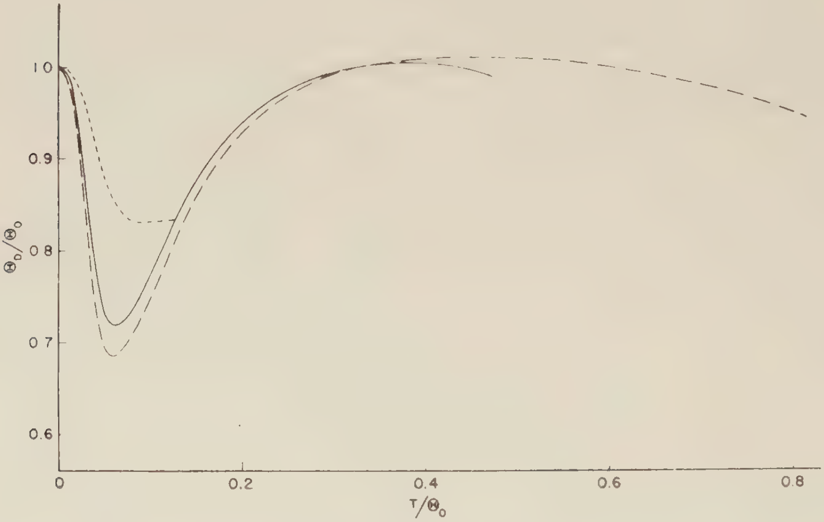

A reduced plot of Θ_D against T for:

diamond - - - - - - - - - - - -
silicon ——————————
and germanium — — — — — —.

We can summarize this section by saying that the present heat capacity results for silicon and germanium are consistent with other measured vibrational properties. However, full use of the accuracy of the heat capacity measurements has not been made in the comparison with other results because of uncertainties inherent in dealing with anharmonic effects. All of the results are inconsistent with the Smith model (Smith 1948) as it has been applied to silicon and germanium by Hsieh (1954). This inconsistency has been dealt with in detail by Brockhouse and Iyengar (1958). On the other hand, the behaviour of the properties of diamond is quite different, as may be seen from fig. 9. It is not clear at present to what extent the Smith model is applicable to diamond because Smith's detailed calculations (1948) were made before accurate values of the elastic constants of diamond were available.

4.2. *Anharmonic Effects*

In the foregoing sections we have suggested that the decrease of Θ_D of both silicon and germanium at higher temperatures is an anharmonic effect of a type which cannot be explained by change of volume alone, It is unlikely that the effect is due to an under-estimation of $C_p - C_v$. As we have seen, $C_p - C_v$ for both solids is small and is known sufficiently accurately. It seems certain also that the decrease of Θ_D cannot be accounted for by the thermal creation of imperfections in the lattices; the energies involved are much too large to give an observable effect on C_p in the temperature region below 300°c. Therefore, the only obvious remaining possibility is that, in the region $T > \Theta_D/3$, the thermal energy is sufficient to make the vibrations markedly anharmonic. When we examine this possibility in more detail, two difficulties become apparent.

In the first place, one would expect the ratio of the amplitude of the vibrations to the interatomic spacing to be the relevant parameter; this ratio is some 30% larger for silicon than it is for germanium, yet the departures of the Θ_D's from the Thirring expansion occur at about the same reduced temperature for both. By contrast it should be mentioned that this parameter correlated reasonably well with similar departures found for alkali halide crystals (Barron *et al.* 1957).

The second difficulty arises from the fact that the crystals have appreciable zero point energy (table 5). In the region of $T \sim \Theta_D/3$ the thermal energy is only about a third of the zero point energy. Hence, we must suppose that zero point energy also introduces anharmonicity in the lattice vibrations even at the lowest temperatures; this point has been stressed previously (Barron *et al.* 1957, 1959). In particular, it has been pointed out that while the analysis of experimental heat capacities gives properties of an effective harmonic frequency spectrum, this spectrum cannot be identified with the spectrum usually derived in theoretical work using only second order terms in the potential energy.

The striking feature of the observed effect at high temperatures is the abruptness with which it appears (fig. 5). This is illustrated in another way in figs. 10 and 11 where differences between C_v computed from C_p and C_v corresponding to the supposed harmonic behaviour of the crystals are plotted against the absolute temperature. Within the precision of the measurements ΔC_v is a linear function of the temperature and $d\Delta C_v/dT$ is nearly the same for both silicon and germanium.

An extensive theoretical study of the effect of anharmonicity on the properties of crystalline lattices has recently been carried out by Ludwig (1958). His results predict for high temperatures an additional term in the heat capacity which is directly proportional to the absolute temperature. A similar result is obtained (Peierls 1955) from a purely classical consideration of the problem and Eastabrook (1957), using a simplified treatment, has estimated that the magnitude of the anharmonic contribution should be less than that of $C_p - C_v$. Reference to figs. 10 and 11 and to table 2 shows that ΔC_v is very much larger than $C_p - C_v$. More important is the fact that ΔC_v is not directly proportional to the absolute temperature.

It would indeed be surprising if ΔC_v did agree with the above predictions which should hold only in the general temperature region $T > \Theta_D$; the

Fig. 10

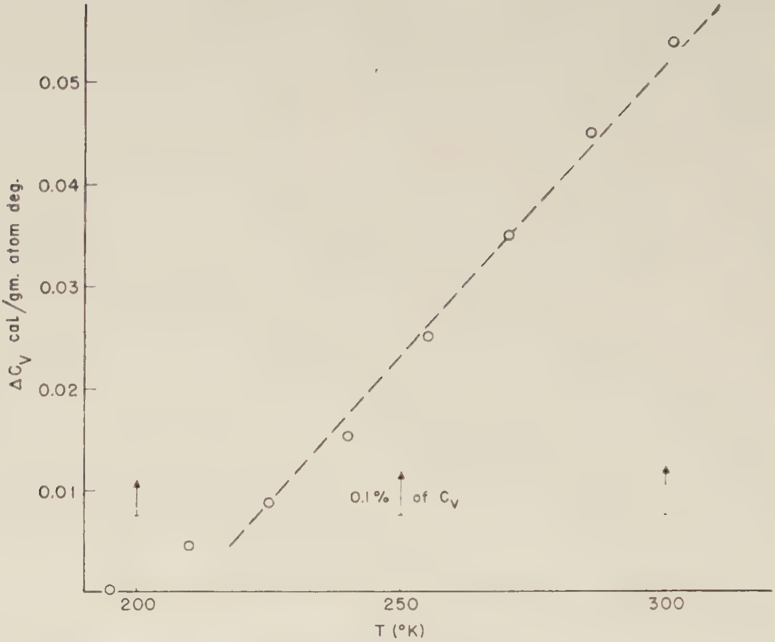

The difference between $C_v(V_0)$ and $C_v(V_0)$ (harmonic) for silicon as a function of T.

Fig. 11

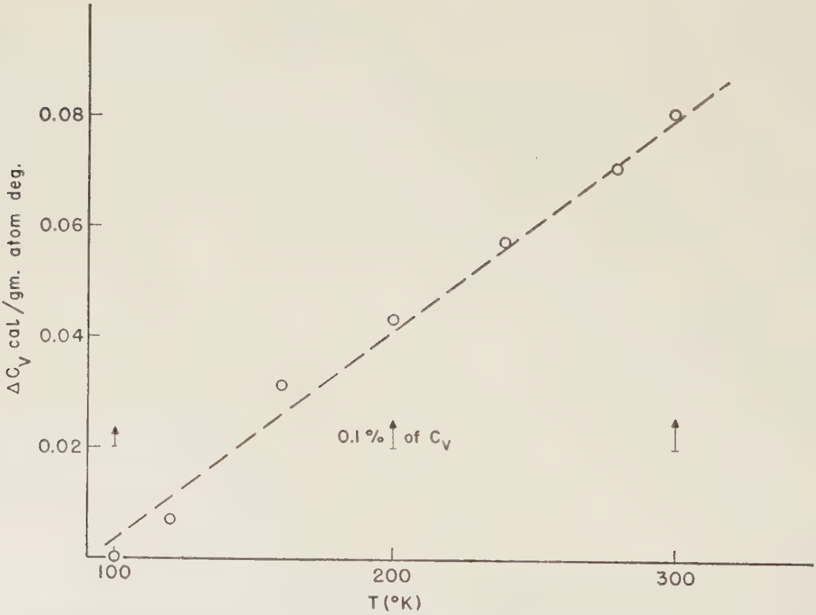

The difference between $C_v(V_0)$ and $C_v(V_0)$ (harmonic) for germanium as a function of T.

highest temperature reached in the experiments was less than Θ_D, even for germanium. Quantum effects in the region $T < \Theta_D$ will reduce the magnitude of ΔC_v below that given by classical mechanics but the precise temperature dependence to be expected is not known. From the experimental evidence alone it is difficult to reach a definite conclusion regarding the exact temperature dependence. This would require either greater precision in the measurements or an extension of the measurements to higher temperatures. Ludwig's work appears to provide the general basis for the treatment of anharmonicity but has so far only been applied in detail to a model of the face centred cubic lattice. A detailed comparison with our results awaits an analysis of Ludwig's theory for the particular case of the diamond structure elements.

ACKNOWLEDGMENTS

We are greatly indebted to Dr. T. H. K. Barron and Dr. G. K. Horton for numerous helpful discussions and for their criticisms of this paper. We have benefited from correspondence with Dr. D. F. Gibbons and Dr. J. C. Phillips and we should like to thank them for sending us results in advance of publication.

REFERENCES

BARRON, T. H. K., BERG, W. T., and MORRISON, J. A., 1957, *Proc. roy. Soc.* A, **242,** 478; 1959, *Ibid.* (in the press).
BARRON, T. H. K., and MORRISON, J. A., 1957, *Canad. J. Phys.*, **35,** 799.
BERG, W. T., and MORRISON, J. A., 1957, *Proc. roy. Soc.* A, **242,** 467.
BROCKHOUSE, B. N., 1958, *International Conference on Semiconductors*, University of Rochester, Rochester, N.Y.
BROCKHOUSE, B. N., and IYENGAR, P. K., 1957, *Phys. Rev.*, **108,** 894; 1958, *Ibid.*, **111,** 747.
CLEMENT, J. R., and QUINNELL, E. H., 1952, *Rev. sci. Instrum.*, **23,** 213.
COLLINS, R. J., and FAN, H. Y., 1954, *Phys. Rev.*, **93,** 674.
CLUSIUS, K., and PIESBERGEN, U., 1958, *Z. Naturf.* (to be published).
DESNOYERS, J. E., and MORRISON, J. A., 1958, *Phil. Mag.*, **3,** 42.
VAN DIJK, H., and DURIEUX, M., 1955, Conférence de physique des basses températures (Annexe 1955–3, Suppl. *Bull. Inst. Int. du Froid*) (Paris). p. 595.
EASTABROOK, J. N., 1957, *Phil. Mag.*, **2,** 1415.
ESTERMAN, I., and WEERTMAN, J. R., 1952, *J. chem. Phys.*, **20,** 972.
GIBBONS, D. F., 1958, *Phys. Rev.*, **112,** 136.
HILL, R. W., and PARKINSON, D. H., 1952, *Phil. Mag.*, **43,** 309.
HSIEH, Y-C., 1954, *J. chem. Phys.*, **22,** 306.
KEESOM, P. H., and PEARLMAN, N., 1953, *Phys. Rev.*, **91,** 1347.
DE LAUNAY, J., 1956, *J. chem. Phys.*, **24,** 1071.
LAX, M., 1958, *Phys. Rev. Letters*, **1,** 133.
LUDWIG, W., 1958, *J. Phys. Chem. Solids*, **4,** 283.
MACFARLANE, G. G., MCLEAN, T. P., QUARRINGTON, J. E., and ROBERTS, V., 1957, *Phys. Rev.*, **108,** 1377.
MCSKIMIN, H. J., 1953, *J. appl. Phys.*, **24,** 988.
MARCUS, P. M., and KENNEDY, A. J., 1959 (to be published).

Morrison, J. A., and Patterson, D., 1956, *Trans. Faraday Soc.*, **52**, 764.

Morrison, J. A., Patterson, D., and Dugdale, J. S., 1955, *Canad. J. Chem.*, **33**, 375.

Pearlman, N., and Keesom, P. H., 1952, *Phys. Rev.*, **88**, 398.

Peierls, R. E., 1955, *Quantum theory of solids* (Oxford: University Press), pp. 34–39.

Pelah, I., Eisenhauer, C. M., Hughes, D. J., and Palevsky, H., 1957, *Phys. Rev.*, **108**, 1091.

Phillips, J. C., 1956, *Phys. Rev.*, **104**, 1263; 1959, *Ibid.* (to be published).

Smith, H. M. J., 1948, *Phil. Trans.* A, **241**, 105.

Woolley, H. W., Scott, R. B., and Brickwedde, F. G., 1948, *J. Research N.B.S.*, **41**, 379.

APPENDIX

Measured Heat Capacities (units—cal/g atom deg)

I. Silicon

T	C_p	T	C_p	T	C_p
7·720	0·0008235	48·63	0·4957	183·00	3·470
8·122	0·0009686	49·80	0·5241	184·61	3·492
8·465	0·001090	50·50	0·5380	186·40	3·526
9·001	0·001330	51·96	0·5741	188·08	3·550
9·471	0·001541	54·38	0·6315	189·94	3·582
9·941	0·001814	55·43	0·6575	191·49	3·607
10·455	0·002133	58·09	0·7271	193·25	3·631
10·894	0·002439	59·01	0·7488	194·86	3·655
11·501	0·002889	61·66	0·8136	196·69	3·684
11·908	0·003274	62·71	0·8396	198·18	3·707
12·435	0·003671	65·10	0·9001	200·08	3·738
12·592	0·003926	66·27	0·9309	201·45	3·760
12·649	0·004151	68·67	0·9852	203·42	3·787
12·927	0·004176	69·74	1·008	204·95	3·804
12·995	0·004283	72·16	1·069	206·71	3·827
13·032	0·004467	73·32	1·101	208·67	3·862
13·618	0·005165	75·57	1·152	210·03	3·877
14·590	0·006620	76·82	1·180	212·34	3·921
14·941	0·007559	80·40	1·269	213·38	3·924
15·527	0·008367	83·95	1·359	216·88	3·970
15·302	0·008035	86·29	1·413	220·56	4·017
15·420	0·008216	89·73	1·502	224·19	4·063
16·256	0·01004	93·20	1·579	227·78	4·107
16·505	0·01050	96·71	1·662	231·26	4·149
17·221	0·01262	100·07	1·740	231·33	4·147
17·529	0·01330	101·46	1·772	234·77	4·186
17·694	0·01380	103·46	1·819	238·24	4·230
18·489	0·01641	106·87	1·902	241·68	4·264
18·686	0·01737	110·15	1·977	245·09	4·309
19·543	0·02038	113·53	2·054	248·64	4·338
19·551	0·02058	117·02	2·137	252·36	4·379
19·606	0·02094	120·39	2·214	256·03	4·418
20·253	0·02416	123·85	2·293	259·68	4·460
21·967	0·03348	124·65	2·311	263·29	4·489
22·101	0·03465	128·05	2·388	266·88	4·521
22·959	0·04054	131·42	2·463	270·43	4·558
23·058	0·04111	134·75	2·537	273·77	4·582
25·17	0·05811	138·00	2·603	277·38	4·621
26·47	0·07150	141·16	2·677	280·85	4·646
28·48	0·09537	144·42	2·744	283·36	4·652
29·80	0·1121	147·78	2·815	284·30	4·680
31·62	0·1387	151·05	2·879	287·71	4·696
32·90	0·1594	154·26	2·944	287·68	4·712
34·67	0·1903	157·51	3·010	291·08	4·735
36·15	0·2175	159·72	3·052	292·90	4·733
37·75	0·2490	160·81	3·076	294·69	4·767
39·43	0·2841	162·97	3·116	295·52	4·770
40·88	0·3140	166·35	3·178	296·63	4·770
42·59	0·3519	169·87	3·243	296·73	4·764
43·96	0·3827	173·16	3·300	298·41	4·785
45·75	0·4249	176·39	3·358	300·33	4·790
46·92	0·4522	179·72	3·423	300·45	4·796

II. Germanium

T	C_p	T	C_p	T	C_p
2·461	0·0001283	24·548	0·3950	123·84	3·928
2·675	0·0001766	25·86	0·4504	127·36	4·006
2·971	0·0002337	27·22	0·5094	130·81	4·079
3·175	0·0003008	28·46	0·5631	134·18	4·150
3·481	0·0003918	29·87	0·6267	135·93	4·178
3·713	0·0004876	31·16	0·6839	139·22	4·245
3·961	0·0005763	32·68	0·7509	142·42	4·308
4·364	0·0007935	33·91	0·8049	145·75	4·363
4·471	0·0008362	35·72	0·8848	149·23	4·427
4·814	0·001077	36·93	0·9376	152·66	4·475
4·963	0·001170	39·00	1·026	156·05	4·529
5·283	0·001446	40·46	1·087	159·39	4·577
5·503	0·001636	42·43	1·168	162·69	4·630
5·774	0·001915	44·29	1·240	166·06	4·668
6·024	0·002188	45·89	1·312	169·50	4·712
6·284	0·002513	47·87	1·393	172·90	4·753
6·506	0·002802	49·37	1·453	176·26	4·796
6·784	0·003247	51·90	1·557	178·49	4·824
7·131	0·003845	53·59	1·622	183·82	4·880
7·510	0·004668	55·63	1·703	189·31	4·931
7·974	0·005757	57·15	1·765	192·91	4·967
8·465	0·007220	59·02	1·840	196·48	4·999
8·948	0·008950	60·39	1·895	200·02	5·034
9·434	0·01104	62·35	1·974	203·54	5·065
10·006	0·01391	63·76	2·029	207·02	5·091
10·442	0·01679	65·81	2·111	210·49	5·119
11·015	0·02103	67·30	2·169	213·92	5·145
11·458	0·02479	69·22	2·239	217·34	5·173
12·011	0·03039	70·73	2·293	222·82	5·219
12·366	0·03512	72·54	2·363	226·53	5·232
12·471	0·03559	74·07	2·421	230·21	5·256
12·902	0·04187	76·00	2·491	233·87	5·286
13·008	0·04265	77·45	2·546	237·50	5·299
13·478	0·04946	79·38	2·617	241·11	5·325
14·002	0·05829	81·09	2·681	244·70	5·349
14·536	0·06767	82·75	2·743	246·40	5·349
15·002	0·07647	84·36	2·801	249·98	5·374
15·192	0·08112	85·97	2·859	253·51	5·390
15·579	0·08827	87·50	2·911	257·02	5·415
15·945	0·09754	89·06	2·973	262·81	5·437
15·961	0·09828	90·70	3·015	268·85	5·461
16·578	0·1127	92·22	3·057	272·84	5·478
16·979	0·1231	93·98	3·120	276·81	5·494
17·579	0·1402	95·46	3·165	280·72	5·510
17·588	0·1399	97·17	3·216	280·90	5·515
18·051	0·1534	98·76	3·266	284·80	5·525
18·493	0·1675	100·27	3·309	286·55	5·537
18·628	0·1701	103·23	3·392	288·66	5·546
19·041	0·1826	106·87	3·502	292·38	5·557
19·632	0·2027	110·39	3·596	292·48	5·560
20·233	0·2256	113·82	3·682	296·23	5·581
21·449	0·2709	117·17	3·768	296·24	5·572
23·186	0·3392	120·44	3·849	300·01	5·609
				300·05	5·600

NOTE: The number of significant figures given reflects the precision of the measurements rather than their absolute accuracy.

The Positions of Dislocations in Arrays†

By A. K. HEAD
Division of Tribophysics,
Commonwealth Scientific & Industrial Research Organization,
University of Melbourne, Australia

[Received November 6, 1958]

ABSTRACT

The equilibrium positions of dislocations in a number of types of array have been found numerically. Arrays considered are:

(i) that generated by a dislocation source which is between two locked dislocations,

(ii) a dislocation pile-up against a locked dislocation which is not on the slip-plane,

(iii) a group of positive dislocations attracted to a group of negative dislocations but prevented from coalescing by locked dislocations,

(iv) a group of positive dislocations attracted by a group of negative dislocations on a parallel slip plane.

A short table of the zeros of the first derivative of the Laguerre polynomials is given.

§ 1. INTRODUCTION

A CENTRAL problem in the dislocation theory of solids is the equilibrium arrangement of a number of mobile dislocations under their mutual interactions and the action of a stress field. As this is a many-body problem exact analytical solutions cannot be expected although Eshelby *et al.* (1951) have shown that there are such solutions for a restricted class of problem. Their solutions follow from properties of the classical orthogonal polynomials which are such that to a polynomial of the nth degree there corresponds an arrangement of n like dislocations, all on the same slip-plane and located at the zeros of the polynomial. These dislocations are in equilibrium under an applied stress field related to the coefficients of the differential equation satisfied by the polynomial. Some of the sets of orthogonal polynomials correspond to dislocation arrangements of great interest but it does not appear possible to extend this method as it is essentially an inverse approach to the problem. It has been suggested (Leibfried 1951, 1954, Haasen and Leibfried 1954) that approximate solutions can be obtained by replacing the discrete dislocations by a continuous dislocation density. In this case the dislocations need not be all of the same sign and the equations of equilibrium become an integral equation which, if the mobile dislocations are all on the same slip plane, can be solved by routine procedures (Head and Louat 1955).

There are still many problems for which neither of the above methods is convenient and for some of these the equations of equilibrium have been solved numerically on the electronic digital computer CSIRAC.

---

† Communicated by the Author.

§ 2. General Method

All dislocations are taken to be of infinite length parallel to the z axis with slip plane parallel to the x axis and in most cases the slip plane is $y=0$. For each array a characteristic length is taken as the unit of distance and the unit of stress defined as the stress at unit distance along the slip plane from an isolated dislocation of the type (screw or edge) being considered and with the sign convention that a positive stress moves a positive dislocation to the left. In these units the equations of equilibrium for n positive dislocations at the points $x_1, x_2, \ldots x_n$, all on the same slip plane are

$$\sum_{\substack{i=1\\ \neq j}}^{n} \frac{1}{x_j - x_i} + P(x_j) = 0, \quad j = 1, 2, \ldots n$$

where $P(x)$ is the stress field due to any applied stress, locked dislocations, etc. In those cases where there are also mobile negative dislocations the positions of these are always related by symmetry to the positions of the positive dislocations and their presence can be allowed for by extra terms in $P(x)$.

This set of equations was solved by relaxation. Starting with approximate positions for the dislocations, each dislocation in turn was moved a distance given by Newton's rule as

$$\delta x_j = \left\{ \sum_{i \neq j} \frac{1}{x_j - x_i} + P(x_j) \right\} \Big/ \left\{ \sum_{i \neq j} \left(\frac{1}{x_j - x_i} \right)^2 - P'(x_j) \right\}.$$

After all dislocations had been moved, any subsidiary conditions were adjusted and the cycle repeated until a sufficiently accurate solution was obtained. In the results given here, the least significant figure has some, but not necessarily full, significance. Incidentally, this is a possible method of computing the zeros of the classical orthogonal polynomials but as it gives only first order convergence it is slow compared with any of the usual methods for finding the zeros of a polynomial.

§ 3. Dislocation Source between Locked Dislocations

The dislocation array of fig. 1 (a) is generated by a dislocation source S which, under the influence of the applied stress σ, emits pairs of positive and negative dislocations. These move off in opposite directions along the slip-plane until the leading pair of dislocations become locked. As all dislocations are in the same slip-plane the same equations hold for either edge or screw. The dislocation source is taken to be midway between the locked dislocations and the unit of length such that the locked positive dislocation is at $x=0$, the dislocation source at $x=1$, and the locked negative dislocation at $x=2$. Since there are equal numbers n of positive and negative dislocations then for a positive dislocation at $x=x_i$ by symmetry there is a negative dislocation at $x=2-x_i$.

The value of σ is taken to be equal and opposite to the back stress of all dislocations on S so that the nett stress at S is zero. For, if σ is greater than this value the source will tend to generate more dislocation pairs and if it is less then dislocation pairs will tend to run back into the source and be annihilated. The equilibrium positions of the positive dislocations and the corresponding value of σ are given in table 1 for $n=2$ to 6.

Fig. 1

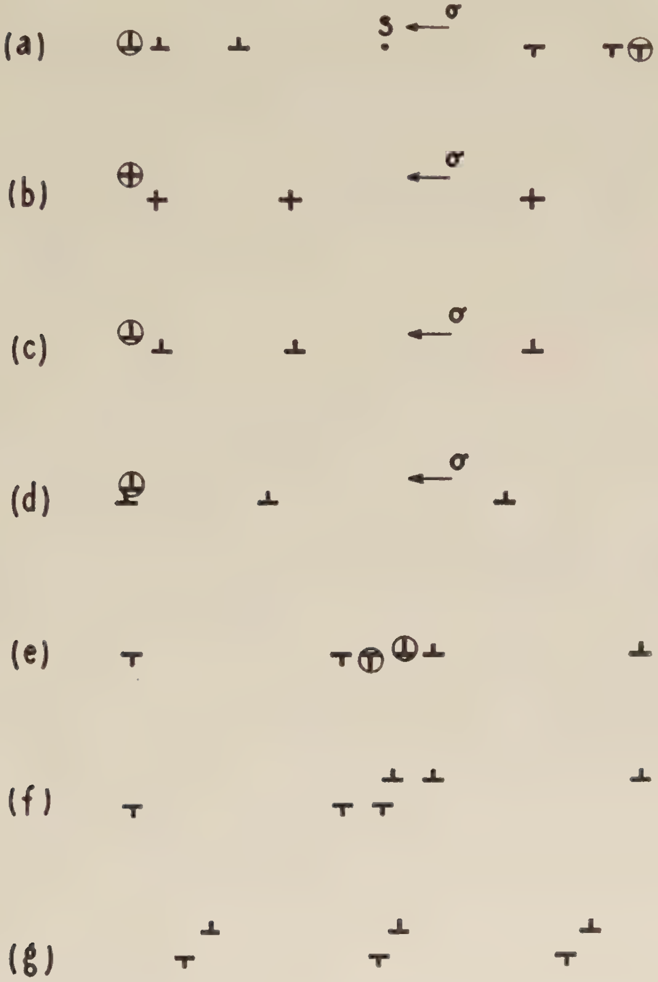

Dislocation arrays for $n=3$. Locked dislocations are circled.
(*a*): Table 1 and § 3.
(*b*): Table 2 and § 4.
(*c*): Table 3 (*a*) and § 4.
(*d*): Table 3 (*b*) and § 4.
(*e*): Table 5 and § 5.
(*f*), (*g*): § 6.

If this problem is solved by Leibfried's approximation (which should be reasonable for n sufficiently large) it is found that $\sigma/n=\pi$. For the exact solution this quantity increases from 2·40 for $n=2$ to 2·79 for $n=6$.

Table 1. Positions of Positive Dislocations and Critical Stress for Fig. 1 (*a*). Negative Dislocations at $2-x$

n	2	3	4	5	6
σ	4·7956	7·7199	10·701	13·714	16·749
x	0 0·28459	0 0·10958 0·42426	0 0·057832 0·20751 0·50672	0 0·035657 0·12448 0·28246 0·56223	0 0·024153 0·083194 0·18351 0·34076 0·60273

§ 4. Pile-up Against Locked Dislocation not on Slip-plane

One of the problems solved by Eshelby *et al.* was the piling up of n like dislocations against a locked dislocation on the slip-plane by a constant applied stress. We consider here the related problem where the locked dislocation is off the slip-plane. In this case for a pile-up of n mobile dislocations, the applied stress σ must be less than some critical value. otherwise some dislocations will be forced past the locked dislocation and be lost from the pile-up. It is necessary to consider screw and edge dislocations separately.

If the slip-plane of the mobile screw dislocations is $y=0$ and the displacement of the locked dislocation from this plane is taken as the unit of length, then the position of the locked dislocation can be taken as (0, 1), (fig. 1 (*b*)). The repulsion from the locked dislocation reaches a maximum on the plane $y=0$ at $x=1$ (Cottrell 1953) and the critical case is when the leading mobile dislocation is at this point. The applied stress necessary to produce this critical case and the positions of the dislocations are given in table 2 for $n=1$ to 6.

The same problem for edge dislocations has two critical cases due to the more complicated variation of the stress field of the locked edge dislocation at (0, 1) on the slip-plane $y=0$ (Cottrell 1953). As the applied stress is increased the n mobile dislocations move towards the locked dislocation until the leading dislocation is at $x=1+\sqrt{2}$, (fig. 1 (*c*)). The repulsion from the locked dislocation is a maximum at this point and any further increase in stress causes the leading dislocation to move past the locked dislocation where it is then held by an attractive force. The stress can then be increased until the leading dislocation reaches $x=1-\sqrt{2}$ (fig. 1 (*d*)) where the attraction is a maximum, any further increase in stress causing the leading dislocation to move off to infinity. The stress and the positions of the dislocations for these two critical cases are given in tables 3 (*a*) and 3 (*b*) for $n=1$ to 6.

Table 2. Positions of Dislocations and Critical Stress for Fig. 1 (*b*)

n	1	2	3	4	5	6
σ	0·5	0·32340	0·24016	0·19128	0·15901	0·13610
x	1	1	1	1	1	1
		6·6625	6·2328	6·0760	5·9989	5·9549
			15·547	14·377	13·895	13·639
				28·045	25·822	24·831
					44·259	40·693
						64·252

Table 3 (*a*). Positions of Dislocations and Critical Stress for Fig. 1 (*c*)

n	1	2	3	4	5	6
σ	0·25	0·16103	0·11943	0·095064	0·079005	0·067609
x	2·4142	2·4142	2·4142	2·4142	2·4142	2·4142
		13·654	12·808	12·499	12·348	12·262
			31·509	29·184	28·222	27·713
				56·677	52·220	50·234
					89·324	82·162
						129·58

Table 3 (*b*). Positions of Dislocations and Critical Stress for Fig. 1 (*d*)

n	1	2	3	4	5	6
σ	0·25	0·16702	0·12536	0·10032	0·083617	0·071681
x	−0·4142	−0·4142	−0·4142	−0·4142	−0·4142	−0·4142
		+11·638	+10·682	+10·328	+10·152	+10·052
			+29·384	+26·184	+25·198	+24·672
				+52·251	+47·886	+45·928
					+82·950	+76·050
						+120·78

When the locked dislocation is on the slip-plane Eshelby *et al.* have shown that for a suitable choice of the unit of length, the mobile dislocations are at the zeros of the first derivative of the $(n+1)$th Laguerre polynomial (table 4). Starting with such a pile-up and keeping the applied stress constant suppose the locked dislocation is moved off the slip-plane a distance d such that dislocations are about to escape from the pile-up. Then d is given by $d/D=\sigma_n/l_n$ where σ_n is the critical stress given in table 2 or 3 (*b*), l_n is the smallest zero of $L_{n+1}'(x)$ (table 4) and D was the distance of the leading mobile dislocation from the locked dislocation when the latter was on the slip-plane. As n increases from 1 to 6 this ratio increases from 0·5 to 0·516 for screw dislocations and from 0·25 to 0·272 for edge dislocations. These calculations are for ideal elastic dislocations and the analysis of Leibfried and Lücke (1949) suggests that the finite core of a real dislocation could be allowed for by decreasing the above values of d by the core diameter. Stroh (1954) has considered dislocation pile-ups in which the leading dislocations are so close together that their cores are overlapping. The present work shows that for such a pile-up to be possible the locked dislocation must be exactly on the same slip-plane as the following dislocations and the pile-up could not be formed by a dislocation source which climbs one atomic plane for each dislocation loop generated (Thompson 1953).

Table 4. Zeros of $L_{n+1}'(x)$

n	1	2	3	4	5	6
x	2	1·2679	0·93582	0·74329	0·61703	0·52766
		4·7321	3·3054	2·5716	2·1129	1·7963
			7·7589	5·7311	4·6111	3·8767
				10·954	8·3983	6·9194
					14·261	11·232
						17·648

§ 5. Positive and Negative Dislocations on Same Slip-Plane

We now consider a group of n positive dislocations attracted to a group of n negative dislocations on the same slip-plane but prevented from coalescing by the locking of the leading positive and negative dislocations (fig. 1 (*e*)). If the origin and the unit of length are chosen so that the locked dislocations are at $x=\pm 1$, then the positions of the positive dislocations are given in table 5 for $n=2$ to 6, and to each positive dislocation at $x=x_i$ there is a negative dislocation at $x=-x_i$. By considering the change in the potential energy of this dislocation array for a small movement of a locked dislocation, the argument of Cottrell (1949) can be adapted to show that the stress at a locked dislocation, due to all other dislocations, is exactly $\frac{1}{2}n$.

Figure 1 (*e*) is also the image representation of the case of n positive dislocations attracted to a free surface at $x=0$ but being held up by a locked dislocation. For screw dislocations such an image representation is exact (Head 1953 a) but is only an approximate representation of the interaction of edge dislocations with a free surface (Head 1953 b).

Table 5. Positions of Positive Dislocations for Fig. 1 (*e*). Negative Dislocations at $-x$

n	2	3	4	5	6
x	1	1	1	1	1
	4·2361	2·6803	2·1427	1·8676	1·7000
		15·088	7·7678	5·4101	4·2593
			44·633	20·300	12·920
				116·88	48·695
					280·44

§ 6. Positive and Negative Dislocations on Parallel Slip-planes

Louat (1953) and Fujita (1954, 1958) have considered the problem of n mobile positive edge dislocations on one slip-plane attracted by n mobile negative edge dislocations on a parallel slip-plane. Fujita argued that when the leading dislocations came sufficiently close there would be a repulsion between them and so there would be an equilibrium arrangement as in fig. 1 (*f*) and that an external applied stress (which he estimated approximately) was necessary to cause the dislocations to interlace as in fig. 1 (*g*).

It was intended to calculate this stress more accurately but from the results of § 5, in particular the magnitude of the stress at the locked dislocation, it appeared probable that in Fujita's problem the attraction of the outer dislocations would outweigh the repulsion of the leading dislocations and that the dislocations would interlace at least partially in the absence of an applied stress. This was confirmed by calculation for the case $n=2$ and so, *a fortiori*, for $n>2$. The distance between the slip-planes was taken as the unit of length and the origin of coordinates at the centre of inversion of the dislocation array so that to a positive dislocation at $x=x_i$, $y=+\frac{1}{2}$ there was a negative dislocation at $x=-x_i$, $y=-\frac{1}{2}$. The leading pair of dislocations were locked at various values of x and the equilibrium position of the other dislocation pair was found. From this the stress field at the locked positive dislocation was calculated. The first five entries of table 6 are for the locked dislocations in the neighbourhood of Fujita's equilibrium position, and it will be seen that although the stress on the locked dislocation has a minimum it does not become zero and so there is no position of equilibrium. The locked dislocations were then moved step by step in the direction of the stress acting on them and it was found that after the dislocations had interlaced each positive dislocation paired off with a negative dislocation and that between the two dislocation pairs there was a weak repulsion, the last entry of table 6 being typical.

Table 6. Fujita's problem, $n=2$

Locked Positive Dislocation $x=$	Mobile Positive Dislocation $x=$	Stress at Locked Positive Dislocation
0·375	2·9877	0·47716
0·3125	2·8355	0·43506
0·25	2·6958	0·41035
0·1875	2·5695	0·41813
0·125	2·4572	0·47009
−4·0	5·0289	0·00569

For $n=2$ then there is no equilibrium arrangement of the dislocations. For $n>2$ it would appear that the dislocations will interlace, at least partially, without an applied stress and that if they interlace completely they split up into positive-negative pairs which are weakly repellent. It is possible that a stable array is formed with the dislocations partially interlaced where a number of dislocations pairs would be formed but prevented from drifting apart by the attraction between the outer unpaired dislocations but the present computer programme is unsuitable for examining this question.

ACKNOWLEDGMENTS

This work has been greatly assisted by the cooperation of the staff of CSIRAC and by discussions with Mr. G. W. Hill, Dr. N. P. Louat and Dr. J. K. Mackenzie.

REFERENCES

COTTRELL, A. H., 1949, *Progress in Metal Physics*, ed. B. Chalmers (London: Butterworths), p. 105; 1953, *Dislocations and Plastic Flow in Crystals* (Oxford: University Press).

ESHELBY, J. D., FRANK, F. C., and NABARRO, F. R. N., 1951, *Phil. Mag.*, **42,** 351.

FUJITA, F. E., 1954, *Sci. Rep. Res. Inst. Tôhoku Univ.* A, **6,** 565; 1958, *Acta Met.*, **6,** 543.

HAASEN, P., and LEIBFRIED, G., 1954, *Nachr. Akad. Wiss., Göttingen, Math. Phys. Kl.*, 31.

HEAD, A. K., 1953 a, *Phil. Mag.* **44,** 92; 1953 b, *Proc. phys. Soc. Lond.* B, **66,** 793.

HEAD, A. K., and LOUAT, N. P., 1955, *Aust. J. Phys.*, **8,** 1.

LEIBFRIED, G., 1951, *Z. Phys.*, **130,** 214; 1954, *Z. ang. Phys.*, **6,** 251.

LEIBFRIED, G., and LÜCKE, K., 1949, *Z. Phys.*, **126,** 450.

LOUAT, N. P., 1953, *Ph.D. Thesis*, University of Bristol, 124.

STROH, A. N., 1954, *Proc. roy. Soc.* A, **223,** 404.

THOMPSON, N., 1953, *Proc. phys. Soc. Lond.* B, **66,** 481.

The Deformation of Lithium, Sodium and Potassium at Low Temperatures: Tensile and Resistivity Experiments†

By D. Hull
A.E.R.E., Harwell

and H. M. Rosenberg
The Clarendon Laboratory, Oxford

[Received November 1, 1958]

Abstract

Stress–strain tests have been made on Li, Na and K at temperatures between 293 and 4·2°K. At higher temperatures the behaviour of all three metals is very similar. They are soft and after the yield point very little hardening is observed. At low temperatures Li and Na transform to f.c.c. and h.c.p. structures respectively on deformation, the character of their stress–strain curves changes accordingly and they harden continuously throughout the test. At 20 and 4·2°K Li deforms with many regions of discontinuous slip and at 4·2°K it fractures in a brittle fashion. Whilst K remains b.c.c. down to 4·2°K it also exhibits an unusual type of hardening at 20 and 4·2°K which is very temperature dependent. The change in the electrical resistivity during low temperature deformation was also measured. There was no detectable change when K was deformed at 4·2°K. This offers further evidence that a large proportion of the resistivity change which is observed when metals are deformed is due to stacking faults. Both Li and Na give considerable resistivity changes when they are deformed at 4·2°K and much of this change is ascribed to the scattering of electrons at the faulted regions within the transformed phases.

§ 1. Introduction

In the past, experiments on the alkali metals have been very limited, mainly because of their high reactivity and the consequent difficulty in the handling and preparation of specimens. They do, however, provide an extremely interesting field for study. At room temperature they all have a body-centred cubic (b.c.c.) structure and are very different from the b.c.c. transition metals which have high melting points and which are susceptible to low temperature brittleness. The properties of sodium and lithium are modified at low temperatures, however, because they undergo martensitic transformations and this puts their behaviour in marked contrast to that of potassium which remains b.c.c. down to the lowest temperatures.

In this paper we shall describe some experiments on the way in which the tensile properties of lithium, sodium and potassium change at temperatures down to 4·2°K. In addition to this the change in the electrical resistivity during deformation has been measured.

---

† Communicated by the Authors.

§ 2. The Experiments

The tensile tests were made using a hard beam machine which is shown diagrammatically in fig. 1. It is a modification for low temperature use of one described by Adams (1958). A constant speed driving motor M lowers the cross beam C via a worm drive, W, and the central threaded rod, R. This extends the specimen, S, because its lower end is connected to the rods P which are in turn fixed to the cross beam. The upper end of the specimen is connected to a load cell, L, by a rod which passes through the centre of R. The sensitivity of the load cell was 5·6 kg per mv. This output potential was fed to an automatic recorder and the specimen was extended at a constant rate of 0·325 mm per minute. A dewar of coolant could be placed around the whole of the lower section of the apparatus. The liquid air container, A, which was attached to the rods P acted as a radiation shield when liquid helium was used in the dewar. The moving joints were sealed with flexible rubber tubing to prevent loss of helium gas. All the low temperature section of the apparatus was made of stainless steel.

The specimens were made by extruding the metal through a circular nozzle under liquid paraffin. The metals rapidly recrystallize at room temperature so that large grained (> 1 mm) polycrystalline specimens were formed. The specimens were about 5 cm long and they had a diameter of 0·165 cm for the electrical resistivity experiments. The stresses required to extend these specimens were too small to measure accurately, however, and so for the tensile tests a diameter of 0·47 cm was used. Each end of the specimen was supported in a holder made of a small block of metal with a conical hole in it (fig. 1, inset), the smallest diameter of the hole being slightly larger than the specimen diameter. About 2 cm of the specimen was passed through this hole and was packed down into the cone, so that when the specimen was pulled the end would not slip out. For the electrical resistivity experiments current and potential leads of fine copper wire were forced into the specimen, the metal being pressed around the wire to ensure good contact. The potential leads were inserted into the specimen through small holes drilled in the sides of the cones whilst the current leads were pushed into the ends of the specimen. Such contacts seemed to be very satisfactory, probably due to the relatively large contraction of the specimens on cooling. Currents of the order of 1 amp were used and the potential produced across the specimen was measured on a galvanometer amplifier.

The section of the apparatus containing the specimen could be surrounded by a dewar vessel and for experiments below room temperature baths of dry ice in acetone (195°K), liquid air (~ 80°K), liquid hydrogen (20·4°K) and liquid helium (4·2°K) were used.

The specimens were fitted into their holders and into the apparatus whilst immersed in a bath of liquid paraffin. For experiments below room temperature the bath was removed and the film of paraffin washed off with carbon tetrachloride just before the specimen was immersed in the

Fig. 1

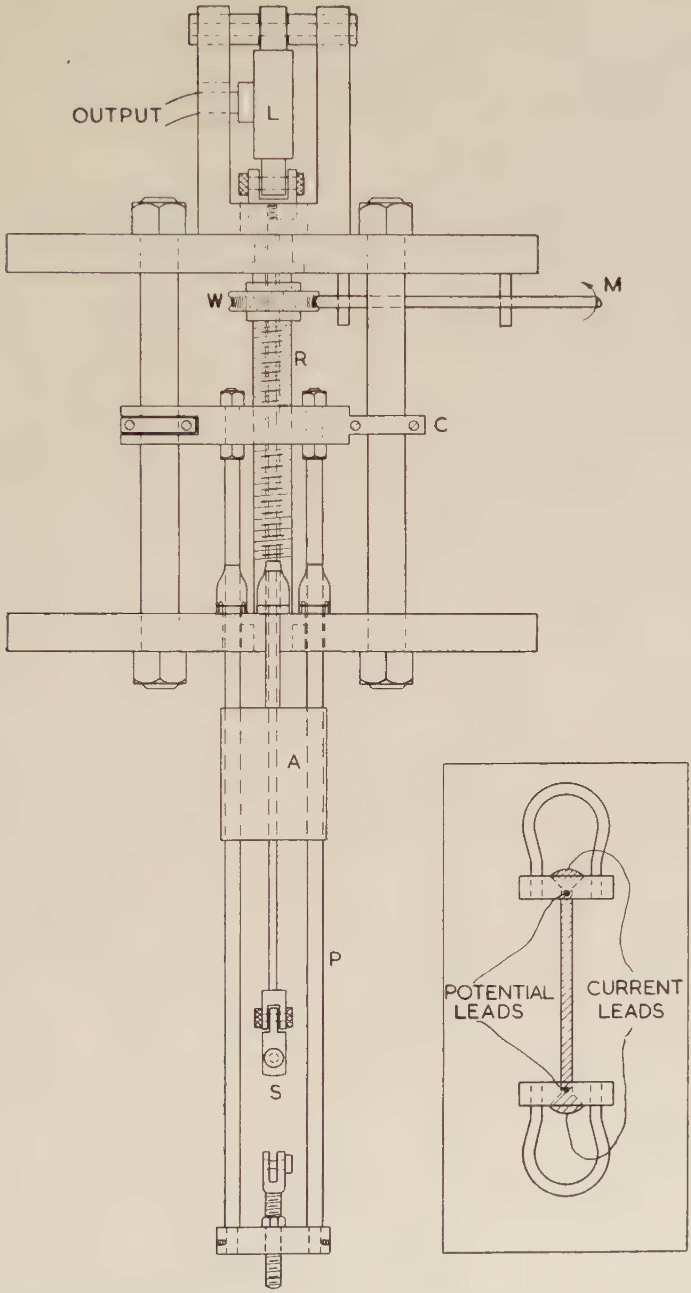

The hard beam tensile apparatus used in the experiments. The inset shows the specimen holders used for the alkali metals.

Fig. 2

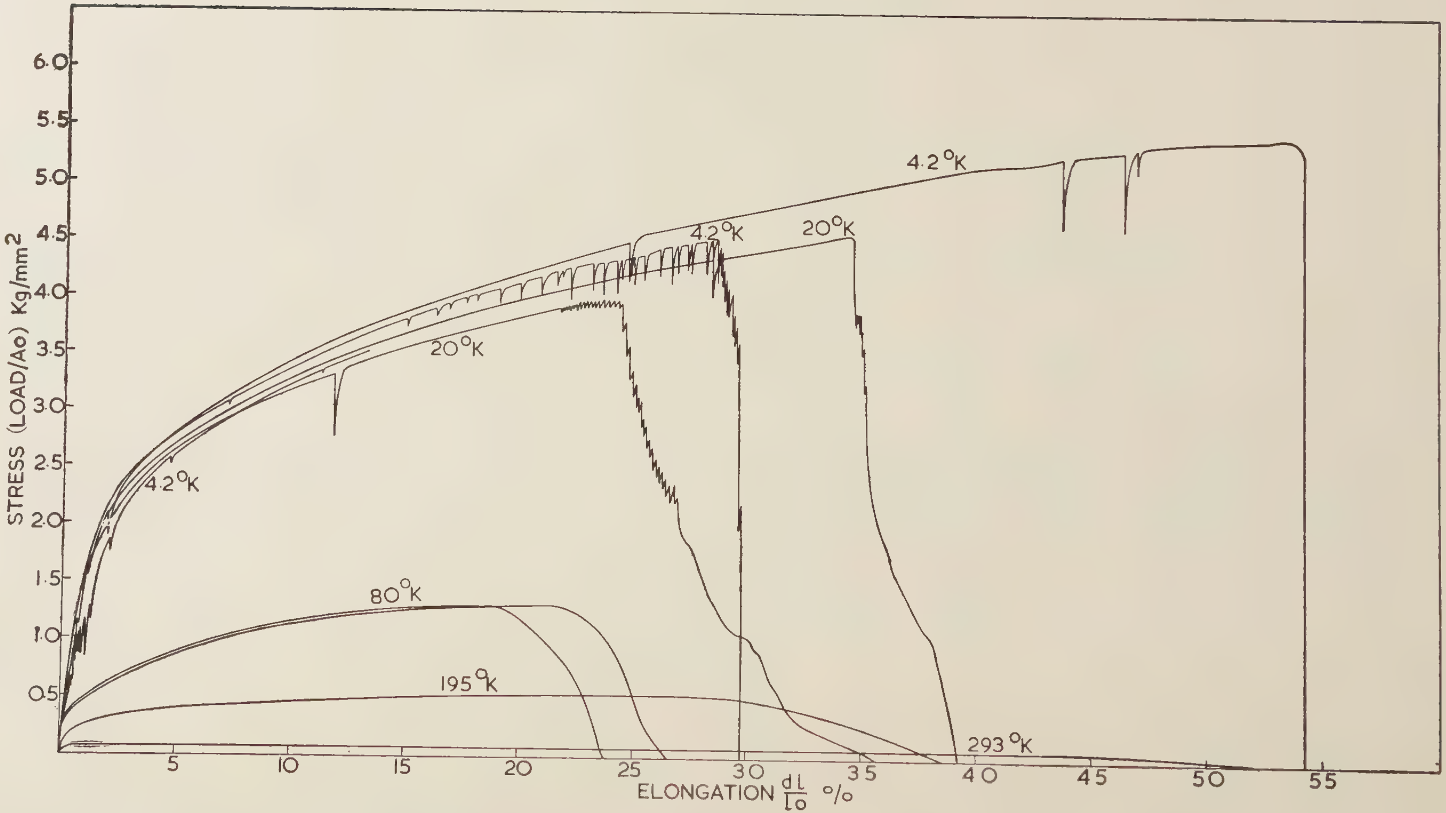

The stress–strain curves for lithium taken at 293, 195, 80, 20 and 4·2°K. The discontinuous slip at 20 and 4·2°K should be noted.

coolant. Whilst this technique prevented large scale oxidation, thin oxide films could not be avoided.

The lithium used was 99·7% pure. Both commercial purity sodium (B.D.H.) (impurity not greater than 0·1%) and high purity vacuum distilled metal (99·998%) were used. All the potassium specimens were made from vacuum distilled metal (99·999%).

§ 3. The Tensile Tests

The stress/strain curves at the various temperatures are shown in figs. 2 to 4 and values of the yield stress are shown in fig. 5. In all cases the yield stresses were very small and difficult to measure accurately with the present machine.

Fig. 3

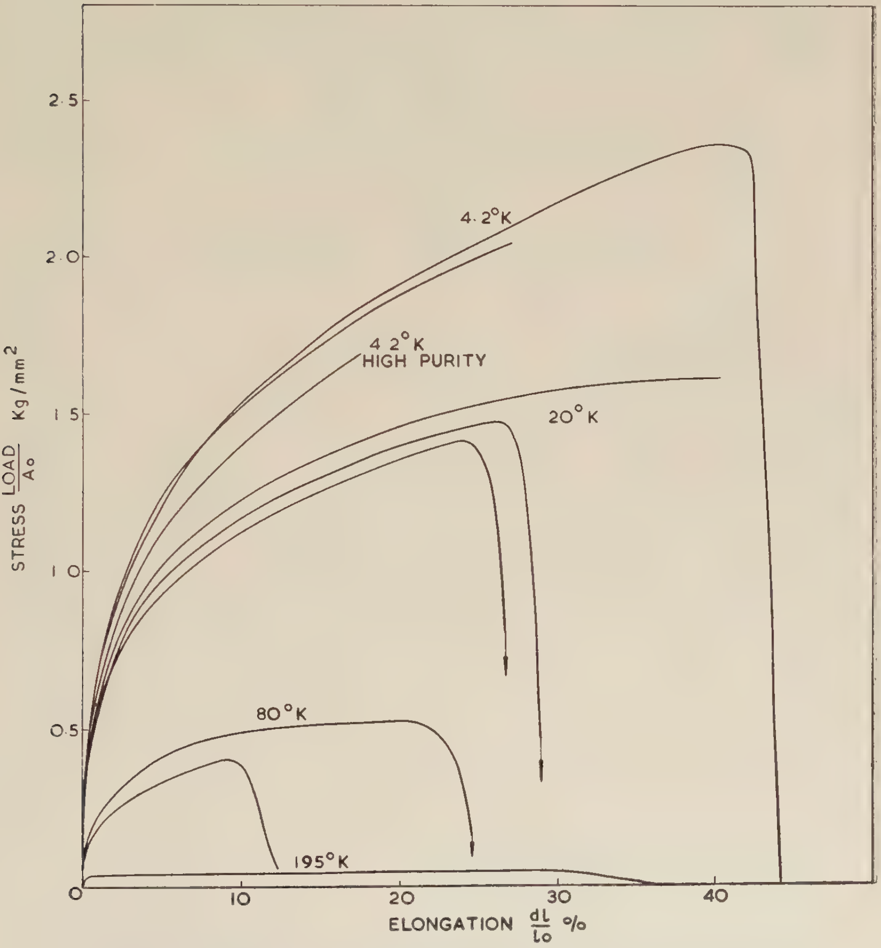

The stress–strain curves for sodium taken at 195, 80, 20 and 4·2°K.

Fig. 4

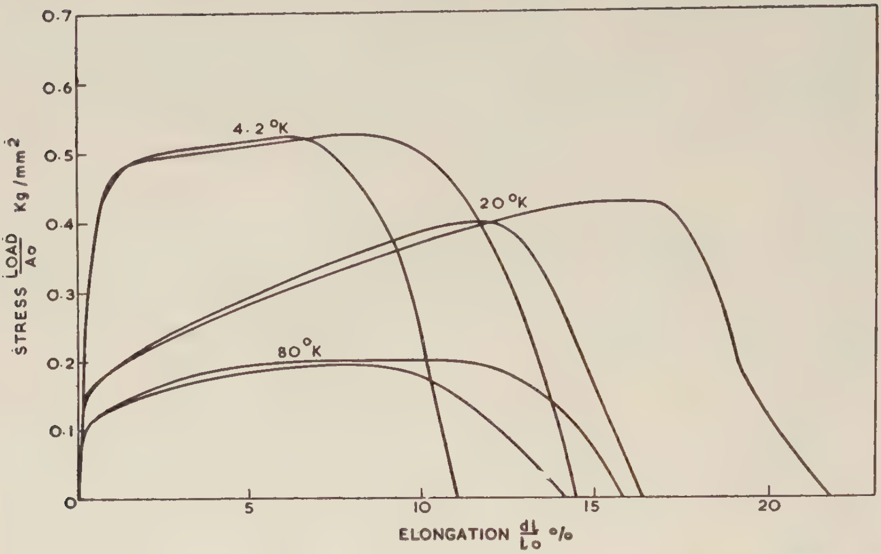

The stress–strain curves for potassium taken at 80, 20 and 4·2°K. Note the very sharp increase in the rate of linear hardening between 20 and 4·2°K.

Fig. 5

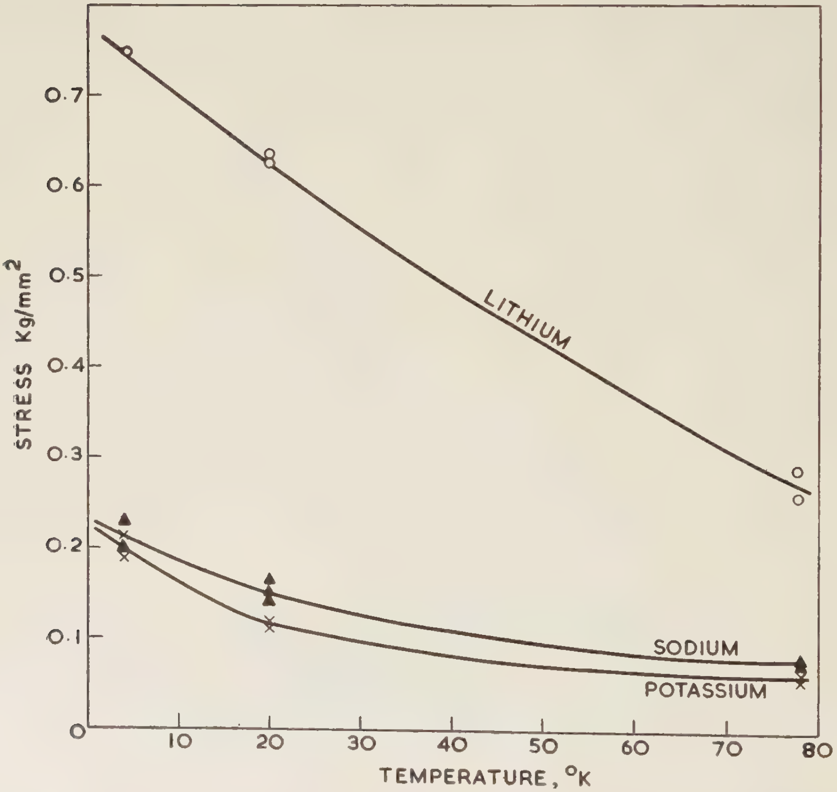

The variation of the yield stress with temperature for lithium, sodium and potassium.

The stress/strain curves of the metals at lower temperatures are quite different from one another. Both sodium and lithium work harden very rapidly to relatively high stresses at 20 and 4·2°K with elongations of about 40%. At both these temperatures, and at 4·2°K in particular, lithium shows a series of very marked yield drops. At 20°K this discontinuous yielding was confined to the second half of the test but at 4·2°K, yield drops were detected in some cases before the yield point was reached. At 4·2°K the specimens did not neck down on fracture, but they snapped in a brittle fashion after an extension of about 30–50% showing a bright fracture face. No signs of any discontinuous yielding were noted in either potassium or sodium. They were extremely ductile at all testing temperatures and the specimens necked down at fracture to a knife edge. Nevertheless, whereas in sodium the hardening continued throughout most of the test, in potassium the initial work hardening rate was not maintained and the maximum stress at 4·2°K was only 20 to 25% that of sodium. One result of this is the smaller elongation of potassium. There is a marked change in the curves of potassium from 20 to 4·2°K. The initial work hardening rate is much higher at 4·2°K than at 20°K where there is a long region of almost linear hardening.

§ 4. The Electrical Resistivity

The change in the electrical resistivity $\Delta\rho$ during deformation was measured at 4·2°K for all three metals and in addition at 20°K for lithium and sodium. A large part of the resistance change is of course due to the increase in the form factor of the specimen as it is being extended. After this has been allowed for, however, there was still a considerable increase in the resistivity of both sodium and lithium after extension in liquid helium. There was, however, practically no change in sodium after deformation at 20°K although if the dependence of $\Delta\rho$ on strain had been of the same magnitude as it was at 4·2°K this could have been observed quite easily. In actual fact a detailed examination of four different runs shows that for the first few per cent of strain the resistivity actually decreases by 2 or 3%. It then begins to increase again, reaching its original value by about 10% strain and thereafter it continues to increase very slightly. No detectable change (less than 1%) in the resistivity of potassium could be detected when it was deformed at 4·2°K. Since it was so soft it could only be extended by a very small amount (3–4%) before it started to neck down and break, and hence very few measurements of the resistivity could be taken and these only after very small amounts of damage had been introduced into the specimen. Nevertheless, it was quite clear that even if there was a slight resistivity change it was very much less than for the other two metals. Logarithmic plots of $\Delta\rho$ against the strain, ϵ, are shown in fig. 6. It will be noted that the relation is approximately linear and is of the form $\Delta\rho = A\epsilon^n$ ohm cm where

$A = 2{\cdot}4 \times 10^{-7}$, $n = 0{\cdot}92$ for lithium at 4·2°K,
$A = 1{\cdot}65 \times 10^{-7}$, $n = 0{\cdot}92$ for lithium at 20°K,
and $A = 2 \times 10^{-8}$, $n = 1{\cdot}1$ for sodium at 4·2°K.

Whilst there was hardly any change in the resistivity of sodium after deformation at 20°K it was noted that if the specimen was warmed up to 80°K after this extension and then re-cooled to 20°K that its resistance had increased by about 10%. This experiment was repeated several times with approximately the same result in each case, independent of whether the specimen was warmed and re-cooled whilst still under tension or with the load removed. On warming to room temperature and re-cooling, nearly all this resistivity increase disappeared. The resistivity change in lithium after deformation at 20°K was similar in form to that obtained when the metal was deformed at 4·2°K except that the value of $\Delta\rho$ for a given strain was about 30% less at 20°K.

Fig. 6

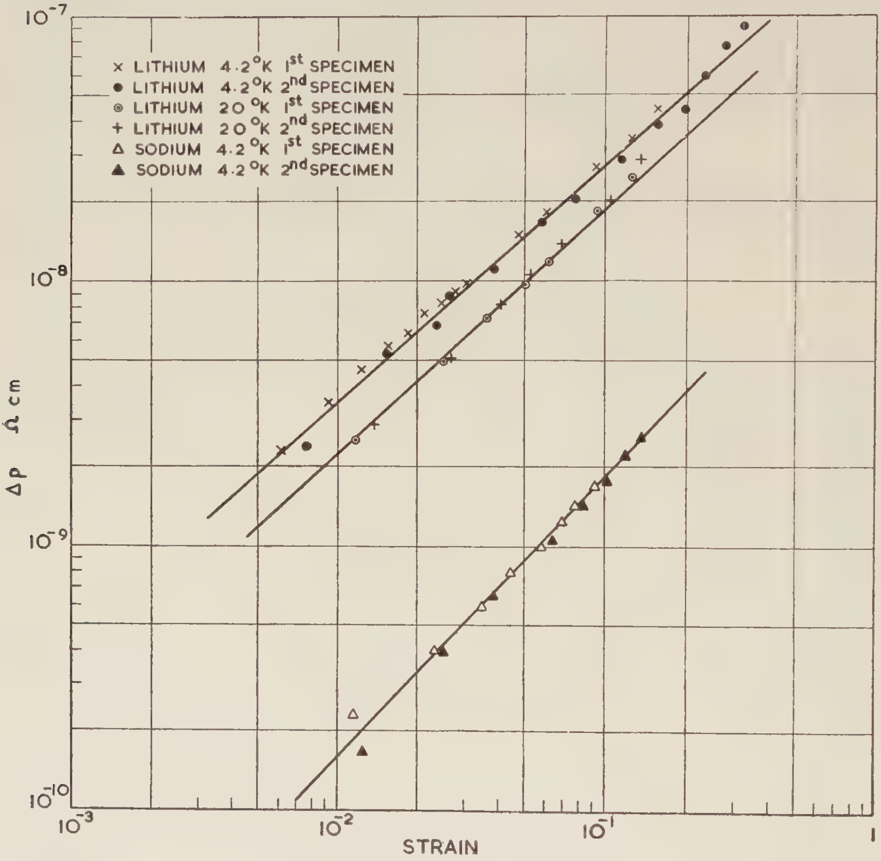

A logarithmic plot of the increase in resistivity, $\Delta\rho$ due to deformation, ϵ, against the strain for lithium at 20 and 4·2°K, and for sodium at 4·2°K. No change in resistivity could be detected when potassium was deformed at 4·2°K and only a very slight change (see discussion) when sodium was deformed at 20°K.

The ratios of the resistivities between 4·2°K and room temperature $\rho_{4\cdot2}/\rho_{RT}$ were $9{\cdot}3\times10^{-3}$ for lithium, $2{\cdot}7\times10^{-4}$ for high purity sodium, and $2{\cdot}4\times10^{-3}$ for potassium.

§ 5. Discussion

5.1. *The Tensile Tests*

The general form of the stress/strain curves can be explained in terms of the transformations which lithium and sodium undergo at low temperatures. Barrett (1948, 1955, 1956) has shown by X-ray diffraction experiments that the following transformations occur:

lithium goes from b.c.c. to h.c.p. below 72°K without cold work,
from b.c.c. or h.c.p. } to f.c.c. (faulted) if cold worked below 110°K,
sodium goes from b.c.c. to h.c.p. (faulted) below 36°K without cold work, if cold worked, below 51°K.

The X-ray data suggest that if the sodium is unworked, about 7% is transformed by 5°K. Severe cold work at 5°K transforms about 50%. Potassium remains b.c.c. down to 5°K and no transformation is observed even if it is severely cold worked at that temperature.

Thus we can take the results for potassium (fig. 4) as being typical of the b.c.c. lattice of the alkali metals. The curve for 80°K shows the general behaviour at relatively high temperatures. Beyond the yield point there is a short region of slight hardening. After this, little further hardening occurs before fracture. This is the same type of curve as is obtained in a b.c.c. transition metal beyond the region of the lower yield point. This last effect has not been detected in the alkali metals. Similar curves are shown for lithium at 293° and 195°K and for sodium at 80°K at which temperatures these metals are still b.c.c. At lower temperatures, however, these two metals transform and this is reflected in their stress/strain curves by the fact that throughout the test the metal continues to harden. The precise nature of this hardening is not yet clear. Two main possibilities suggest themselves. Firstly, a hardening due to the hold-up of dislocations at the boundaries between the phases and secondly, a hardening within the faulted phase itself.

In sodium there is a considerable difference between the 20 and 4·2°K curves. This is because the transformation temperature is relatively low and hence much less transformation product will be formed at 20 than at 4·2°K.

In lithium the transformation takes place during deformation at 80°K, as is shown by the continuous hardening during the test at that temperature. By 20°K the transformation to the h.c.p. lattice is practically complete, as is shown by the similarity of the work hardening at 20 and 4·2°K. Whilst the general form of these curves is similar to those for sodium, there is of course the very considerable difference that discontinuous yielding is only observed for lithium. In sodium the transformation on cold work is from b.c.c. to h.c.p., whereas the transformation for lithium at 20 and

4·2°K is from h.c.p. to f.c.c. It is suggested, since no serrations are observed for sodium, that the discontinuous yielding in lithium is due to a catastrophic change from h.c.p. to f.c.c.

It should be noted that a strain of a few per cent would be produced if the whole of the specimen transformed from h.c.p. to f.c.c., and whilst this would account satisfactorily for the integrated strain produced in the regions of discontinuous yielding, the large total strain must result from other forms of deformation.

The curves for potassium also show some interesting features. Whereas at 80°K very little hardening is observed, by 20°K a very long region of practically linear hardening occurs. At 4·2°K this linear hardening has become so great that it is practically indistinguishable from the elastic part of the deformation. The mechanism for such an extemely temperature dependent hardening is not yet clear and it would not seem profitable to propose one without more detailed experiments. In the transition group b.c.c. metals such hardening (if it exists) is presumably masked by the yield point effect. It should be noted that beyond the region of rapid hardening at 4·2°K a softening mechanism occurs (presumably due to the breakdown or the avoidance of dislocation barriers analogous to stage III in f.c.c. metals) so that the stress/strain curve is practically horizontal. This softening is probably the same as that which occurs in the horizontal region at 80°K and also in the higher temperature curves of sodium and lithium. Thus it seems that in a pure b.c.c. metal at low temperatures there is a region of intense hardening after the metal has yielded. As the temperature is raised this hardening rapidly decreases and at still higher temperatures it becomes so small that once the metal has yielded the hardness remains approximately constant right up to fracture. It should be noted, however, that in spite of the very large increase in hardness in potassium between 20 and 4·2°K, a comparison of the ordinate scales of figs. 2 to 4 shows that even at 4·2°K the metal is still very soft compared with sodium and lithium.

As the temperature is reduced the yield stress of all three metals increases in a similar manner to that observed in the b.c.c. transition metals. The fact that even in the transformation region of lithium and sodium the yield stress continues to rise would seem to suggest that we are measuring the yield stress of the b.c.c. phase since previous workers have shown that the yield stress of h.c.p. and f.c.c. metals is not very temperature dependent.

5.2. *The Electrical Resistivity*

The increase in the electrical resistivity during deformation at 4·2°K is usually considered to be due to three main causes: the scattering of the conduction electrons by (1) the point defects produced during the deformation, (2) the dislocations, and (3) the stacking faults if the dislocations can dissociate into partials with a ribbon of fault between them. Considerable experimental evidence is now available (e.g. Christian and Spreadborough 1956, Seeger 1956, Lomer and Rosenberg 1959) to bear out the suggestion first made by Broom (1952) that in metals in which the dislocations are able to separate into partial dislocations nearly all the extra resistivity associated with the dislocations is due to the scattering of the electrons by the stacking faults, rather than scattering by the dislocations themselves. This hypothesis is further supported by the present experiments in which no resistivity increase could be detected when potassium was deformed at 4·2°K, because stacking faults are not thought to occur in the b.c.c. lattice and hence little or no resistivity change should be expected. The fact that no resistivity change is observed would also suggest that in the b.c.c. lattice very few point defects are produced on deformation unless, for example, they are able to diffuse away at 4·2°K in potassium. This would require an activation energy of motion of very much less than 0·01 ev, which seems rather unlikely, unless a crowdion mechanism is invoked.

One cannot be certain about the cause of the resistivity increases which are detected in lithium at 20 and 4·2°K and in sodium at 4·2°K. The X-ray experiments of Barrett (1948, 1956) show that in deformed specimens the regions of h.c.p. and f.c.c. are heavily faulted and there would seem to be no doubt that in addition to point defect resistivity some of the increases must be due to the scattering of the electrons by these faults. But there is also the possibility that the electrons are scattered at the interface boundaries between the phases, or by the strain field associated with those boundaries. In actual fact it is not thought that this would be a very large effect since the area of the interface boundary will be very small compared with the area of stacking fault.

It should be noted that the resistivity change for sodium is about ten times less than that for lithium at any given strain, but that the strain dependence is very similar. This might be due to the fact that very much less of the material is transformed, particularly if we assume that there is no contribution to the deformation resistivity from the b.c.c. parts of the specimen. (Barrett only got a 50% transformation and his method of cold work was much more drastic than ours.) Another possibility is that the stacking fault probability might be much greater in f.c.c. lithium than in h.c.p. sodium.

The resistivity measurements taken when sodium was deformed at 20°K are rather interesting. It will be recalled that there seemed to be very little change in the resistivity when the specimen was extended but that after it had been warmed up to 80°K and then re-cooled to 20°K the resistivity increased. A tentative explanation of this behaviour can be given in the light of the recent work by Gugan and Dugdale (1958) on the change in the resistivity of sodium when it transforms. The resistivity of a metal can be divided into two parts. The first is the residual resistivity, ρ_0, produced by the scattering of the electrons by the static defects in the specimen and which accounts for practically the whole of the resistivity which is measured at 4·2°K. This is the resistivity with which this discussion has so far been concerned. There is also the resistivity ρ_i, caused by the scattering of the electrons by the lattice vibrations. This decreases rapidly as the temperature is lowered but at 20°K, in our sodium specimens, it still accounted for about 90% of the total resistance of the specimen. Gugan and Dugdale have shown that the value of ρ_i for the h.c.p. phase of sodium is considerably less than that for the b.c.c. phase at the same temperature. Now as we deform sodium at 20°K we transform more of the metal to the h.c.p. phase and hence we tend to decrease the value of ρ_i. At the same time, however, we introduce dislocations and possibly other types of defect which will increase ρ_0. By chance these two effects practically cancel one another out, hence giving the impression that no resistivity changes are occurring. As has already been stated the results actually show that during the first few per cent of strain the total resistivity decreases very slightly and thereafter it begins to increase again so that an exact cancellation of the two effects does not occur.

When the specimen is now warmed up to 80°K a great deal of this extra h.c.p. phase, which was introduced by the deformation, reverts to b.c.c. and even when we re-cool to 20°K again, whilst some will transform back to h.c.p., there will be very much less of that phase present than before we warmed up. Hence the resistivity will increase and this is what is observed. The magnitude of this increase, $\Delta\rho'$, will be approximately equal to the decrease in the resistivity due to the change to the h.c.p. phase during the original deformation. Since as has been explained this decrease in resistivity must be approximately equal to the increase in resistivity due to dislocations and other defects we can get a measure of this increase from the value of $\Delta\rho'$.

Some support for this argument is obtained when we look at the values of $\Delta\rho'$ which were obtained. Three runs in which strains of 0·16, 0·13 and 0·12 were introduced at 20°K gave values of $\Delta\rho'$ on warming to 80°K and then re-cooling to 20°K of 1·1, 2·2 and 3×10^{-9} ohm cm respectively. These figures are of the same order of magnitude as the extra resistivity introduced when sodium is strained at 4·2°K by these amounts. At 4·2°K we assume that the resistivity changes observed are due only to the defects produced by the deformation. The fact that one does get this rough agreement between these two sets of results suggests that a considerable part of the resistivity increase produced by deformation at 4·2°K must be due to dislocations rather than to point defects, because otherwise $\Delta\rho'$, after warming to 80°K, would be reduced by the annealing out of point defects at that temperature.

Nevertheless, some of the resistivity increase might be ascribed to point defects which are produced during the deformation and in this connection we should point out that when copper is deformed at low temperatures the corresponding values for the parameters A and n are about $5{\cdot}5 \times 10^{-8}$ and 1·3 to 1·5 respectively, i.e. $\Delta\rho$ is about twice that observed in our sodium specimens. Of this resistivity change about half can be ascribed to point defect scattering (see for example van Bueren 1955). This gives the order of magnitude which might be expected but it is obvious that the complications of the phase changes in the present case are such that any more detailed comparison would be pointless.

The resistivity changes in lithium at 20°K were about 30% less than those at 4·2°K. This reduction might also be due to a decrease in the value of ρ_i for the transformed phases of lithium. Since the Debye θ of lithium is much higher than that of sodium only a few per cent of the resistivity at 20°K will be due to ρ_i, but it is conceivable that the change in ρ_i might be large enough to give the difference between the results at 20 and 4·2°K which is observed.

ACKNOWLEDGMENTS

We should like to thank Mr. G. W. Horsley of A.E.R.E., Harwell, for supplying the high purity metals and Mr. J. Lamming for assistance in constructing the apparatus and in taking some of the measurements. We are also grateful to Dr. F. J. Bradshaw, Professor F. C. Frank, F.R.S., and Dr. J. W. Christian for most useful consultation. This work which was carried out at the Clarendon Laboratory formed part of a joint programme of research between the Laboratory and the Metallurgy Division of A.E.R.E., Harwell.

REFERENCES

ADAMS, M. A., 1958 (to be published).
BARRETT, C. S., 1948, *Phys. Rev.*, **72,** 245 ; 1955, *J. Inst. Met.*, **84,** 43 ; 1956, *Acta Cryst.*, **9,** 671.
BROOM, T., 1952, *Proc. phys. Soc.* B, **65,** 871.
CHRSITIAN, J. W., and SPREADBOROUGH, J., 1956, *Phil. Mag.*, **1,** 1069.
GUGAN, D., and DUGDALE, J. S., 1958, *Canad. J. Phys.*, **36,** 1248.
LOMER, J. N., and ROSENBERG, H. M., 1959, *Phil. Mag.* (in the press).
SEEGER, A., 1956, *Canad. J. Phys.*, **34,** 1219.
VAN BUEREN, H. G., 1955, *Acta Met.*, **3,** 519.

The Preparation of Smooth Single Crystal Surfaces of Silver by an Evaporation Technique†

By D. W. Pashley‡
Physics Department, Imperial College, London, S.W.7

[Received September 16, 1958]

Abstract

An electron diffraction study has been made of the growth of evaporated silver layers on cleaved mica surfaces, with the substrate at various temperatures during the deposition. It is shown that good orientation (epitaxy) occurs over a wide range of temperatures, but that the nature of the orientation depends upon both the substrate temperature and the film thickness. Under certain conditions of preparation it is found that the surface of the silver deposit is very smooth on an atomic scale. These surfaces are of value as substrates for other experiments, both on epitaxy and on specimen preparation for high resolution electron microscopy of metals, and examples of these applications are quoted.

§ 1. Introduction

Detailed studies of the oriented growth of thin surface deposits in single crystal substrates (epitaxy) require the use of substrate surfaces which are very smooth on an atomic scale. Systematic work (for a general review see Pashley (1956)) has been carried out with cleavage surfaces as substrates, but when metal single crystal substrates are required, cleavage is rarely possible. Electropolished surfaces may be prepared on metallic single crystals, but these are usually quite undulating (Kranert *et al.* 1944), and not always suitable as substrates. Several years ago the author developed a method of preparing good smooth single crystal surfaces of silver by evaporation on to mica, following upon earlier work by Rudiger (1937) and Tull (1951). These surfaces have since been used for a number of different experiments on epitaxy (Newman and Pashley 1955, Kehoe *et al.* 1956 a, b, Newman 1957, Mason 1958, Grunbaum 1958, Grunbaum *et al.* 1958). Further, the silver substrates have also been used as the first stage in the preparation of detached single crystal films of gold and other metals for use as specimens in high resolution microscopy (Pashley 1959, Pashley *et al.* 1957, Bassett *et al.* 1958).

Since no detailed account of the technique of preparing the silver surfaces has been published to date, the investigations which resulted in the determination of the optimum preparation conditions are presented in this paper. The work consists of an investigation by reflection electron diffraction of the structure of layers of silver evaporated on to a mica cleavage surface under a variety of conditions. Rudiger (1937) was the first to show that a good single crystal orientation of silver may be obtained on mica, and Tull (1951) prepared such layers which were also quite smooth on an atomic scale (see, however, § 4).

---

† Communicated by the Author.

‡ Present address: Tube Investments Research Laboratories, Hinxton Hall, Cambridge.

§ 2. THE EVAPORATION TECHNIQUE

Preliminary investigations were carried out by heating pieces of freshly cleaved mica inside a small porcelain tube surrounded by an electric heater, and depositing various thicknesses of silver at different substrate temperatures, inside a standard type of evaporating plant. It was immediately established that good orientation of the silver could be obtained, and that the perfection of the orientation and the smoothness of the substrate surface depended upon substrate temperature, rate of deposition and deposit thickness. An arrangement which allowed these parameters to be controlled was therefore constructed.

The mica substrates were placed on a hotplate consisting of a composite cylindrical copper block, heated by an internal nichrome winding, and supported on three quartz pillars. The temperature of the hotplate was measured by a copper-constantan thermocouple embedded in its surface. Once thermal equilibrium is established, the temperature of the mica surface should be within one degree centigrade of this temperature. The silver was deposited from a heated tungsten spiral. With this arrangement it was found initially that only very imperfect orientation could be obtained, and this became worse as the substrate temperature was raised. It was established that the cause of the discrepancy arose from the distillation of low melting point impurity metals from the copper block, which was of commercial impurity only. Mica specimens were heated on the hotplate and then examined by reflection electron diffraction without any silver layer being deposited. It was found that small amounts (probably less than 10 Å in average thickness) of two substances had deposited on the mica surface. These substances gave bright and clear diffraction patterns consistent with the two alloys SnAs and SnTe, which have structures of the rocksalt type and lattice constants of 5·68 Å and 6·29 Å respectively. Both alloys were very well oriented as follows:

$$(111) \text{ alloy parallel to mica } (001),$$
$$\text{with } [1\bar{1}0] \text{ and } [\bar{1}10] \text{ alloy parallel to mica } [100].$$

The occurrence of the metals Sn, As and Te as impurities seems quite likely, since such metals are sometimes added to improve machining properties. Clearly the presence of these thin alloy deposits was affecting the subsequent growth of the silver deposits. To overcome this difficulty, a second hotplate was constructed of 'specpure' copper, with a nominal purity of better than 99·999%. This gave results which were always consistent, good orientation being obtained under the appropriate conditions. Attempts to construct a furnace of electrolytic copper resulted in the formation of films with poor orientation. Although no impurity deposits could be detected in this case, it is presumed that very small amounts did occur, and influence the growth of the silver deposit.

It was found also that even with the furnace constructed of specpure copper, the surface smoothness could not be reliably controlled unless certain further precautions were taken. It was necessary to minimize the effect of the radiant heat from the tungsten spiral, which caused rises in the surface temperature of the silver film during preparation. This was carried out by using suitable shields, the final arrangement being shown in fig. 1. The evaporating distance was about 12 cm and the vacuum was better than 10^{-4} mm Hg. This gave good reproducible results in all respects. The specimens were always prepared in a separate evaporating plant and transferred to an electron diffraction camera for examination.

Fig. 1

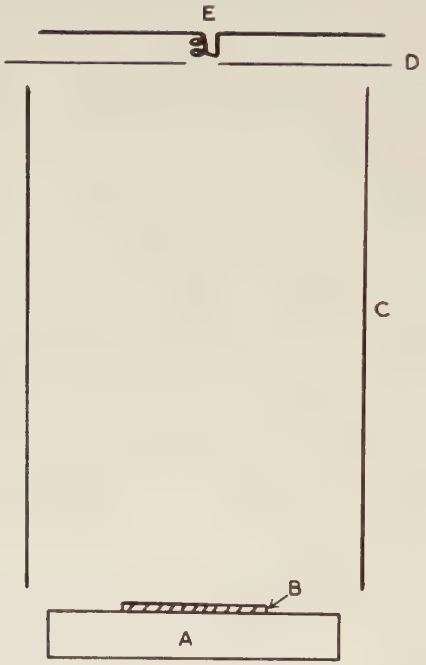

The arrangement for specimen preparation. A is the furnace; B is the specimen; C is a cylindrical aluminium shield coated internally with graphite; D is a flat shield with an aperture through which the silver passes; E is the tungsten spiral from which the silver is evaporated.

§ 3. Experimental Observations

3.1. *The Effect of Substrate Temperature*

Preliminary experiments indicated that thicknesses greater than a few hundred ångströms are required for good surface smoothness and coherence of deposit. Thus a series of specimens of about 1000 Å in thickness was prepared, at various substrate temperatures from 20°c to 500°c. The results are summarized in the table, and illustrated by the photos of figs. 2 to 4 (Pl. 43), the interpretation of which is indicated in fig. (5). The orientation referred to as single positioning is

$$\left.\begin{array}{ll}(111) & \text{Ag parallel to (001) mica cleavage,}\\ {[1\bar{1}0]} & \text{Ag parallel to [010] mica.}\end{array}\right\} \quad . \quad . \quad . \quad (1)$$

Furnace temp. (°c)	Random orientation	Single positioning	Double positioning	{111} twinning	Crystal size	Degree of surface smoothness
20	S	N	S	S	Very small	N
40	M	N	S	S	Very small	N
60	W	N	S	S	Very small	W
75	VW	N	S	S	Small	M
90	N	N	S	W	Small	M
250–300	N	S	VW	N	Very large	Complete
500	N	—	S	S	Very large	N

S = strong, M = medium, W = weak, VW = very weak, N = none.

For double positioning, the following orientation occurs also.

$$\left.\begin{array}{ll}(111) & \text{Ag parallel to (001) mica cleavage,}\\ {[\bar{1}10]} & \text{Ag parallel to [010] mica.}\end{array}\right\} \quad . \quad . \quad . \quad (2)$$

Twinning was prominent in many cases, and occurred on all of the {111} planes. As the substrate temperature is increased the orientation gradually improves, the twinning becomes less prominent, the crystal size increases and the surface becomes smoother, until at 250–300°c a good single crystal orientation without twinning or double positioning occurs, and the surface of the film is very smooth. Above the substrate temperature of 300°c the surface structure gradually changes again. In particular the surface is no longer smooth, and prominent twinning reappears.

3.2. *The Effect of Film Thickness*

The influence of the film thickness on the structure of the deposit has been investigated with the substrate temperature at its optimum value of about 275°C. In the very early stages the deposit consists of small isolated nuclei of a few tens of ångströms in linear dimensions. Many are oriented in the usual way, but some are randomly oriented, and prominent twinning on all {111} planes occurs also. Figure 6 (Pl. 43) shows the diffraction pattern obtained from a deposit of 50 Å. Diffuse rings appear also at earlier stages. As the thickness is increased, the orientation becomes more perfect and the rings disappear from the diffraction pattern. The spots sharpen laterally, and elongate perpendicular to the shadow edge. At a thickness of about 200 Å the diffraction pattern is similar to that of fig. 3. Further increases in thickness produce a continuation of these trends, together with a gradual weakening of the diffraction spots due to twinning. The twinning at the surface disappears completely at a thickness of about 500 Å. At a thickness of 1000 Å the smooth well-oriented surface described above is obtained.

Fig. 5

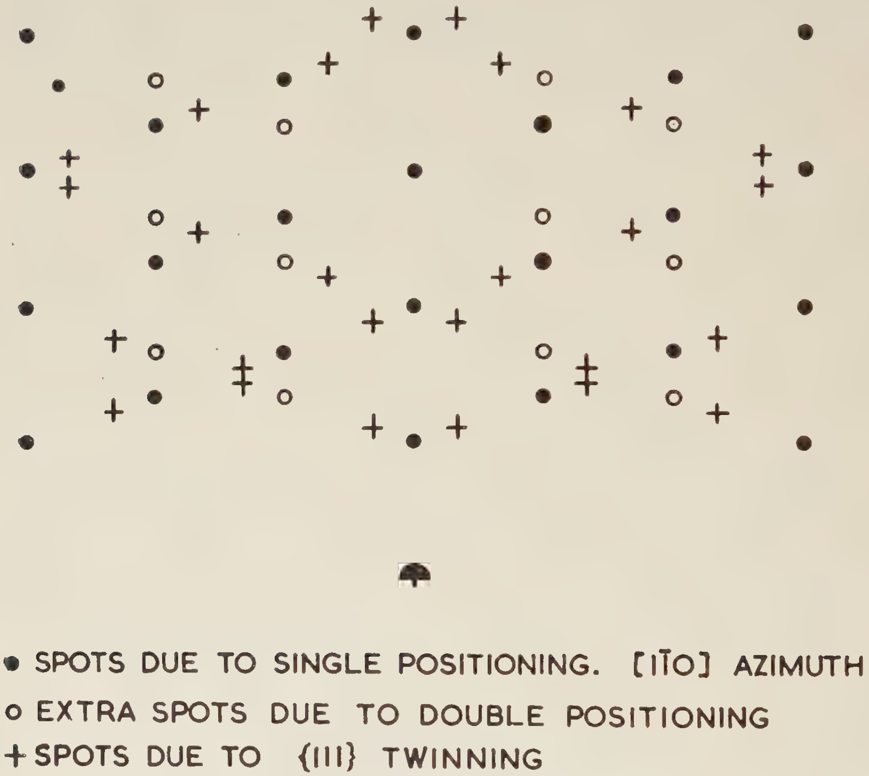
● SPOTS DUE TO SINGLE POSITIONING. [11̄0] AZIMUTH
○ EXTRA SPOTS DUE TO DOUBLE POSITIONING
+ SPOTS DUE TO {111} TWINNING

The interpretation of figs. 2, 3, 4 and 6.

A further technique which has been used to study the silver films is that of high-angle Kikuchi lines (Alam *et al.* 1954). The high-angle Kikuchi patterns may be obtained with a much larger glancing angle of incidence for the electrons, and the depth of penetration is correspondingly larger. By means of the technique the single and double positioning are more easily distinguished than from a pattern such as that of fig. 4. It was confirmed that with a substrate temperature of 250–300°c complete single positioning does occur at a thickness of 1000 Å. However, even with thinner deposits, which were partly doubly positioned according to the conventional reflection diffraction pattern, prominent single positioning was indicated by the high-angle Kikuchi patterns. This demonstrates that the double positioning occurs mainly in the surface layers, and not throughout the depth of the deposit. Figure 7 (Pl. 44) shows a high-angle Kikuchi pattern from a 1000 Å layer deposited at 270°c. In addition to indicating the complete single positioning of the silver, the sharpness of the pattern also indicates the high degree of perfection of the orientation.

3.3. *The Rate of Deposition*

Since this work is concerned with the preparation of films of at least several hundred ångströms in thickness, slow rates of deposition lead to a long time of evaporation, with the result that large increases in the surface temperature of the silver surface occur due to radiant heat from the evaporation source. This affects, in particular, the surface smoothness of the deposit. A deposition rate of approximately 500 Å/min has therefore been used in all this work.

§ 4. SUMMARY AND DISCUSSION

It has been established that over a wide temperature range silver is well oriented on a mica cleavage surface in the orientations given in § 3. This is consistent with the work of Tull (1951), but does not agree well with that of Rudiger (1937) and Thirsk (1950), who found other orientations also. In view of the stringent conditions found in the present experiments (see § 2) concerning the need for cleanliness of the substrate during the deposition, it is concluded that the results of Rudiger and Thirsk were affected by slight traces of impurity. The consistent results obtained for the structure of the deposit grown as described in § 2, in at least three different pieces of apparatus over a period of several years, supports the view that the orientation described above is the one characteristic of a clean mica substrate. This orientation has a fairly good fit, as illustrated in fig. 8. Along the mica [100] the misfit is -4%, and is the same along the mica [010], if a fit of three silver atom distances with the corresponding mica distance is considered.

The surfaces obtained with a substrate temperature of about 270°c reflect as a good optical mirror, in contrast with those obtained by Tull (1951), which were somewhat dull in appearance. The exact conditions under which Tull's specimens were prepared were not specified, so that no direct correlation is possible. It is deduced that a substrate temperature of greater than 300°c was used. Although the surfaces were not optically smooth, they appeared smooth according to the electron diffraction evidence, as indicated by the extent to which refraction of the electrons occurred at the surface. Tull was able to measure the inner potential for silver as 23 volts. The main requirement for this type of measurement is that the surface is atomically smooth over areas of linear dimension of about a few hundred ångströms. Thus irregularities such as steps, pits, etc. may be present, but must be greater than about 1000 Å apart. Such surface irregularities could, of course, affect the optical reflectivity. It is deduced that the surfaces obtained by depositing 1000 Å of silver at a substrate temperature of 250–300°c as described in §2 are more generally smooth than those prepared by Tull. No accurate inner potential measurements were made on these specimens, but it was confirmed that the refractive effect was consistent with a value of about 20 volts. The surfaces are therefore considered to be smooth to near atomic dimensions over areas of at least about 1000 Å in linear dimension. Various kinds of irregularity might be present within this limitation, but these are not sufficient to affect the optical reflectivity appreciably.

Fig. 8

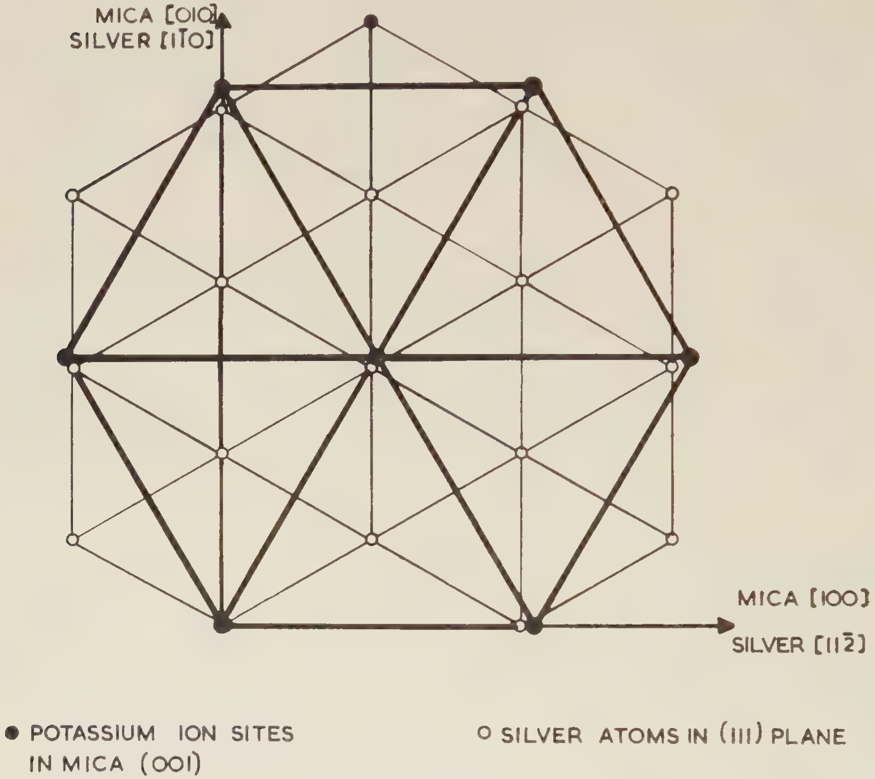
MICA [010]
SILVER [1$\bar{1}$0]
MICA [100]
SILVER [11$\bar{2}$]
● POTASSIUM ION SITES IN MICA (001)
○ SILVER ATOMS IN (111) PLANE

The fit of the main silver orientation on mica.

The value of the (111) silver surfaces as substrates for other experiments has been demonstrated by the applications quoted in § 1. In addition to these applications, the author has studied the growth of silver bromide and silver chloride on the silver surfaces, by direct chemical attack with halogen vapour. The orientations found are those expected for growth on a smooth (111) surface, as previously determined (Pashley 1952), and no evidence for any growth on a facet oblique to the surface was obtained. This result was checked with the high-angle Kikuchi patterns, as well as by conventional reflection diffraction. Thus there was no possibility of any appreciable amount of halide growing in another orientation, and in a place on the surface not accessible for diffraction by the conventional technique. From this evidence it is deduced that no facets of appreciable size and number exist oblique to the surface.

It is interesting to note that the perfection of orientation improves as the thickness of the film is increased. Two explanations are possible. Either the well-oriented nuclei grow faster, and gradually predominate as the film is made thicker, or the well-oriented nuclei grow at the expense of the badly oriented nuclei (including randomly oriented and twinned nuclei), so that a ‘recrystallization’ of the film occurs as it is made thicker. The possibility of the latter mechanism is supported by the fact that if a 1000 Å film is deposited at room temperature, when it is very poorly oriented (see table), a subsequent anneal at 300°c produces a well-oriented film.

ACKNOWLEDGMENTS

I wish to thank Dr. M. Blackman for his interest in this work, which was carried out partly during the tenure of a Senior Research Award of the Department of Scientific and Industrial Research, and partly during the tenure of an Imperial Chemical Industries Research Fellowship in the University of London.

REFERENCES

ALAM, N., BLACKMAN, M., and PASHLEY, D. W., 1954, *Proc. roy. Soc.* A, **221,** 224.
BASSETT, G. A., MENTER, J. W., and PASHLEY, D. W., 1958, *Proc. roy. Soc.* A, **246,** 345.
GRUNBAUM, E., 1958, *Proc. phys. Soc.*, **72,** 459.
GRUNBAUM, E., NEWMAN, R. C., and PASHLEY, D. W., 1958, *Phil. Mag.*, **3,** 1337.
KEHOE, R. B., NEWMAN, R. C., and PASHLEY, D. W., 1956 a, *Brit. J. appl. Phys.*, **7,** 29; 1956 b, *Phil. Mag.*, **1,** 783.
KRANERT, W., LEISE, K. H., and RAETHER, H., 1944, *Z. Phys.*, **122,** 248.
MASON, B. J., 1958, *Advanc. Phys.*, **7,** 235.
NEWMAN, R. C., 1957, *Phil. Mag.*, **2,** 750.
NEWMAN, R. C., and PASHLEY, D. W., 1955, *Phil. Mag.*, **46,** 927.
PASHLEY, D. W., 1952, *Proc. roy. Soc.* A, **210,** 355; 1956, *Advanc. Phys.*, **5,** 173; 1959, *Phil. Mag.*, **4,** 324.
PASHLEY, D. W., MENTER, J. W., and BASSETT, G. A., 1957, *Nature, Lond.*, **179,** 752.
RUDIGER, O., 1937, *Ann. Phys.*, **30,** 505.
THIRSK, F. R., 1950, *Proc. phys. Soc.*, B, **63,** 833.
TULL, V. F. G., 1951, *Proc. roy. Soc.* A, **206,** 219.

The Observation of Dislocations in Thin Single Crystal Films of Gold Prepared by Evaporation†

By D. W. Pashley
Tube Investments Research Laboratories, Hinxton Hall, Cambridge

[Received September 16, 1958]

Abstract

An evaporation technique has been developed to allow thin (approx. 200 Å thick) detached single crystal films of gold to be prepared. These films are very coherent and uniform in thickness. Dislocation lines are observed in these films with a density of 10^{10}–10^{11}/cm^2. The dislocations may be observed to move inside the electron microscope. A prominent feature of the movement is the occurrence of wide ribbons of stacking fault due to the splitting of a dislocation in to two partial dislocations. Cross-slip is observed also.

Annealing of the films has produced some regular arrays of dislocations, including hexagonal networks and arrays at low angle boundaries.

Small loops are also found in some of the films and are interpreted as dislocation loops resulting from the collapse of discs of vacancies.

§ 1. Introduction

The application of transmission electron microscopy to the direct study of the microstructure of metals is largely limited by the techniques available for preparing suitable thin specimens. Various methods have been employed. Beaten gold foil (approx. 1000 Å thick) may be examined directly or after further thinning by a chemical etchant (Hirsch *et al.* 1955). Chemical thinning of a thicker beaten foil (0·5 μ aluminium) is also possible (Hirsch *et al.* 1956). Heidenreich (1949) used an electro-polishing technique for thinning aluminium, and this has been extended and improved by Bollmann (1956) and Tomlinson (1958) to allow a variety of metals to be thinned. Nicholson *et al.* (1958) have used the electro-polishing technique to thin aluminium alloys.

Thinning can also be carried out by ionic bombardment (Castaing 1955) and thin sections of metals may be cut by means of an ultra-microtome (Haanstra 1955, Fernandez-Moran 1956). Thin films which are suitable for transmission electron microscopy can be prepared directly by electrodeposition (Weil and Read 1950, Reimer 1956).

All of these methods provide specimens which are either non-uniform in thickness locally, or which are of a uniform thickness over only quite small areas. Since the author has been concerned with carrying out experiments on controlled deformation of metal films inside the electron microscope (this work will be reported in a later paper), it seemed desirable to produce films which are uniform in thickness over reasonably large areas. For this reason the preparation of thin metallic films by means of evaporation techniques has been investigated. A further advantage of the evaporation technique is that it is possible, by using single crystal substrates, to produce oriented ‘single crystal’ films.

---

† Communicated by the Author.

Often, evaporated films of metals of only a few hundred ångströms or less in thickness are quite granular in structure, and not very continuous or homogeneous. An improvement in continuity may be obtained by the use of thicker films, but this is often undesirable because the electron transmission is then poor. Most attempts at making thin detached films by evaporation techniques (see for example Raether 1952, Ogawa and Watanabe 1954) have involved the use of non-metallic substrates, particularly alkali halides. This paper describes a technique involving the use of metallic substrates which are themselves produced by evaporation (Pashley 1959). Good coherent single crystal films of gold are obtained, and dislocations and their movement are observed in these films.

§ 2. THE PREPARATION AND STRUCTURE OF THE FILMS

The main difficulty in the use of metallic substrates concerns the surface preparation. Electro-polishing is a possible method, but this normally produces a wavy surface, and it would be difficult to avoid small amounts of local surface contamination which might cause gross imperfections in the films (see, however, Brame and Evans 1958). It seemed more promising to prepare the initial surface by an evaporation technique, since this may be carried out conveniently for the case of a (111) silver surface (see previous paper). Such a surface is very smooth on an atomic scale, and is an ideal substrate for gold since the misfit for parallel orientation is only 0·2%. Also, the gold film is readily detached by dissolving the silver in nitric acid.

It is found that (111) gold films of 150 Å and upwards in thickness may be prepared in this way. The deposition of the silver and gold is carried out in quick succession by means of two evaporation sources built in to a standard evaporation unit. The substrate is heated to about 270°C during both depositions, by being placed on a small hotplate constructed of ‘specpure’ silver with mica as an insulating material and pure molybdenum wire as a heater. The results described in this paper were obtained with gold films of approximately 200 Å in thickness. The films are good single crystals over large areas (many mm^2), as indicated by transmission electron diffraction patterns. Examination in the electron microscope (Siemens Elmiskop I) indicates that the films are coherent and non-granular. When the films are stripped and mounted on a supporting grid by lifting from the surface of water, local buckling occurs. This leads to prominent extinction contours on the image.

An extreme case of local bending is shown in fig. 1 (Pl. 45), where complex contours are visible. Similar contours have been obtained previously with lead iodide (Mollenstedt 1953) and mica (Rang 1953 a, b) and have been attributed to the occurrence of bubbles in the films, as shown in fig. 2 (*a*). With the gold films the effect may be explained as due to the presence of small 'dimpled regions' in the film, as illustrated in fig. 2 (*b*). These would arise if the silver and gold is deposited on the surface of mica which contains the bubble-like features shown in fig. 2 (*a*). It is assumed that the lattice is elastically strained so that the [111] axis is always perpendicular to the local plane of the film. The contours obtained represent the loci of points in the film which are diffracting in the same way; i.e. regions for which the same reciprocal lattice point is intersected by the sphere of reflection. On this basis, the effect of a dimpled region approximated to the shape $H = Ae^{-\alpha r^2}$ (see fig. 3 (*a*)) has been calculated, and the resulting contour pattern is shown in fig. 3 (*b*), for the case of the electron beam directed along the normal to the general film plate. The parameters A and α were chosen such that the maximum slope dH/dr is 0·08 radians at a value of $r = 0{\cdot}16\,\mu$ (see fig. 3 (*a*)). The radius of the dimpled region is then a few tenths of a micron, and the value of H at $r = 0$ is 210 Å. The resulting contour pattern shown in fig. 3 (*b*) is symmetrical, whereas the features shown in fig. 1 are not. This is because the beam is not exactly perpendicular to the general film plane. If a tilt of only 0·05 radians is allowed for, the contour pattern takes the form of fig. 3 (*c*). This is asymmetrical in a manner similar to that of the features shown in fig. 1. The calculated example is intended only as an illustration of the main features of the contour patterns from the dimpled regions, particularly the effect of tilting. No attempt has been made to calculate in any detail

Fig. 2

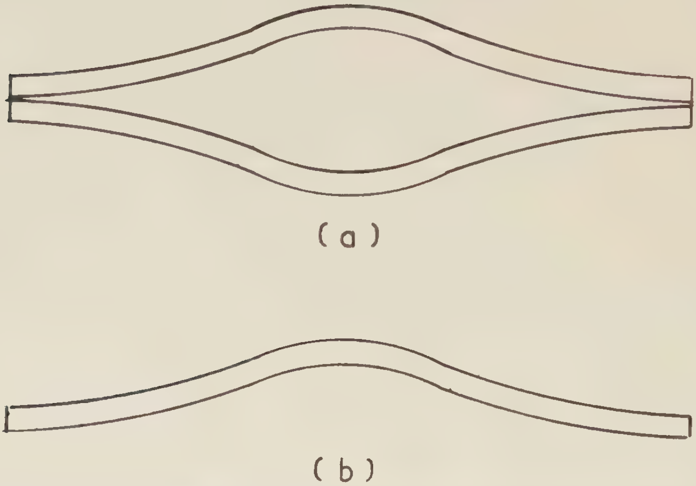

(*a*) The type of bubble observed in a thin film of lead (Mollenstedt 1953) and in mica (Rang 1953 a, b).

(*b*) Dimpled region occurring in a gold film.

Fig. 3

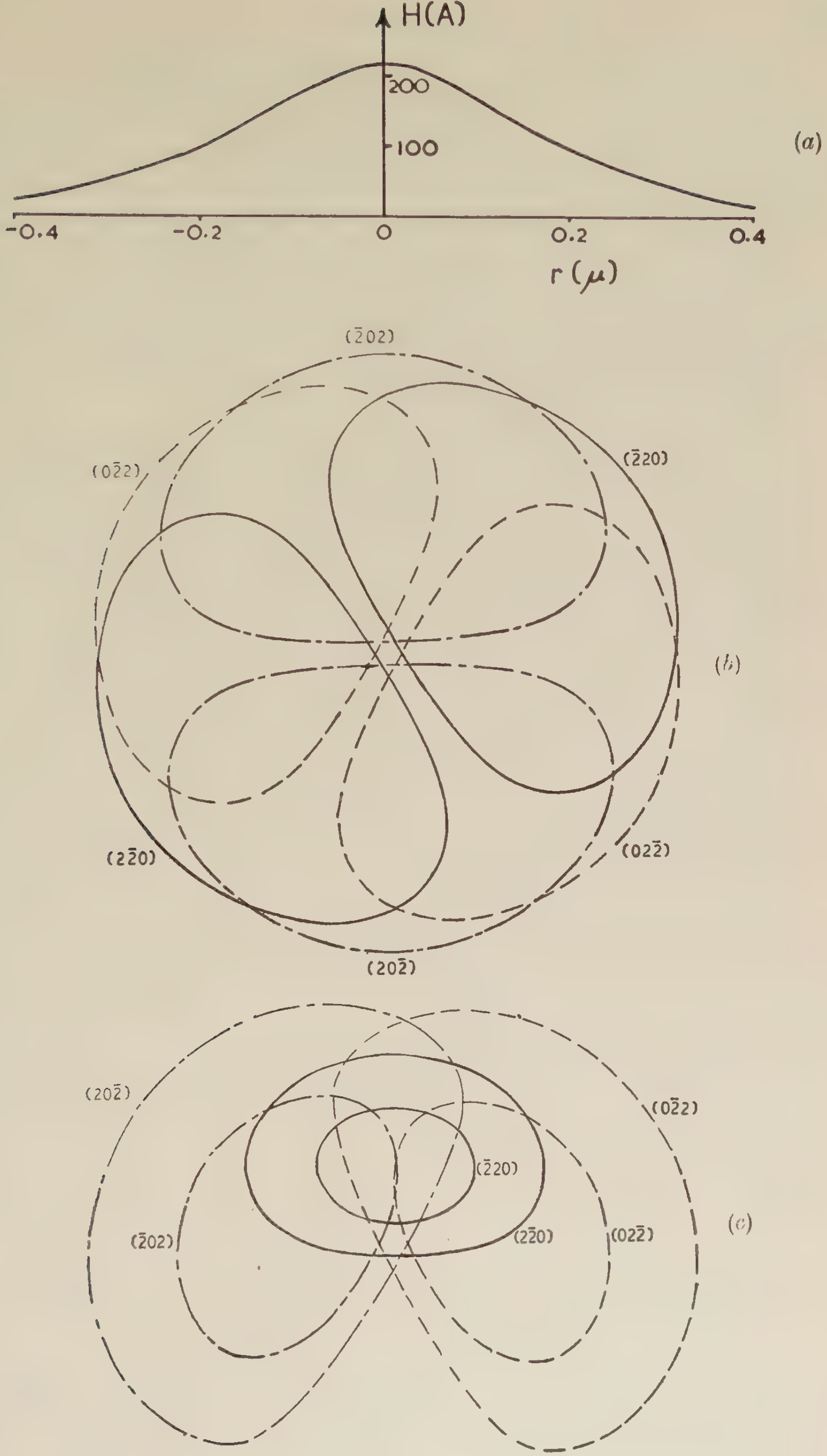

(*a*) The shape of the dimpled region used for calculating the extinction contour patterns of figs. 3 (*b*) and (*c*).

(*b*) The $\{20\bar{2}\}$ extinction contours for the beam perpendicular to the general film plane.

(*c*) The $\{20\bar{2}\}$ extinction contours for the beam rotated by 0·05 radians about $[11\bar{2}]$ with respect to the orientation of (*b*).

the exact shape of the film corresponding to the contours of fig. 1. A method for doing this has been given by Rang (1953 a).

The use of mica as the initial substrate provides single crystal gold films with their (111) planes parallel to the film plane. Attempts have been made to produce films in (100) orientation, by using rocksalt in place of the mica, and retaining the intermediate silver layer of about 2000 Å. This technique produces gold films which are uniform, continuous and well oriented, but they contain many grown-in twins, as shown both by transmission diffraction and by microscopy (see fig. 4 (Pl. 45)). Occasionally areas of 0·1 mm dimension may be prepared free of twins, but no control of this behaviour has been obtained.

§ 3. THE OBSERVATION OF DISLOCATIONS AND THEIR MOVEMENT

Dislocations in the gold films may be observed by diffraction contrast, following the technique first used by Hirsch *et al.* (1956) and Bollmann (1956). The dislocations are formed in the specimens during the growth process. All the observed dislocations lie in the $(11\bar{1})$, $(1\bar{1}1)$ and $(\bar{1}11)$ slip planes which make angles of 70·5° with the plane of the film, so that the projected width of the slip plane projected on to (111) is given by $t \cot 70{\cdot}5°$, where t is the thickness of the film. With $t \sim 200$ Å, the projected width is only about 70 Å. The $(11\bar{1})$, $(1\bar{1}1)$ and $(\bar{1}11)$ slip planes intersect (111) along $[1\bar{1}0]$, $[10\bar{1}]$ and $[01\bar{1}]$, which are three directions at 60° to one another. The dislocations pass from top to bottom of the film, and tend to assume their shortest possible length within the slip plane. Their distribution throughout the area of the film appears to be random. Dislocation lines running approximately parallel to the film plane are not observed. The projected length of the dislocation lines is very short (also about 70 Å), and in most cases the dislocations appear as dots on the electron microscope image, usually black (on a positive print), sometimes white and sometimes black-white in character. The white dots appear only in regions which are diffracting strongly, i.e. in an extinction contour. The visibility or contrast of a dislocation varies with the general diffraction conditions in the immediate vicinity of the dislocation, and is often quite low. The dislocations in the (111) films are more readily detected as they move (see below).

Dislocations are more easy to detect unambiguously in the (100) gold films, partly because of the more favourable geometry. The four {111} planes make angles of 54·8° with the (100) film plane, and the projected width of the slip plane for a film of 200 Å in thickness is approximately 140 Å. The dislocations appear on the images as short lines, with pronounced intensity maxima at the two ends (see fig. 4). Because of the greater ease of detection, it is possible to make a reliable estimate of the dislocation density in the (100) films. A value of 10^{10}–$10^{11}/\mathrm{cm}^2$ is obtained, in good agreement with the estimates of $10^{11}/\mathrm{cm}^2$ made on the (111) gold films by means of moiré patterns (Bassett *et al.* 1958).

In addition to the dislocations described above, a number of the (111) specimens has contained a high density of small loops (see fig. 5 (Pl. 45)). These are very similar to the dislocation loops recently observed by Hirsch *et al.* (1958) in quenched aluminium, and often have the appearance of double lines (see A, fig. 5) as frequently observed by Hirsch *et al.* (see their §3.1). The loops are always less than 100 Å in diameter, the smallest distinguishable loop being about 30 Å across. No control of the preparation of specimens containing the loops has been obtained. Because the appearance of the loops is very similar to that of the loops observed by Hirsch *et al.*, it is assumed that they are dislocation loops of the same kind, i.e. they arise from collapsed discs of vacancies in which a Shockley partial is nucleated so that a prismatic $\frac{1}{2}[110]$ dislocation is produced (Read 1953). Presumably large numbers of vacancies become built into the lattice during the deposition process. In these circumstances the formation of the loops might well depend upon the rates of deposition at various stages of the growth. This factor is not well controlled in the present experiments, and requires further investigation.

The dislocations observed in the gold films may be caused to move by use of an intense and localized illuminating electron beam, as obtained with the double condenser lens of the Siemens Elmiskop I. Dislocation movement induced in this way has already been observed by Hirsh *et al.* (1956, 1957) with aluminium films and Whelan *et al.* (1957) with films of stainless steel. The detailed mechanism which causes the motion is not clear, but it is assumed that the main effect arises from the compressive stresses which occur in the plane of the film, as a result of the extremely localized heating by the incident electrons. There is a remarkable influence of the time of electron bombardment on the behaviour of the specimen. When an area is first examined at high local illumination, no marked dislocation movement is observed, until that particular area has been illuminated for a period of about one minute, after which pronounced dislocation movement is usually observed. This induction period does not arise because a finite time is required for a certain temperature to be reached, since the illumination may be removed from the particular area for a period of two or three minutes, and pronounced dislocation movement occurs immediately the illumination is restored. Apparently the dislocations are in some way locked in the film as prepared, and intense localized electron bombardment results in the unlocking of the dislocations. Alternatively the formation of a carbon contamination film may be in some way responsible, although deposition of a thin carbon film on each side of the specimen before observation by the method described by Bradley (1954) causes no change in the general behaviour of the specimen. In both cases, the detailed mechanism is obscure.

Various kinds of motion of the dislocation lines are observed:

(1) A wandering and extremely slow ($< 10^{-5}$ cm/sec) motion not confined to any particular slip plane; these are presumably screw dislocations.

(2) A faster and sudden motion confined to one well-defined slip plane; this motion results in the formation of a slip trace, as observed by Hirsch *et al.* (1956), which fades after a period of about 10–20 sec.

(3) Motion as indicated in (2) except that single and multiple cross-slip occurs.

(4) The sudden splitting of a dislocation into two partial dislocations, with the production of a wide ribbon of stacking faults.

In addition, the dislocation loops such as shown in fig. 5 sometimes disappear suddenly during observation, and sometimes appear equally suddenly. No details of their motion have been observed. Hirsch *et al.* (1958) have given details in the case of the movement of loops in aluminium.

Fig. 7

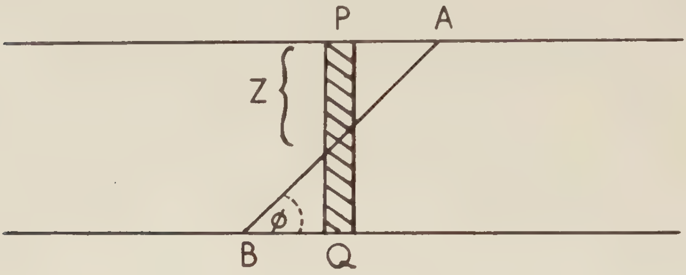

A stacking fault AB in a thin film.

The first three types of motion have already been described by Hirsch *et al.* (1956) for aluminium foils, and no further description will be given here. The fourth motion will be considered in more detail. This process shows itself by the appearance of fine lines on the micrograph, as shown in fig. 6 (Pl. 45) and fig. 8 (Pl. 46). The lines appear very suddenly, some disappear equally suddenly, and the total number increases as the electron bombardment is continued. The lines do not disappear as the electron illumination is reduced.

This type of feature was not properly understood until the theory for the contrast produced by a stacking fault was worked out by Whelan and Hirsch (1957 a, b). According to their theory, if a stacking fault occurs on a crystal plane AB (see fig. 7) inclined at an angle ϕ to the plane of the film, and if the shear corresponding to the stacking fault has a non-zero component perpendicular to the lattice planes which are giving rise to a Bragg reflection, the intensity of the Bragg reflection from a column of the film such as PQ will depend upon the depth z of the stacking fault below the surface. When z is equal to an integral multiple of the extinction distance s for a particular Bragg reflection, the diffracted beam from the part of the column PQ above the faulting plane is zero. Similar conditions apply to the lower part. It is shown that as a result of this effect the intensity of the diffracted beam, and hence also the intensity of the undeviated transmitted beam, depends periodically on z and well-defined fringes are observed on the image with a spacing of $s \cot\phi$. This analysis applies when the crystal is set nearly, but not exactly, at the Bragg angle: at the exact setting the fringe spacing is $\frac{1}{2}s \cot\phi$. With the (111) gold films used in the work described in this paper, the main reflections which occur are {220}. The estimation of extinction distance involves a knowledge of the atomic scattering factor f_s for electrons. Values of s have been deduced from the f_s values given recently by Ibers (1958), and these are given in the table, the value for {220} being about 250 Å. This is approximately equal to the thickness of the film, so that only one fringe, or at the most two fringes, of the stacking fault contrast can be expected in this case. Films of much greater thickness do not give rise to the wide ribbons of stacking fault during observation in the Elmiskop I, so no confirmation of the detailed contrast can be made in this way. With the films of 200–300 Å in thickness, the contrast in the stacking faults can be changed by tilting the specimens. This is arranged to allow {111} and {200} Bragg reflections to occur, so that extinction distances of 155 Å and 175 Å are brought into operation and the path length of the electrons passing through the film is increased by a factor $\sec\theta$ (θ = angle of tilt) so that more than one fringe appears; by a suitable choice of the tilting direction the projected width of the stacking fault may be increased to allow the individual fringes to be resolved more readily. This technique is illustrated in fig. 8. The tilting is such that one set of stacking faults is on {111} planes steeply inclined to the electron beam, and two fringes are observed, whereas the other set of stacking faults is on {111} planes not so steeply inclined, and the two fringes are not resolved, so that the normal fine lines appear. The stacking faults appear also during the observation of the (100) gold films, but these have not been studied in such detail. With these films the {002} reflections are predominant, and two fringes may be observed without any tilting.

Extinction Distance (s) for Gold Based upon Atomic Scattering Amplitudes for Electrons (f_s) as given by Ibers (1958)

Reflection (*hkl*)	f_s (Å)	s (Å) for accelerating potential of 80 kv
(111)	7·6	155
(200)	6·7	176
(220)	4·8	248

A further observation is that the stacking fault fringes sometimes have a twisted appearance, as shown in fig. 9 (Pl. 46). This effect is predicted by the theory of Whelan and Hirsch (1957 a, b). A final piece of evidence that the observed fine lines are due to stacking faults is that when they disappear suddenly, a single dislocation may be observed to appear simultaneously at one end of the original line. This is as expected since one partial dislocation moves and combines with the other partial to produce an unsplit dislocation as the stacking fault is eliminated.

The width of the stacking faults (i.e. the separation between the two partials) may be as high as one micron. This is much larger than the estimated equilibrium separation of about 35 Å for gold (Seeger 1955). The reason why such wide stacking faults can be produced seems to be associated with the effect of dislocation pinning which occurs at the surfaces of the film. Such pinning has been discussed previously (Hirsch *et al.* 1956, Whelan *et al.* 1957), and is considered to be due to the presence of a surface oxide film in some cases. Although no surface oxide is present on the gold films, the specimens rapidly become covered by a film of carbon contamination during examination in the electron microscope. This contamination is likely to provide an effective means of pinning dislocations by hindering the formation on the surface of the steps associated with the movement of dislocation. On this mechanism the pinning will depend upon the Burgers vector of the dislocation, since the step is given by the component of the Burgers vector resolved perpendicular to the surface. Thus of the two partial dislocations into which a dislocation splits, one may be more effectively pinned than the other. Further, the stress acting on a dislocation constraining it to move also depends, for a given stress system, on its Burgers vector, so that the stress acting on one partial may be much higher than that acting on the other. As a result of these two effects, one partial may be caused to move whilst the other remains stationary, a certain stress being required to keep them apart. Since the partials do not automatically come together again once the stress is removed, it is assumed that the carbon contamination film which forms after the one partial has moved and formed a surface step, hinders the removal of that step, and so prevents the reversal of the movement.

Ciné films of the movement of dislocations have been taken by direct photography of the fluorescent screen, with an instrumental magnification of 40 000 ×. It is found that the maximum permissible frame speed is about 10/sec. Under these conditions the stacking faults appear between the two successive exposures, so that they appear in less than 10^{-1} sec.

§ 4. The Effect of Annealing the Gold Films

Attempts at annealing the gold films have resulted in quite uncontrolled behaviour. At about 500°c the films often develop many small holes which gradually produce a lace-work structure. Sometimes this is accompanied by a considerable increase in the thickness of the remaining parts of the films. A complete recrystallization may occur in this way, leading to thick crystals several microns in lateral extent in random orientation. These crystals are often too thick to allow adequate electron transmission for microscopy, but thin regions of 2000 Å and less may be examined at an accelerating potential of 100 kv. Complicated dislocation structures are then visible; these include many long dislocation lines which run approximately parallel to the plane of the film (cf. §3 for the arrangement of dislocations in the film as prepared).

Regular dislocation arrays are also found in these annealed specimens. Figure 10 (Pl. 46) shows an array of dislocations at low angle grain boundaries. Figure 11 (Pl. 46) shows an array which appears to have arisen from the interaction of two sets of dislocations on near neighbouring slip planes. If it is assumed that during the annealing process the dislocations on the near neighbouring slip planes climb towards one another so as to intersect with each other as shown in fig. 12 (*a*), and that the dislocations have identical Burgers vectors, the dislocations will rearrange themselves as shown in fig. 12 (*b*). This rearrangement is illustrated in fig. 12 (*c*). At each intersection the slip plane is divided into four areas A, B, C and D; over areas B and C the crystal is slipped by one Burgers vector unit, and over area D the crystal is slipped by two units with respect to the slip over A. The areas B and C therefore join, and the interaction occurs as indicated in fig. 12 (*b*). Hexagonal networks are also produced in the annealed films.

Fig. 12

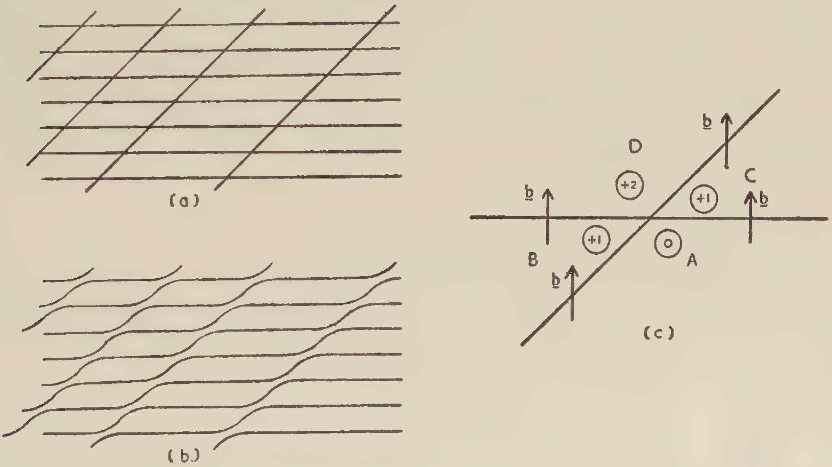

The mechanism by which the dislocation array of fig. 11 is formed; (*b*) is the Burgers vector of the dislocations.

§ 5. Summary and Discussion

It has been shown that good coherent and uniform single crystal films of gold may be produced by an evaporation technique, with a thickness (approx. 200 Å) suitable for obtaining bright transmission electron micrographs at high magnification. Preliminary investigations suggest that it will be possible to prepare films of platinum, palladium and rhodium in the same way. The development of similar techniques for preparing thin films of other metals depends upon finding suitable smooth substrates on which the deposit metal may be grown as a coherent film, and from which the deposit film may be conveniently detached.

Dislocations are observed in the gold films, their density being 10^{10}–10^{11}/sm^2. The movement of the dislocations resulting from the use of a highly localized intense illuminating electron beam has been observed. A prominent feature is the occurrence of wide ribbons of stacking fault, due to dislocations splitting into two partials which separate by as much as one micron.

Whelan *et al.* (1957) have compared the nature of the dislocation movements induced in aluminium and stainless steel. Extensive cross-slip but no occurrence of stacking faults was observed with aluminium; with stainless steel no cross slip was observed, but the stacking faults were prominent. This was interpreted in terms of the very high stacking fault energy for aluminium (approximately 200 ergs/cm^2) compared with that for stainless steel (approximately 15–20 ergs/cm^2). The gold appears to be an intermediate case, since both cross-slip and stacking faults are prominent. This is consistent with the intermediate stacking fault energy of approximately 40 ergs/cm^2 estimated by Seeger (1955).

Finally, it must be emphasized that both the original dislocation arrangements and the behaviour of the dislocations under any form of applied stress are characteristic of thin films, and not bulk materials. On the other hand the techniques of thinning bulk materials to obtain the thin film gives rise to dislocation arrangements which are to a large extent characteristic of the bulk material, although any movement of the dislocations is still essentially a thin film behaviour.

ACKNOWLEDGMENTS

I am grateful to Dr. J. W. Menter for valuable discussions during the course of this work. This paper is published by permission of the Chairman of Tube Investments Limited.

REFERENCES

BASSETT, G. A., MENTER, J. W., and PASHLEY, D. W., 1958, *Proc. roy. Soc.* A, **246,** 345.
BOLLMANN, W., 1956, *Phys. Rev.*, **103,** 1588.
BRADLEY, D. E., 1954, *Brit. J. appl. Phys.*, **5,** 65.
BRAME, D. R., and EVANS, T., 1958, *Phil. Mag.*, **3,** 971.
CASTAING, R., 1955, *Rev. Métall.*, **52,** 669.
FERNANDEZ-MORAN, H., 1956, *Indian dia. Rev.*, **16,** 128.
HAANSTRA, H. B., 1955, *Philips tech. Rev.*, **17,** 178.
HEIDENREICH, R. D., 1949, *J. appl. Phys.*, **20,** 993.
HIRSCH, P. B., KELLY, A., and MENTER, J. W., 1955, *Proc. phys. Soc.* B, **68,** 1132.
HIRSCH, P. B., HORNE, R. W., and WHELAN, M. J., 1956, *Phil. Mag.*, **1,** 677; 1957, *Lake Placid Conference Report* (New York: Wiley).

HIRSCH, P. B., SILCOX, J., SMALLMAN, R. E., and WESTMACOTT, K. H., 1958, *Phil. Mag.*, **3**, 897.

IBERS, J. A., 1958, *Acta Cryst.*, **11**, 178.

MOLLENSTEDT, G., 1953, *Optik*, **10**, 72.

NICHOLAS, R., THOMAS, G., and NUTTING, J., 1958, *Brit. J. appl. Phys.*, **9**, 25.

OGAWA, S., and WATANABE, D., 1954, *J. phys. Soc. Japan*, **9**, 475.

PASHLEY, D. W., 1959, *Phil. Mag.*, **4**, 316.

RAETHER, H., 1952, *Z. angew. Phys.*, **4**, 53.

RANG, O., 1953 a, *Optik*, **10**, 90; 1953 b, *Z. Phys.*, **136**, 465.

READ, W. T., 1953, *Dislocations in Crystals* (New York: McGraw-Hill).

REIMER, L., 1956, *Z. Naturf.*, **11(a)**, 649.

SEEGER, A., 1955, *Report of conference on defects in crystalline solids* (London : Physical Society), p. 328.

TOMLINSON, H. M., 1958, *Phil. Mag.*, **3**, 867.

WEIL, R., and READ, H. J., 1950, *J. appl. Phys.*, **21**, 1068.

WHELAN, M. J., and HIRSCH, P. B., 1957 a, *Phil. Mag.*, **2**, 1121; 1957 b, *Phil. Mag.*, **2**, 1303.

WHELAN, M. J., HIRSCH, P. B., HORNE, R. W., and BOLLMANN, W., 1957, *Proc. roy. Soc.* A, **240**, 524.

The Excitation of Molecular Vibration and Rotation by Impact of Slow Electrons†

By H. S. W. Massey, F.R.S.
University College, London

[Received November 10, 1958]

Abstract

A new approximate formula is derived for the cross sections for excitation of molecular vibration and rotation by impact of slow electrons. Account is taken of the fact that in such impacts the incident electron is moving much faster than the nuclei in the molecule while its wave function suffers considerable distortion by the molecular field.

§ 1. Introduction

Comparatively little attention has been paid to the theory of the excitation of nuclear motion in molecules by electron impact. All of the calculations which have been carried out so far have employed Born's approximation. This is certainly not valid in many cases when the electron wavelength is comparable with molecular dimensions, though there may be exceptions to this. Examples in which use of the approximation would appear to be justified have been given, as in the excitation of rotation due to interaction with the permanent electric dipole or quadrupole moment of a molecule (Massey 1932, Gerjuoy and Stein 1955). In most cases of practical interest, as in microwave breakdown in a molecular gas, or in the Luxemburg effect, the electron wavelength is comparable with molecular dimensions and to obtain reliable results a more accurate approximation is required.

In seeking this, it is natural to turn one's attention to the distorted wave method which has been recently used with some success in dealing with excitation of atoms by electrons with energies close to the threshold. This method replaces the plane waves which represent the wave functions of the incident and scattered electron waves by waves respectively distorted by the mean field of the atom in its initial and final states. The difficulty in applying this directly to excitation of nuclear motion in a molecule is that, although the electrons are slow, as judged from the relation of the wavelength to molecular dimensions, they are nevertheless moving rapidly compared with the nuclei and it would not seem to be a good approximation to regard the distortion as due to the mean molecular field averaged over all orientations of the molecule. It is the purpose of this note to develop an alternative method in which the distortion is produced by the molecular field with a fixed orientation and nuclear separation, the rate of excitation of the nuclear motion being then determined by the rate of change of the distortion with orientation and nuclear separation. If the molecular field is small the formula obtained reduces to Born's approximation.

---

† Communicated by the Author.

§ 2. DERIVATION OF THE FORMULA FOR THE INELASTIC CROSS SECTION

We confine ourselves in the first instances to diatomic molecules. Electron exchange effects will be ignored initially and it will be supposed throughout that no change in the electronic state of the molecule occurs. Such questions as coupling between the molecular rotation and electron spin will not be considered.

We denote the vector separation of the nuclei by $\mathbf{R}$, the coordinates of the n molecular electrons relative to the centre of mass of the nuclei by $\mathbf{r}_{sm}$, $s=1, \ldots, n$ and those of the colliding electrons by $\mathbf{r}$. The wave equation for the system can be written

$$\left[T_m(\mathbf{r}_{sm}) - \frac{\hbar^2}{2m}\nabla^2 - \frac{\hbar^2}{2M}\nabla_R{}^2 - E_k - E_0 + V(\mathbf{r}_{sm}, \mathbf{R}) + U(\mathbf{r}, \mathbf{r}_{sm}, \mathbf{R}) + \frac{Z_1Z_2e^2}{R}\right]\Psi = 0, \quad . \quad . \quad . \tag{1}$$

where $V(\mathbf{r}_{sm}, \mathbf{R})$ is the potential energy of interaction of the molecular electrons with the nuclei and with each other and $U(\mathbf{r}, \mathbf{r}_{sm}, \mathbf{R})$ that of the colliding electron with the nuclei and the molecular electrons. Z_1e and Z_2e are the nuclear charges, E_0 is the energy of the initial state of the molecule and E_k the kinetic energy of the incident electron.

In the absence of the colliding electron the molecular wave function is represented with good accuracy by

$$\Phi = \phi_0(\mathbf{r}_{sm}, \mathbf{R})\chi_0(\mathbf{R}), \quad . \quad . \quad . \quad . \quad . \quad . \quad . \quad . \tag{2}$$

where ϕ_0 is the wavefunction for the electronic motion and χ_0 for the nuclear rotation and vibration. ϕ_0 and χ_0 are proper functions which satisfy the equations

$$\left[T_m(\mathbf{r}_{sm}) + V(\mathbf{r}_{sm}, \mathbf{R}) + \frac{Z_1Z_2e^2}{R} - \epsilon(R)\right]\phi_0(\mathbf{r}_{sm}, R) = 0, \tag{3}$$

$$\left[\frac{\hbar^2}{2M}\nabla_R{}^2 + E_0 - \epsilon(R) + \frac{\hbar^2}{2M}\int \phi_0 \nabla_R{}^2\phi_0 \, d\tau_{r_{sm}}\right]\chi_0 = 0. \tag{4}$$

If we write the solution of (1) in the form

$$\Psi = \phi_0(\mathbf{r}_{sm}, \mathbf{R})\Lambda(\mathbf{R}, \mathbf{r}), \quad . \quad . \quad . \quad . \quad . \quad . \quad . \quad . \tag{5}$$

then on substitution in (1) we find, using (2) that

$$\phi_0\left[\frac{\hbar^2}{2m}\nabla^2 + \frac{\hbar^2}{2M}\nabla_R{}^2 + E_k + E_0 - \epsilon(R) - U(\mathbf{r}, \mathbf{r}_{sm}, \mathbf{R})\right]\Lambda + \frac{\hbar^2}{2M}[\Lambda\nabla_R{}^2\phi_0 + 2\,\mathrm{grad}_R\Lambda \,.\, \mathrm{grad}_R\phi_0] = 0. \quad . \quad . \quad . \tag{6}$$

Multiplying by ϕ_0^* and integrating over $d\tau_{sm}$ we have, since ϕ_0 is normalized to unity for all $\mathbf{R}$,

$$\left[\frac{\hbar^2}{2m}\nabla^2+\frac{\hbar^2}{2M}\left\{\nabla_R{}^2+\int\phi^*\nabla_R{}^2\phi\,d\tau_{sm}\right\}+E_k+E_0-\epsilon(R)\right.$$
$$\left.-\int U(r,r_{sm},R)|\phi_0(\mathbf{r}_{sm})|^2\,d\tau_{sm}\right]\Lambda=0. \quad . \quad . \quad . \quad (7)$$

The term in grad ϕ_0 vanishes if ϕ_0 is real because

$$\int\phi_0\,\mathrm{grad}_R\,\phi_0\,d\tau_{sm}=\tfrac{1}{2}\,\mathrm{grad}_R\int\phi_0{}^2\,d\tau_{sm}=0.$$

This equation for Λ is satisfied approximately by taking

$$\Lambda=\Lambda_j=F_j(\mathbf{r},\mathbf{R})\chi_j(\mathbf{R}) \quad . \quad . \quad . \quad . \quad . \quad . \quad . \quad . \quad . \quad (8)$$

where χ_j is the wave function for the jth state of molecular motion which satisfies (4) with E_0 replaced by E_j and F_j is the wave function for motion of the free electron of the appropriate energy in the field of the molecule, when the nuclear separation is R, averaged over the coordinates of the molecular electrons. Thus

$$\nabla^2F_j+\left[k_j{}^2-\frac{2m}{\hbar^2}\int U(\mathbf{r},\mathbf{r}_{sm},\mathbf{R})|\phi_0(\mathbf{r}_{sm})|^2\,d\tau_{sm}\right]F_j=0. \qquad (9)$$

where $$k_j{}^2=\frac{2m}{\hbar^2}(E_k+E_j-E_0).$$

The terms which do not cancel when (8) is substituted in (7) are

$$\frac{\hbar^2}{2M}(\chi_j\nabla_R{}^2F_j+2\,\mathrm{grad}_R\,\chi_j\,.\,\mathrm{grad}_R\,F_j). \quad . \quad . \quad . \quad . \quad (10)$$

We may now regard these terms as giving rise to transitions between states with different j, i.e. between states with different wave functions $\chi(\mathbf{R})$ for nuclear vibration and rotation. Applying the usual perturbation theory we have that the number of transitions per second from an initial state 0 of nuclear motion to a final state j is

$$\frac{2\pi}{\hbar}\left|\int\frac{\hbar^2}{2M}\chi_j{}^*F_j(\chi_0\nabla_R{}^2F_0+2\,\mathrm{grad}_R\,\psi_0\,.\,\mathrm{grad}_R\,F_0)\,d\tau_R\,d\tau_r\right|^2. \qquad (11)$$

By appropriate normalization of F_0 and F_j this yields for the differential cross section in which the electron is scattered in the direction (ζ,μ) (the incident direction being taken as axis) after producing the appropriate excitation

$$I_{0j}(\zeta)\sin\zeta\,d\zeta\,d\mu$$
$$=\frac{k_j}{k_0}\left|\frac{m}{4\pi M}\int\chi_j{}^*F_j(\mathbf{r},\mathbf{R})(\chi_0\nabla_R{}^2F_0+2\,\mathrm{grad}_R\,\chi_0\,.\,\mathrm{grad}_R\,F_0)\,d\tau_R\,d\tau_r\right|^2$$
$$\times\sin\zeta\,d\zeta\,d\mu, \quad . \quad . \quad . \quad (12)$$

where $$F_0\sim\exp(i\mathbf{k}_0\,.\,\mathbf{r})+f_0(\theta,\mathbf{R})r^{-1}\exp(ik_0r)$$
$$F_j\sim\exp(-i\mathbf{k}_j\,.\,\mathbf{r})+f_j(\pi-\Theta,\mathbf{R})r^{-1}\exp(ik_jr).$$

with $$\cos\Theta=\cos\theta\cos\zeta+\sin\theta\sin\zeta\cos(\phi-\mu).$$

§ 3. RELATION TO BORN'S APPROXIMATION

We write

$$\int U(\mathbf{r},\mathbf{r}_{sm},\mathbf{R})|\phi_0(\mathbf{r}_{sm})|^2\,d\tau_{sm}=U_{00}(\mathbf{r},\mathbf{R}). \quad . \quad . \quad . \quad (13)$$

If U_{00} can be treated as small

$$F_0=\exp(i\mathbf{k}_0\,.\,\mathbf{r})-\frac{m}{2\pi\hbar^2}\int U_{00}(\mathbf{r}',\mathbf{R})\,\frac{\exp(ik_0|\mathbf{r}-\mathbf{r}'|)}{|\mathbf{r}-\mathbf{r}'|}\exp(i\mathbf{k}_0\,.\,\mathbf{r}')\,d\tau_{r'} \quad (14)$$

so that

$$\nabla_R F_0=-\frac{m}{2\pi\hbar^2}\int\frac{\exp(ik_0|\mathbf{r}-\mathbf{r}'|)}{|\mathbf{r}-\mathbf{r}'|}\exp(ik_0\,.\,\mathbf{r}')\,\nabla_R U_{00}(\mathbf{r}',\mathbf{R})\,d\tau_{r'}.$$

Hence to this approximation

$$\int\int\chi_j^*F_j(\chi_0\,.\,\nabla_R^2F_0+2\,\mathrm{grad}_R\,\chi_0\cdot\mathrm{grad}_R\,F_0)\,d\tau_r\,d\tau_R$$
$$=-\frac{m}{2\pi\hbar^2}\int\int\int\chi_j^*\exp(-i\mathbf{k}_j\,.\,\mathbf{r})(\chi_0\nabla_R^2U_{00}+2\,\mathrm{grad}_R\,\chi_0\cdot\mathrm{grad}_R\,U_{00})$$
$$\times\frac{\exp(ik_0|\mathbf{r}-\mathbf{r}'|)}{|\mathbf{r}-\mathbf{r}'|}\exp(i\mathbf{k}_0\,.\,\mathbf{r})\,d\tau_r\,d\tau_{r'}\,d\tau_R. \quad . \quad . \quad . \quad (15)$$

We have now that

$$\int\exp(i\mathbf{k}_j\,.\,\mathbf{r})\,\frac{\exp(ik_0|\mathbf{r}-\mathbf{r}'|)}{|\mathbf{r}-\mathbf{r}'|}\,d\tau_r=\frac{4\pi}{k_0^2-k_j^2}\exp(-i\mathbf{k}_j\,.\,\mathbf{r}'), \quad (16)$$

so that (15) reduces to

$$-\frac{m}{2\pi\hbar^2(k_0^2-k_j^2)}\int\int\exp[i(\mathbf{k}_0-\mathbf{k}_j)\,.\,\mathbf{r}'](\chi_0^*\chi_j\nabla_R^2U_{00}+2\chi_0^*$$
$$\times\,\mathrm{grad}_R\,\chi_j\cdot\mathrm{grad}_R\,U_{00})\,d\tau_{r'}\,d\tau_R. \quad . \quad . \quad . \quad (17)$$

Now

$$\int\chi_j^*\chi_0\nabla_R^2U_{00}\,d\tau_R=\int\nabla_R^2(\chi_j^*\chi_0)U_{00}\,d\tau_R,$$

$$\int\chi_j^*\,\mathrm{grad}_R\,\chi_0\cdot\mathrm{grad}_R\,U_{00}\,d\tau_R=-\int U_{00}\nabla_R\cdot(\chi_j^*\,\mathrm{grad}\,\chi_0)\,d\tau_R.$$

so, since

$$\nabla_R^2(\chi_j^*\chi_0)-2\nabla_R\cdot(\chi_j^*\nabla_R\chi_0)=\chi_0\nabla_R^2\chi_j^*-\chi_j^*\nabla_R^2\chi_0,$$

(15) becomes

$$-\frac{m}{2\pi\hbar^2(k_0^2-k_j^2)}\int\int\exp[i(\mathbf{k}_0-\mathbf{k}_j)\,.\,\mathbf{r}']\,U_{00}(\mathbf{R},\mathbf{r}')(\chi_0\nabla_R^2\chi_j-\chi_j^*\nabla_R^2\chi_0)$$
$$\times\,d\tau_{r'}\,d\tau_R. \quad . \quad . \quad . \quad (18)$$

Now, because χ_0 and χ_j satisfy equations of the form (4),

$$\chi_0\nabla_R^2\chi_j^*-\chi_j^*\nabla_R^2\chi_0=\frac{2M}{\hbar^2}(E_0-E_j)\chi_0\chi_j^*=\frac{M}{m}(k_0^2-k_j^2)\chi_0\chi_j^*,$$

so that, on substitution in (12)

$$I_{0j}(\zeta)=\frac{k_j}{k_0}\left|\frac{m}{2\pi\hbar^2}\int\int\chi_j^*\chi_0\exp[i(\mathbf{k}_0-\mathbf{k}_j)\,.\,\mathbf{r}']\,U_{00}(\mathbf{R},\mathbf{r}')\,d\tau_{r'}\,d\tau_R\right|^2 \quad (19)$$

which is Born's approximation.

On the other hand, when the approximation (14) is not valid it is no longer possible to reduce the integral in (12) to the form (18) with the plane waves replaced by the appropriate distorted waves.

§ 4. CONCLUDING REMARKS

The application of the formula (12) to specific cases is difficult because it requires that the functions F_0, F_j should be known with sufficient accuracy for their derivatives with respect to the nuclear separations to be obtainable to a reasonable degree of approximation. An attempt is being made nevertheless to carry out the calculations for molecular hydrogen.

ACKNOWLEDGMENT

I wish to thank Dr. S. Zienau who read this paper in draft and made useful suggestions.

REFERENCES

GERJUOY, E., and STEIN, S., 1955, *Phys. Rev.*, **97,** 1671; **98,** 1848.
MASSEY, H. S. W., 1932, *Proc. Camb. phil. Soc.*, **28,** 99.

A Generalization of Grüneisen's Theory of Solids and its Application to Solid Argon†

By R. O. Davies and S. Parke
Physics Department, Queen Mary College, Mile End Road, London

[Received September 7, 1958]

Abstract

The quasi-harmonic model of a solid (a harmonic model which takes only partial account of anharmonicity) is examined and a general notation established. The theory involves the quantities $[\epsilon_i]^{[n]} \equiv (V^n/\nu_i)\ (\partial^n \nu_i/\partial V^n)$, where ν_i are the spectral frequencies. By evaluating averages of $[\epsilon_i]^{[n]}$ appropriate at high and low temperatures it is shown that Grüneisen-type assumptions are reasonable for the inert gas solids. This confirms work by Barron on Grüneisen's γ (in our notation $\gamma = -\langle [\epsilon_i]^{[1]} \rangle_{\text{Av}}$).

Grüneisen's equation of state $pV = -VU_0'(V) + \gamma U_T$, where U_T and U_0 are the thermal and non-thermal contributions to the internal energy U, is extended to yield an equation of the form $V/\kappa_T = V^2 U_0''(V) + \gamma' U_T - \gamma^2 T C_V$ where $\gamma' (= \langle [\epsilon_i]^{[2]} \rangle_{\text{Av}})$ is a 'second' Grüneisen constant. It may be estimated from measurements of the variation of compressibility with temperature in much the same way as the first Grüneisen constant γ is determined from measurements on expansivity, specific heat and compressibility.

Experimental results for argon are compared with the theory, assuming a Lennard–Jones 6-12 potential. Good agreement is obtained except above 40°K where anharmonicity must be considered explicitly.

Our estimates of γ are consistent with those of previous writers; from the theory we conclude that for argon γ' has a value of about 10 and this is confirmed by a direct use of experimental results on compressibility.

§ 1. Introduction

The most useful approximate theory of the equation of state of simple solids is that associated with Mie and Grüneisen. It has been summarized by Grüneisen (1926) and its main feature is the introduction of an empirical constant γ which is a measure of the anharmonicity of the interatomic forces. From the point of view of lattice dynamics, the Mie–Grüneisen theory is best understood by using a harmonic model of the solid and assuming that the dimensionless derivatives of the frequencies of the normal modes with respect to the volume, $\partial \ln \nu_i/\partial \ln V$, are the same for each mode. They are the negative of the Grüneisen γ. We wish to consider a generalization of this theory in which not only the first but also higher derivatives of the frequencies are considered and are replaced by appropriate constants. To explain exactly what we shall do, it is best to start from first principles.

---

† Communicated by the Authors.

The thermodynamic properties of a simple mechanical system under isotropic stress can be obtained from the Helmholtz free energy (F) when it is expressed as a function of temperature (T) and volume (V). Indeed, working from $\beta F (\beta = 1/kT)$ one has

$$\left.\begin{aligned} \beta U &= \beta \partial(\beta F)/\partial\beta, \\ \beta V p &= -V\partial(\beta F)/\partial V, \\ C_v/k &= -\beta^2\partial^2(\beta F)/\partial\beta^2, \\ (V/k)(\alpha/\kappa) &= V\partial/\partial V(\beta\partial/\partial\beta - 1)(\beta F), \\ V\beta(1/\kappa) &= V^2\partial^2(\beta F)/\partial V^2, \end{aligned}\right\} \quad . \; . \; . \quad (1)$$

where U is the internal energy, α is the expansivity and κ is the isothermal compressibility.

In a number of systems one can express βF in the form

$$\beta F = f(\beta\epsilon) \quad (\epsilon = \epsilon(V)) \quad . \; . \; . \; . \; . \; . \; . \; . \quad (2)$$

or else as a sum of such functions, $\sum_i f_i(\beta\epsilon_i)$. In particular the latter is the case for the harmonic model of a solid; the right-hand side of (2) then consists of a pure potential term $\beta\Phi$—the corresponding function $f(x)$ being x—where $\Phi(V)$ is the potential energy of the undisplaced lattice and a sum of ' thermal ' terms $\sum_i f(\beta\epsilon_i)$ where $f(x) = \frac{1}{2}x + \log[1 - \exp(-x)]$, and $\epsilon_i(V) = h\nu_i(V)$ (the ν_i are the spectral frequencies of the lattice).

If eqn. (2) is substituted into eqn. (1) we obtain

$$\left.\begin{aligned} \beta U &= f^{[1]}, \\ \beta p V &= -f^{[1]}[\epsilon]^{[1]}, \\ C_v/k &= -f^{[2]}, \\ (V/k)(\alpha/\kappa) &= f^{[2}\,[\epsilon]^{[1]}, \\ V\beta/\kappa &= f^{[1]}[\epsilon]^{[2]} + f^{[2]}[\epsilon]^{[1]2}, \\ \text{where} \qquad f^{[n]} &= x^n\partial^n f/\partial x^n \quad (x = \beta\epsilon), \\ \text{and} \qquad [\epsilon]^{[n]} &= (V^n/\epsilon)(\partial^n\epsilon/\partial V^n). \end{aligned}\right\} \quad . \; . \; . \quad (3)$$

For manipulation of these quantities it is convenient to note that

$$\left.\begin{aligned} (x\partial/\partial x)f^{[n]} &= f^{[n+1]} + nf^{[n]}, \\ V\partial/\partial V &= [\epsilon]^{[1]}x\partial/\partial x, \\ (V\partial/\partial V)[\epsilon]^{[n]} &= [\epsilon]^{[n+1]} + n[\epsilon]^{[n]} - [\epsilon]^{[1]}[\epsilon]^{[n]}. \end{aligned}\right\} \quad . \; . \; . \quad (4)$$

In order to apply (3) to the harmonic model of a solid it must, in accordance with what was said above, be summed. We therefore need: (i) the potential energy of the lattice (Φ) and its first two derivatives $\Phi^{[1]}$ and $\Phi^{[2]}$; (ii) the energies of the normal modes and the distributions of $[\epsilon]^{[1]}$ and $[\epsilon]^{[2]}$ over the modes. The thermal f-functions are known, and can be obtained by successive differentiation of

$$f(x) = \tfrac{1}{2}x + \log[1 - \exp(-x)].$$

Hence the final result comes from carrying out appropriate summations.

This programme is not easy to carry through and for numerical work it is desirable to refer all the lattice calculations to a reference volume (V_0) and to expand the thermodynamic functions in powers of the dilatation $\delta = (V - V_0)/V_0$. To the second power of δ, the thermodynamic coefficients may be found from $A_r(\beta)$ in the expansion

$$\beta F = A_0 + A_1\delta + \tfrac{1}{2}A_2\delta^2 + \tfrac{1}{6}A_3\delta^3 + \tfrac{1}{24}A_4\delta^4, \quad . \quad . \quad . \quad . \qquad (5)$$

where

$$\left.\begin{aligned} A_0 &= f^{[0]}, \\ A_1 &= f^{[1]}[\epsilon]^{[1]}, \\ A_2 &= f^{[1]}[\epsilon]^{[2]} + f^{[2]}[\epsilon]^{[1]2}, \\ A_3 &= f^{[1]}[\epsilon]^{[3]} + f^{[2]}3[\epsilon]^{[1]}[\epsilon]^{[2]} + f^{[3]}[\epsilon]^{[1]3} \\ A_4 &= f^{[1]}[\epsilon]^{[4]} + f^{[2]}(4[\epsilon]^{[1]}[\epsilon]^{[3]} + 3[\epsilon]^{[2]2}) + f^{[3]}6[\epsilon]^{[1]2}[\epsilon]^{[2]} + f^{[4]}[\epsilon]^{[1]4}, \end{aligned}\right\} \qquad (6)$$

all quantities on the right of (6) being evaluated at the reference volume V_0.

In the simplest form of Grüneisen's theory of the solid state one works from eqn. (3), treating $[\epsilon]^{[1]}$ and $[\epsilon]^{[2]}$ as constant in all the thermal terms. ($[\epsilon]^{[1]}$ is the negative of Grüneisen's γ and $[\epsilon]^{[2]}$—which appears, for example, in Born and Huang (1954), eqns. (4.55) and (17.15)—can be regarded as a second Grüneisen constant but it is not usually considered in detail.) The potential energy terms must be dealt with separately; for them $f(x) = x$ and $f^{[n]} = 0 (n \geqslant 2)$.

We propose to test on solid argon a simple generalization of Grüneisen's theory: we work from eqn. (6) and replace the coefficients of the f-functions in all the thermal terms, viz. $[\epsilon]^{[1]}$, $[\epsilon]^{[2]}$, $[\epsilon]^{[1]2}$, $[\epsilon]^{[1]}$. $[\epsilon]^{[2]}$, etc. by appropriately chosen constant average values ('generalized Grüneisen constants'); the potential energy term is dealt with separately and without further approximation.

Granted the (unjustified) use of a harmonic model, the only arbitrary element in our procedure is the choices of averages in forming the generalized Grüneisen constants. The choices we make here are explained in § 3 and are suggested by the work of Domb and Salter (1952), Salter (1954), Barron (1955), Barron and Domb (1955). In carrying out the calculations we have drawn extensively on numerical work by the same authors. We shall work with a Lennard–Jones potential (chosen in § 2) with no further fitting of constants. (It is of course possible that another choice of intermolecular potential would yield different results.) The summed 'f-functions' required are obtained with the help of the frequency distribution of Leighton (1948) (§ 4). The final results are compared in § 5 with the experiments of Clusius (1936), Barker and Dobbs (1955), Dobbs *et al.* (1956), Stewart (1955, 1956) and with previous calculations by Kane (1939), Henkel (1955), Domb and Zucker (1956), Zucker (1956, 1958). An experimental estimate of the second Grüneisen constant ($[\epsilon]^{[2]} \equiv \gamma'$) is obtained in § 6. The usefulness of the model is assessed in § 7.

§ 2. The Interatomic Potential and Lattice Energy of Argon

To fit the two constants in the Lennard–Jones potential

$$\phi(r^2)=4\epsilon[(\sigma/r)^{12}-(\sigma/r)^6] \quad . \quad . \quad . \quad . \quad . \quad . \quad (7)$$

we have adopted the experimental values cited by Dobbs and Jones (1957),

$$\left.\begin{aligned} a_0&=5{\cdot}31\pm0{\cdot}01\,\text{Å},\\ -U_0=L_0&=1850\pm12\text{ cal (g mole)}^{-1},\end{aligned}\right\} \quad . \quad . \quad . \quad . \quad (8)$$

for the lattice constant and the latent heat at absolute zero and zero pressure. The harmonic theory of Salter was recalculated, taking all neighbours into account in the zero point energy as well as in the potential term, and it was found that the zero point energy and pressure are given by

$$\left.\begin{aligned} \frac{U_0}{N\epsilon}&=\frac{6{\cdot}0659}{V^{*4}}-\frac{14{\cdot}454}{V^{*2}}+\frac{3{\cdot}295\Lambda^*}{V^{*7/3}}R^{1/2},\\ p^*&=\frac{24{\cdot}264}{V^{*5}}-\frac{28{\cdot}908}{V^{*3}}+\frac{4{\cdot}394}{V^{*10/3}}\frac{(3{\cdot}626-V^{*2})}{R^{1/2}},\end{aligned}\right\} \quad . \quad . \quad . \quad . \quad (9)$$

$$(R\equiv 2{\cdot}072-V^{*2})$$

where $V^*=2(a_0/2\sigma)^3$, $\Lambda^*=h/\sigma(m\epsilon)^{1/2}$. (The numbers here differ by about 4% from those of Salter.) The elastic moduli at absolute zero were also recalculated.

Substituting the experimental values of (8) into (9) we find for ϵ and σ the values given in the first entry of table 1. These values are used in the remainder of this paper.

Table 1. The Interatomic Potential of Argon $\phi(r^2)=4\epsilon[(\sigma/r)^{12}-(\sigma/r)^6]$

$10^{14}\epsilon$/erg	σ, Å	
1·64(4)	3·401	Harmonic calculation, all neighbours (this work)
1·69	3·402	Anharmonic calculation, all neighbours (Zucker 1956)
1·65	3·405	Virial coefficient (Hirschfelder *et al*. 1954)

Table 2. Values of $\Phi^{[n]}\equiv V^n\partial^n\Phi/\partial V^n$ in k cal mole^{-1} Obtained from Eqn. (9) for the Reference Volume at Absolute Zero ($V^*=0{\cdot}9514$)

$\Phi^{[0]}$	$\Phi^{[1]}$	$\Phi^{[2]}$	$\Phi^{[3]}$	$\Phi^{[4]}$
−2·026	+0·5489	+12·37	−119·6	+1018

The corresponding values of V^* and Λ^* are 0·9514 and 0·1865 respectively; they lead to a zero-point thermal energy of 176 cal. mole^{-1}, the potential energy of the lattice at absolute zero being 2026 cal mole^{-1} and the volume at absolute zero being 22·57 cm^3 mole^{-1}.

The first two terms of eqn. (9) give the lattice energy (Φ) and from them the successive derivatives of table 2 can be found. The last term gives the zero point thermal energy (U_z) which is needed § 3.

§ 3. CALCULATION OF GENERALIZED GRÜNEISEN CONSTANTS

Since the harmonic model which we are using is most likely to be accurate at low temperatures, we shall evaluate the averages of $[\epsilon]^{[1]}$, $[\epsilon]^{[2]}$, . . . etc. at low temperatures, and assume that these are temperature independent.

From the form of the thermal function, $f(x) = \frac{1}{2}x + \log[1 - \exp(-x)]$, and the definition, $f^{[n]} = x^n \partial^n f / \partial x^n$, it is easy to verify that sums of the type $\sum_i f^{[n]}(x_i)(x = \beta\epsilon_i)$ have two kinds of behaviour for $T \to 0$ ($\beta \to \infty$): (A) for $n = 1$ the sum is proportional to β and the high frequency part of the spectrum is important; (B) At low enough temperatures the frequency spectrum in any element of solid angle is proportional to ν^2. Therefore for $n \geqslant 2$ the sum is proportional to β^{-3} and only the low frequency part of the spectrum is important.

The 'type A' sums—involving $f^{[1]}$—are more difficult to deal with and such progress as has been made appears in the work on zero point energy due to Domb and Salter (1952). Luckily we can draw on their results for our purpose, as we shall now show.

3.1. '*Type A*' *Averages*

For any quantity η_i distributed over the vibrational modes of the crystal we define 'type A' averages—denoted by a bar—as

$$\bar{\eta} = \underset{\beta\to\infty}{\mathrm{Lt}} \left\{ \frac{\sum_i f^{[1]}(\beta\epsilon_i)\eta_i}{\beta} \bigg/ \frac{\sum_i f^{[1]}(\beta\epsilon_i)}{\beta} \right\}. \quad . \quad . \quad . \quad . \quad (10)$$

Now by eqn. (3) the zero point thermal energy is

$$U_z = \underset{\beta\to\infty}{\mathrm{Lt}} \{\textstyle\sum_i f^{[1]}(\beta\epsilon_i)/\beta\}. \quad . \quad . \quad . \quad . \quad . \quad . \quad . \quad (11)$$

Differentiate eqn. (11) successively with respect to volume and make use of the fact—noted above— that for $\beta \to \infty$ sums involving $f^{[1]}$ are of order β whereas those involving $f^{[n]}$ ($n \geqslant 2$) are of order β^{-3}. We then find that

$$V^n \frac{\partial^n U_z}{\partial V^n} = \underset{\beta\to\infty}{\mathrm{Lt}} \{\textstyle\sum f^{[1]}(\beta\epsilon_i)[\epsilon_i]^{[n]}/\beta\}. \quad . \quad . \quad . \quad . \quad (12)$$

Finally, combine eqns. (10), (11) and (12), and we have

$$\overline{[\epsilon]^{[n]}} = \frac{V^n}{U_z} \frac{\partial^n U_z}{\partial V^n}. \quad . \quad . \quad . \quad . \quad . \quad . \quad . \quad . \quad (13)$$

Equation (13) allows us to calculate the 'type A' average values which we now choose for the first terms on the right side of eqn. (6). To do this we differentiate the expression for U_z obtainable from eqn. (9). The results are given in table 3. Since the Domb–Salter approximation for U_z depends on the second moment of the spectrum, 'type A' averages are likely to be better at high temperatures.

Table 3. 'Type A' Averages of eqn. (10) Calculated from eqns. (13) and (9)

$\overline{[\epsilon]^{[1]}} = -3{\cdot}109$	$\overline{[\epsilon]^{[2]}} = +10{\cdot}02$	$\overline{[\epsilon]^{[3]}} = -45{\cdot}36$	$\overline{[\epsilon]^{[4]}} = +234{\cdot}3$

3.2. '*Type B*' *Averages*

We turn now to the other terms on the right of eqn. (6). For these we adopt a method due to Born (1923) and used by Barron. He has observed that the appropriate low-temperature averages involving $f^{[n]}(n \geqslant 2)$ for a quantity $\theta_{i\Omega}$ depending on the acoustic mode and on the direction of propagation of the long waves are defined by

$$\langle \theta \rangle = \sum_{i=1}^{3} \iint \theta_{i\Omega} v^{-3}{}_{i\Omega}\, d\Omega \Big/ \sum_{i=1}^{3} \iint v^{-3}{}_{i\Omega}\, d\Omega, \qquad (14)$$

where $v_{i\Omega}$ is the velocity of the ith acoustic mode ($i = 1, 2, 3$) in the direction Ω. We call these the 'type B' (B for Born) averages.

Taking into account only nearest neighbours, it may be shown that the velocities of long waves are given by

$$\frac{m}{2a^2} v_i^2 = r^2 \phi''(r^2) b_i + \phi'(r^2), \qquad (15)$$

where b is an eigenvalue of

$$b_{rs} = \tfrac{1}{2}\delta_{rs} + \cos \alpha_r \cos \alpha_s (1 - \tfrac{1}{2}\delta_{rs}), \qquad (16)$$

$\cos \alpha_s$ being the direction cosines of the propagation vector. It follows that

$$[\epsilon_i]^{[1]} = \frac{V}{\epsilon_i} \frac{\partial \epsilon_i}{\partial V} = \frac{3}{4} \frac{r^2}{v_i^2} \frac{\partial V_i^2}{\partial r^2}. \qquad (17)$$

If we choose as reference volume that corresponding to minimum intermolecular potential†, then $\phi'(r^2) = 0$ and (15) becomes

$$[\epsilon_i]^{[1]} = \frac{3}{4} \left\{ r^2 \frac{\phi'''(r^2)}{\phi''(r^2)} + 1 + 1/b_i \right\}. \qquad (18)$$

This quantity and its 'type B' average has been found by Barron. By continuing the differentiation of (17) one can form expressions for every combination of ϵ appearing on the right side of eqn. (6); the formulae are analogous to (18) but more complex. They are given in Appendix I. The main point is that they involve derivatives of the potential of the type

$$F_n \equiv \frac{r^{2(n-1)} \phi^{(n)}(r^2)}{\phi''(r^2)}$$

evaluated where $\phi'(r^2) = 0$. These are listed in table 4 for the potential function of § 2.

---

† This is not the same choice as was made in evaluating 'type A' averages; the effect of this inconsistency is being investigated.

In carrying out the averages it is necessary to evaluate the integrals

$$I_n \equiv \iint \sum_{i=1}^{3} b_i^{-(n+3/2)}\, d\Omega \Big/ \iint \sum_{i=1}^{3} b_i^{-3/2}\, d\Omega.$$

These can be found with the help of values of b_i tabulated by Barron and Domb (1955). The results are shown in table 4.

With these results and the formulae of Appendix I we may compile the 'generalized Grüneisen constants' as the 'type B' averages of table 5.

Comparing tables 3 and 5 we note the good agreement between averages derived by methods A and B. This means that to a good approximation we may take the same averages both at high and low temperatures. Hence the approximation of replacing the individual values of $[\epsilon]^{[1]}$, etc. by constants is not unreasonable.

Table 4. Values of F_n and I_n (see text) Evaluated where $\phi'(r^2)=0$

	F_n	I_n
$n=1$	$-\ 12$	2·72
$n=2$	$+\ 128$	8·097
$n=3$	$-\ 1400$	25·47
$n=4$	$+16240$	83

Table 5. 'Type B' Averages Defined by eqn. (14), Calculated from Formulae of Appendix I

$\langle[\epsilon]^{[1]}\rangle = -2{\cdot}760$	$\langle[\epsilon]^{[2]}\rangle = 9{\cdot}082$	$\langle[\epsilon]^{[3]}\rangle = -40{\cdot}20$	$\langle[\epsilon]^{[4]}\rangle = 202{\cdot}8$
$\langle[\epsilon]^{[1]2}\rangle = 7{\cdot}692$	$\langle[\epsilon]^{[1]}[\epsilon]^{[2]}\rangle = -25{\cdot}27$	$\langle[\epsilon]^{[1]}[\epsilon]^{[3]}\rangle = 111{\cdot}5$	
$\langle[\epsilon]^{[1]3}\rangle = -21{\cdot}66$	$\langle[\epsilon]^{[1]2}[\epsilon]^{[2]}\rangle = 70{\cdot}84$		
$\langle[\epsilon]^{[1]4}\rangle = 61{\cdot}64$	$\langle[\epsilon]^{[2]2}\rangle = 82{\cdot}66$		

§ 4. CALCULATION OF THERMAL FUNCTIONS

The remaining functions required in eqn. (6) involve successive derivatives of the function

$$f(x) = \tfrac{1}{2}x + \log\,[1-\exp\,(-x)], \quad \text{viz.} \quad f^{[n]}(x) \equiv x^n f^{(n)}(x).$$

These may be written in the form

$$\left.\begin{aligned} f^{[1]}(x) &= \tfrac{1}{2}x + \frac{x}{e^x-1}, \\ f^{[n+1]}(x) &= (-)^n \frac{x^{n+1}\sum\limits_{\omega=1}^{n} c_n^{\,\omega} e^{\omega x}}{(e^x-1)^{n+1}} \qquad (n \geqslant 1), \\ \text{where} \qquad c_n^{\,\omega} &= c_n^{\,n-\omega+1} \qquad (1 \leqslant \omega \leqslant n) \\ &= (-)^\omega \sum_{j=1}^{n} (-)^j \binom{n-j}{n-\omega} j!\; s_n^{\,j}, \end{aligned}\right\} \quad . \quad . \quad . \quad (19)$$

and s_n^j are Stirling numbers of the second kind tabulated, for example, by Jordan (1950, p. 170). This result is proved in Appendix II.

Some values of c_n^ω are given in table 6.

Table 6. Values of c_n^ω Defined by

$$(-)^n(e^x-1)^{n+1}d^{n+1}f/dx^{n+1}=\sum_{\omega=1}^{n} c_n^\omega \text{ where } f(x)=\tfrac{1}{2}x+\log\left[1-\exp(-x)\right]$$

$n+1$	n	$\omega=1$	2	3	4	5	6	7	8	9
2	1	1								
3	2	1	1							
4	3	1	4	1						
5	4	1	11	11	1					
6	5	1	26	66	26	1				
7	6	1	57	302	302	57	1			
8	7	1	120	1191	2416	1191	120	1		
9	8	1	247	4293	15619	15619	4293	247	1	
10	9	1	502	14608	88234	156190	88234	14608	502	1

From this table it follows, for example, that

$$f^{[4]}(x)=-x^4\{e^x+4e^{2x}+e^{3x}\}/(e^x-1)^4.$$

Graphs showing $(-)^n f^{[n+1]}/n!$ are drawn in fig. 1.

Table 7. The Summed f-functions: Values of S_n (Θ/T) (eqn. (20)). Values of $f^{[n]}$ from fig. 1; $G(\Lambda)$ from Leighton (1948) with $\gamma/\alpha=-0{\cdot}067$ (argon); ($\Theta=44{\cdot}51$°K for argon)

Θ/T	S_0	S_1	S_2	S_3	S_4
0·00	$-\infty$	2·954	2·954	5·908	17·72
0·20	−4·040	2·974	2·935	5·908	17·72
0·45	−1·607	3·049	2·860	5·903	17·73
0·55	−0·990	3·096	2·815	5·898	17·73
0·75	−0·013	3·216	2·704	5·875	17·75
1·00	+0·934	3·411	2·531	5·813	17·78
1·25	+1·724	3·655	2·332	5·701	17·80
1·50	+2·415	3·938	2·120	5·532	17·79
2·00	+3·637	4·609	1·694	5·029	17·47
2·50	+4·750	5·383	1·312	4·373	16·60
3·00	+5·803	6·228	0·998	3·671	15·19
3·50	+6·828	7·120	0·752	3·004	13·40
4·50	+8·841	8·987	0·427	1·927	9·77
9·00	+17·75	17·765	0·052	0·277	1·75

In eqn. (6) we need the sums $\sum_i f^{[n]}(\beta\epsilon_i)$ taken over the energy eigenvalues of the lattice. Leighton (1948) has calculated a normalized distribution of energy eigenvalues in terms of the dimensionless parameter Λ, where the energy is $\epsilon=\frac{1}{2}\epsilon_{\max}\Lambda(0\leqslant\Lambda\leqslant 2)$ and $\epsilon_{\max}$ is a parameter determined by the force constants of the lattice. Denoting this distribution by $G(\Lambda)$, the sums in eqn. (6) involve

$$S_n\left(\frac{\Theta}{T}\right) \equiv \int_0^2 f^{[n]}\left(\frac{\Theta\Lambda}{T}\right) G(\Lambda)\, d\Lambda \qquad . \quad . \quad . \quad . \quad (20)$$

where instead of $\epsilon_{\max}$ we now use the parameter $\Theta \equiv \epsilon_{\max}/2k$. $\epsilon_{\max}$ is in fact given by

$$\epsilon_{\max} = 2\frac{h}{\pi}\left(\frac{\alpha}{2m}\right)^{1/2}$$

where m is the atomic mass; and $G(\Lambda)$ has been obtained by Leighton

Fig. 1

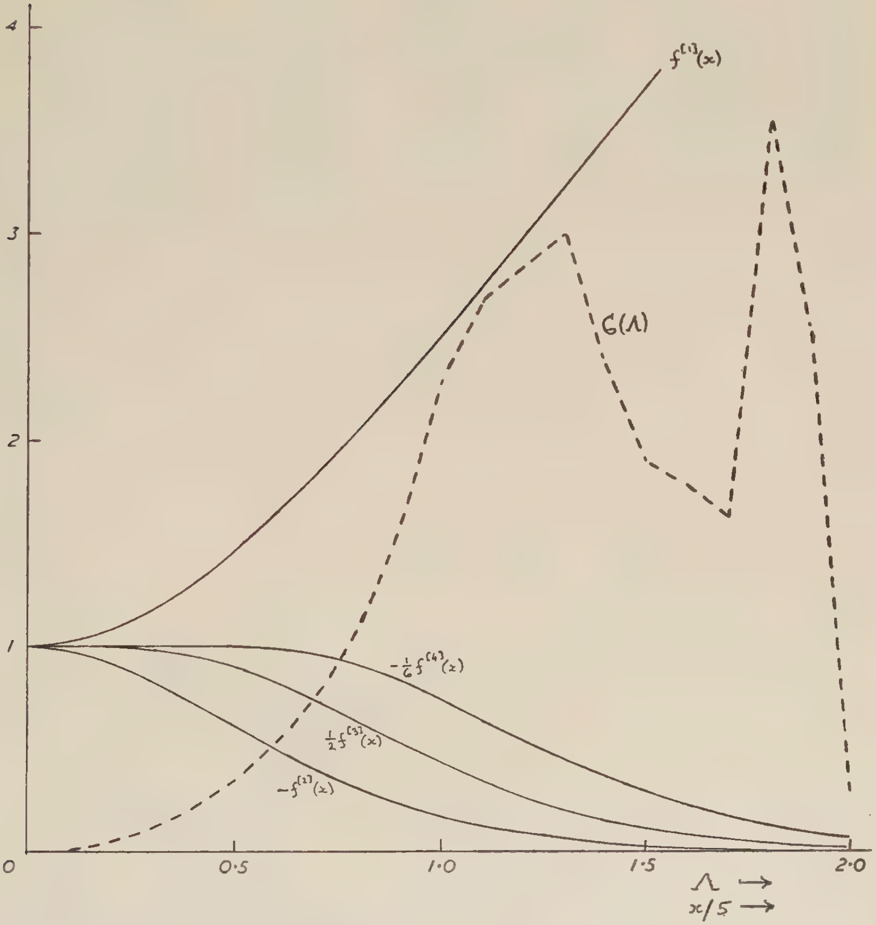

Graphs of the thermal functions (eqn. (19)) and frequency distribution (eqn. (20)). Plotted are $(-1)^{n-1}f^{[n]}(x)/(n-1)!$ (against $x/5$) and $G(\Lambda)$ (against Λ).

for two values of the force constant γ/α. For argon $\alpha = a_0 c_{44}$, $\gamma = (a_0/4)(c_{11} - c_{12} - c_{44})$ where, by using the work of Salter (1954), one may calculate $c_{11} = 3{\cdot}59 \times 10^{10}$ dyne cm^{-2}, $c_{12} = 2{\cdot}04 \times 10^{10}$ dyne cm^{-2} and $c_{44} = 2{\cdot}12 \times 10^{10}$ dyne cm^{-2}. Hence, with a_0 from eqn. (8), $\gamma/\alpha = -0{\cdot}067$ and $\Theta = 44{\cdot}51$°K. The corresponding curve for $G(\Lambda)$ is shown dotted on fig. 1.

Values of $S_n(\Theta/T)$ are given in table 7.

§ 5. THE FREE ENERGY AND OTHER THERMODYNAMIC PROPERTIES OF SOLID ARGON

With the help of the summed f-functions (table 7), the generalized Grüneisen constants (tables 3 and 5) and the derivatives of the lattice energy Φ (table 2) we may now tabulate the values of the coefficients A_r (eqn. (6)) which determine the free energy. This is done in table 8. Finally, by differentiation in accordance with eqn. (1), we may compute the thermodynamic coefficients C_p, α and κ. These are displayed, together with experimental results and the results of certain other calculations on figs. 2–5.

Fig. 2

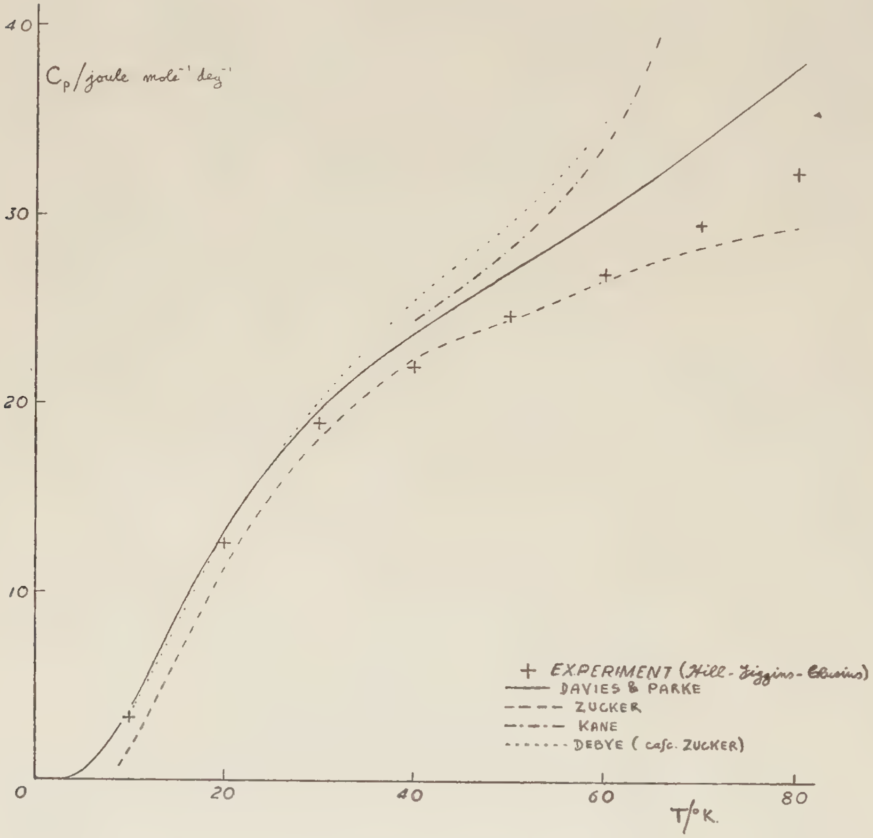

The specific heat of solid argon at constant pressure (C_p) as a function of temperature (T).

+ experimental points obtained from a smooth curve drawn through the results of Hill *et al.* (see Dobbs and Jones 1957).

——the generalized Grüneisen theory of this paper (calculated from eqns. (1) and (5) with the help of table 8).

– – –anharmonic calculations of Zucker (1958).

—.—.—.—harmonic theory of Kane (1939).

. . . . . .calculation based on Debye's model (Zucker 1958).

Table 8. The Expansion of the Free Energy: Values of A_r/β (see eqn. (6)) found from Tables 2, 3, 5 and 7. (The Potential Energy Contribution to A_r is $\beta\Phi^{(r)}$, see Table 2.)

Θ/T	T(°K)	A_0/β	A_1/β	A_2/β in kcal mole^{-1}	A_3/β	A_4/β
∞	0	−1·852	+0·0067	14·12	−127·5	1059
9·0	4·94	−1·852	+0·0063	14·12	−127·5	1059
4·5	9·89	−1·853	0	14·08	−127·8	1058
3·5	12·74	−1·854	−0·0103	14·03	−127·9	1059
3·0	14·84	−1·856	−0·0218	13·98	−128·0	1059
2·5	17·80	−1.858	−0·0430	13·92	−128·0	1060
2·0	22·25	−1·866	−0·0846	13·84	−127·9	1061
1·6	20·67	−1·884	−0·1728	13·74	−127·7	1060
1·25	35·60	−1·905	−0·2547	13·69	−127·5	1058
1·00	44·51	−1·944	−0·3888	13·67	−127·4	1055
0·75	59·34	−2·028	−0·6296	13·72	−127·6	1051
0·55	80·92	−2·186	−0·9984	13·88	−128·4	1048

Fig. 3

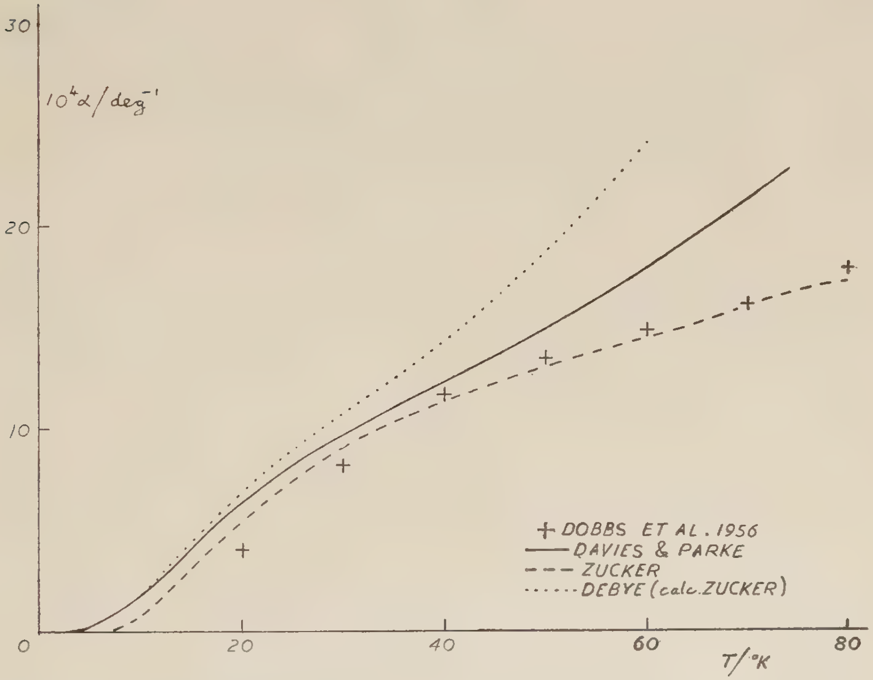

The variation with temperature (T) of the expansivity (α) of solid argon.
+ experimental results of Dobbs *et al.* (1956).
———evaluated from the theory (eqns. (1) and (5) and table 8).
– – – –anharmonic calculation (Zucker 1958).
......harmonic (Debye) theory (Zucker 1958).

Fig. 4

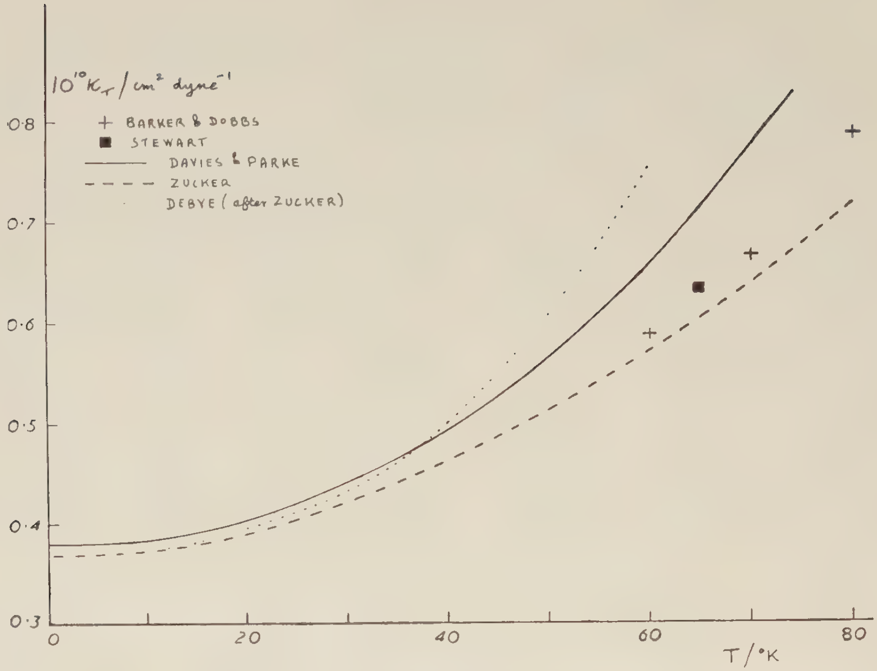

The variation of isothermal compressibility (κ_T) with temperature (T) at zero pressure.

+ experimental results of Barker and Dobbs (1955).
■ experimental result of Stewart (1956) at 65°K.
———the harmonic theory of this paper.
– – –anharmonic calculation (Zucker 1958).
. . . . . .Debye-type calculation (Zucker 1958).

Fig. 5

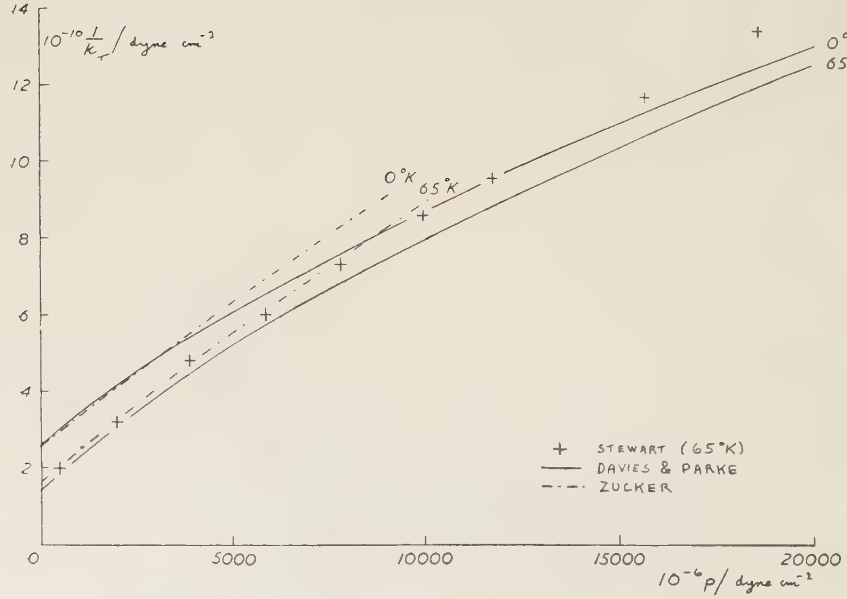

The isothermal bulk modulus ($1/\kappa_T$) as a function of pressure (p).
+experimental results of Stewart (1956) at 65°K.
———the generalized Grüneisen theory of this paper,
–·–·–anharmonic calculation (Zucker 1958).

§ 6. A DIRECT ESTIMATE OF THE SECOND GRÜNEISEN CONSTANT FROM EXPERIMENTAL DATA

In the work of §§ 3–5 we have obtained generalized Grüneisen constants by making reasonable theoretical estimates based on a single intermolecular potential function. It is interesting that, just as one can estimate the first Grüneisen constant, $[\epsilon]^{[1]}=[(V/\epsilon)(\partial\epsilon/\partial V)]_{\text{Av}}\equiv-\gamma$ directly from measurements of the expansivity, specific heat and compressibility, so can one estimate the second Grüneisen constant,

$$[\epsilon]^{[2]}=[(V^2/\epsilon)(\partial^2\epsilon/\partial V^2)]_{\text{Av}}\equiv\gamma'$$

(say), directly from measurements of the variation of compressibility with temperature, together with certain further information. In the case of argon we have obtained an estimate of γ' by this method which agrees satisfactorily with the theoretical estimates given earlier (tables 3 and 5).

Table 9. Experimental Values of the Quantities in eqn. (24) for Argon, using $\gamma=2{\cdot}44$ and taking Φ from the Intermolecular Potential of eqn. (7)

$T(^\circ\text{K})$	V/κ	γ^2TC_v	$V^2\dfrac{\partial^2\Phi}{\partial V^2}$	U	Φ
	(all in kcal mole^{-1})				
0	13·2	0	12·4	−1·85	−2·03
20	12·9	0·46	12·1	−1·83	−2·03
40	11·3	1·44	10·7	−1·75	−2·01
60	9·7	2·41	8·5	−1·62	−1·99
80	7·5	3·60	6·5	−1·49	−1·94

Taking the potential terms and thermal terms into the right side of eqn. (3) and making the generalized Grüneisen assumption of treating $[\epsilon]^{[1]}$ and $[\epsilon]^{[2]}$ as constants, we may eliminate the thermal functions $f^{[1]}$ and $f^{[2]}$ to obtain three independent relations.

$$\beta pV=-\beta V(\partial\Phi/\partial V)-[\epsilon]^{[1]}\beta(U-\Phi), \qquad (21)$$

$$(V/k)(\alpha/\kappa)=-[\epsilon]^{[1]}C_v/k, \qquad (22)$$

$$\beta(V/\kappa)=\beta V^2(\partial^2\Phi/\partial V^2)+[\epsilon]^{[2]}\beta(U-\Phi)-[\epsilon]^{[1]2}C_v/k. \qquad (23)$$

Equations (21) and (22) are familiar results. Equation (23) is less familiar and is the one that we wish to use. It may be rewritten for convenience as

$$V/\kappa=V^2(\partial^2\Phi/\partial V^2)-\gamma^2C_vT+\gamma'(U-\Phi). \qquad (24)$$

Using the sources cited earlier we have obtained V, κ, C_v and U from experimental results, we have assumed the first Grüneisen constant to be 2·44 (which is the mean of the four values of γ given by Dobbs and Jones (1957), Appendix III, for $T=20^\circ\text{K}$, 40°K, 60°K and 80°K) and we have calculated Φ and $V^2(\partial^2\Phi/\partial V^2)$ from the intermolecular potential used earlier. The results are given in table 9.

A graph combining these results is shown in fig. 6. From it we estimate $\gamma' = [\epsilon]^{[2]} = 11{\cdot}2 \pm 1{\cdot}0$. This value may be compared with the theoretical estimates given earlier: 'type A' averages gave $[\epsilon]^{[2]} = 10{\cdot}0$ and 'type B' averages gave $[\epsilon]^{[2]} = 9{\cdot}1$. The value obtained for γ' by the method we have just used depends sharply on the value adopted for γ. Thus if we had used the value $\gamma = 2{\cdot}8$ (which is close to Barron's—and our—'type B' average) we would find $\gamma' = 14{\cdot}5 \pm 1{\cdot}0$.

Fig. 6

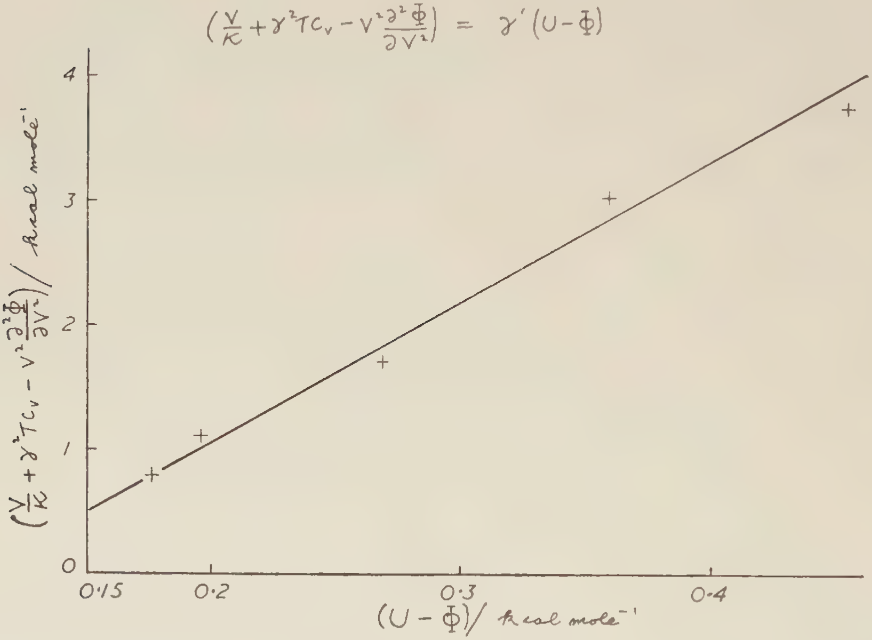

Test of the relation $\frac{V}{\kappa_T} = V^2\frac{\partial^2\Phi}{\partial V^2} - \gamma^2 T C_v + \gamma'(U-\Phi)$ for $\gamma = 2{\cdot}44$. Φ is the lattice energy (§ 2). γ is the 'first' Grüneisen constant $\left(= \left\langle -\frac{V}{\epsilon}\cdot\frac{\partial\epsilon}{\partial V}\right\rangle_{\text{Av}}\right)$ and γ' is the second Grüneisen constant $\left(= \left\langle \frac{V^2}{\epsilon}\cdot\frac{\partial^2\epsilon}{\partial V^2}\right\rangle_{\text{Av}}\right)$. (See §§ 1 and 6.) The remaining quantities are obtained from experiments (Dobbs and Jones 1957).

The slope of the line yields $\gamma' = 11{\cdot}2 \pm 1{\cdot}0$.

§ 7. Conclusions

The main results of the calculations, as displayed on figs. 2–5, show that our generalized Grüneisen theory is in reasonable agreement with experimental results on argon from absolute zero up to about 40°K. Above this temperature it is definitely inferior to the theory of Zucker. This is perhaps not surprising because our theory gives only a partial account of anharmonicity; in effect we have assumed harmonic modes of vibration, with frequencies depending parametrically on the volume. Zucker on the other hand deals with an anharmonic, one-atom model so that it is not surprising that his theory is less successful at low temperatures.

In favour of our theory is that, now that the main calculations of 'type B' averages and thermal f-functions have been made, it can be extended to deal with other rare gases. Certain other extensions (e.g. to anisotropic crystals) are also possible.

The γ values obtained by us are: 3·11 ('type A') and 2·76 ('type B'). It is not surprising that the latter is close to Barron's value of 2·82 because our method of averaging is the same as his. Zucker obtains $\gamma=2{\cdot}8$, while Dobbs and Jones quote experimental values in the range 2·4–2·8.

Our three estimates of the second Grüneisen constant,

$$\gamma' = [(V^2/\epsilon)(\partial^2\epsilon/\partial V^2)]_{\mathrm{Av}},$$

are: 10·0 ('type A'), 9·1 ('type B') and 11·2 (from experiment, see § 6). It seems reasonable to conclude that γ' is a new approximate 'constant' (like γ) with a value near to 10 for argon. This 'constant' has not previously been discussed and estimated. It clearly constitutes a second measure of anharmonicity (γ is the first) and it would be interesting to investigate its value in other systems.

APPENDIX I

To carry out the calculations of 'type B' averages in § 3 and other manipulations of the type discussed here, there are some elementary formulae which are of great value.

Let $f(x)$ be any differentiable function of x. Denote the type of differentiation by superscripts as follows:

$$f^{(n)} \equiv \frac{\partial^n f}{\partial x^n}\,;\quad f^{[n]} \equiv x^n \frac{\partial^n f}{\partial x^n}\,;\quad f^{\{n\}} = \frac{\partial^n f}{\partial(\ln x)^n} \qquad . \quad . \quad . \quad (25)$$

and denote the type of function to be differentiated by brackets:

$$(f)^{(n)} \equiv f^{(n)} = \frac{\partial^n f}{\partial x^n}\,;\quad [f]^{(n)} = \frac{1}{f}\frac{\partial^n f}{\partial x^n}\,;\quad \{f\}^{(n)} = \frac{\partial^n \ln f}{\partial x^n}. \qquad . \quad . \quad (26)$$

Thus the symbolism admits nine types of nth derivatives. The conversion from ( ) to [ ] in either of the rows (25) and (26) is immediate:

$$f^{[n]} = x^n f^{(n)}\,;\quad (f)^{(n)} = f[f]^{(n)}. \qquad . \quad . \quad . \quad . \quad . \quad . \quad . \quad (27)$$

The conversion from [ ] to { } is more complicated and the relevant formulae are:

$$\left.\begin{aligned}
f^{[1]}&=f^{\{1\}},\\
f^{[2]}&=f^{\{2\}}-f^{\{1\}},\\
f^{[3]}&=f^{\{3\}}-3f^{\{2\}}+2f^{\{1\}},\\
f^{[4]}&=f^{\{4\}}-6f^{\{3\}}+11f^{\{2\}}-6f^{\{1\}},
\end{aligned}\right\}\quad . \quad . \quad . \qquad (28)\dagger$$

$$\left.\begin{aligned}
f^{\{1\}}&=f^{[0]},\\
f^{\{2\}}&=f^{[2]}+f^{[1]},\\
f^{\{3\}}&=f^{[3]}+3f^{[2]}+f^{[1]},\\
f^{\{4\}}&=f^{[4]}+6f^{[3]}+7f^{[2]}+f^{[1]}.
\end{aligned}\right\}\quad . \quad . \quad . \qquad (29)\dagger$$

The results of (28) and (29) are *true for all forms of the function being differentiated.*

$$\left.\begin{aligned}
\{f\}^{(1)}&=[f]^{(1)},\\
\{f\}^{(2)}&=[f]^{(2)}-[f]^{(1)2},\\
\{f\}^{(3)}&=[f]^{(3)}-3[f]^{(1)}[f]^{(2)}+2[f]^{(1)3},\\
\{f\}^{(4)}&=[f]^{(4)}-4[f]^{(1)}[f]^{(3)}-3[f]^{(2)2}+12[f]^{(1)2}[f]^{(2)}-6[f]^{(1)4},
\end{aligned}\right\}\quad . \qquad (30)\ddagger$$

$$\left.\begin{aligned}
[f]^{(1)}&=\{f\}^{(1)},\\
[f]^{(2)}&=\{f\}^{(2)}+\{f\}^{(1)2},\\
[f]^{(3)}&=\{f\}^{(3)}+3\{f\}^{(1)}\{f\}^{(2)}+\{f\}^{(1)3},\\
[f]^{(4)}&=\{f\}^{(4)}+4\{f\}^{(1)}\{f\}^{(3)}+3\{f\}^{(2)2}+6\{f\}^{(1)2}\{f\}^{(2)}+\{f\}^{(1)4}.
\end{aligned}\right\}\quad . \qquad (31)\ddagger$$

The results of (30) and (31) are *true for all types of differentiation.*

With the help of eqns. (26)–(31) we can easily make conversions between any of the nine types of derivative. Thus one can form the expressions required for $[\epsilon]^{[2]}$, $[\epsilon]^{[1]2}$, etc. in eqn. (6) in terms of the derivatives of ϕ in eqn. (15).

APPENDIX II

To prove the formulae of (19) for the nth derivative of

$$f(x)=\tfrac{1}{2}x+\log\,[1-\exp(-x)],$$

set $e^{x}=u$, $e^{-x}=v$ so that

$$\frac{d}{dx}=\frac{d}{d\ln u}=-\frac{d}{d\ln v}.$$

---

† The coefficients in (28) and (29) are Stirling numbers of the first and second kind respectively; see Appendix II.

‡ Equations (30) and (31) are familiar to statisticians as giving, respectively the conversion from cumulants to moments and *vice versa* (see Kendall (1947), p. 62).

Now differentiating n times the formula

$$f^{(1)}(x)=\tfrac{1}{2}+\frac{1}{u-1}=-\tfrac{1}{2}+\frac{1}{1-v} \quad . \quad . \quad . \quad . \quad . \quad (32)$$

we have

$$f^{(n+1)}(x)=\frac{d}{d(\ln u)^n}\left(\frac{1}{u-1}\right)=(-)^n\frac{d}{d(\ln v)^n}\left(\frac{1}{1-v}\right). \quad . \quad . \quad (33)$$

Invoking one of the main properties of Stirling numbers of the second kind $s_n^{\ j}$ (see Jordan, 1950), viz.

$$\frac{d^n}{d(\ln u)^n}=\sum_{j=1}^{n} s_n^{\ j} u^j \left(\frac{d}{du}\right)^j \quad . \quad . \quad . \quad . \quad . \quad . \quad . \quad (34)$$

we therefore have

$$f^{(n+1)}(x)=\frac{\sum_{j=1}^{n} s_n^{\ j} u^j (-)^j j!\,(u-1)^{n-j}}{(u-1)^{n+1}}. \quad . \quad . \quad . \quad . \quad (35)$$

$$=\frac{\sum_{j=1}^{n} (-)^n s_n^{\ j} v^j j!\,(1-v)^{n-j}}{(1-v)^{n+1}} \quad . \quad . \quad . \quad . \quad (36)$$

or, finally, writing $v=1/u$ in (36),

$$f^{(n+1)}(x)=\frac{\sum_{j=1}^{n} (-)^n s_n^{\ j} j!\,(u-1)^{n-j} u}{(u-1)^{n+1}}. \quad . \quad . \quad . \quad . \quad (37)$$

Equation (37) is virtually the same as (19) of the text and comparing it with (35) we see immediately the symmetry relation $c_n^{\ \omega}=c_n^{\ n-\omega+1}$ among the coefficients; because of this relation it is necessary to work out the c_n only for $\omega=1, 2, \ldots [n+1/2]$—as is clear from table 6.

ACKNOWLEDGMENTS

We wish to thank Professor G. O. Jones for helping us, Dr. E. R. Dobbs for making results available to us before publication, Dr. E. H. Sondheimer for constructive remarks on the subject of Appendix II and Mr. L.Finegold for providing us with some numerical data.

One of us (S. P.) wishes to thank the Ministry of Education for a research grant.

REFERENCES

BARKER, J. R., and DOBBS, E. R., 1955, *Phil. Mag.*, **46,** 1069.
BARRON, T. H. K., 1955, *Phil. Mag.*, **46,** 720.
BARRON, T. H. K., and DOMB, C., 1955, *Proc. roy. Soc.* A, **227,** 447.
BORN, M., 1923, *Atomtheorie des Festen Zustandes* (Berlin: Teubner).
BORN, M., and HUANG, K., 1954, *Dynamical Theory of Crystal Lattices* (Oxford : Clarendon Press).
CLUSIUS, K., 1936, *Z. phys. Chem.*, B **31,** 459.

Dobbs, E. R., Figgins, B. F., Jones, G. O., Piercey, D. C., and Riley, D. P., 1956, *Nature, Lond.*, **178,** 483.

Dobbs, E. R., and Jones, G. O., 1957, *Rep. Progr. Phys.*, **20,** 516.

Domb, C., and Salter, L., 1952, *Phil. Mag.*, **43,** 1083.

Domb, C., and Zucker, I. J., 1956, *Nature, Lond.*, **178,** 484.

Grüneisen, E., 1926, *Handbuch der Physik*, Vol. X (Berlin: Springer), p. 1.

Henkel, J. H., 1955, *J. chem. Phys.*, **23,** 681.

Hirschfelder, J. O., Curtiss, C. F., and Bird, R. B., 1954, *Molecular Theory of Gases and Liquids* (New York: Wiley).

Jordan, C., 1950, *Calculus of Finite Differences* (New York: Chelsea).

Kane, G., 1939, *J. chem. Phys.*, **7,** 603.

Kendall, M. G., 1947, *The Advanced Theory of Statistics*, Vol. I (London: Griffin).

Leighton, R. B., 1948, *Rev. mod. Phys.*, **20,** 165.

Salter, L., 1954, *Phil. Mag.*, **45,** 360.

Stewart, J. W., 1955, *Phys. Rev.*, **97,** 578; 1956, *J. Phys. Chem. Solids*, **1,** 146.

Zucker, I. J., 1956, *J. chem. Phys.*, **25,** 915; 1958, *Ph.D. Thesis*, University of London.

The Electromechanical Properties of Barium Titanate†

By H. L. ALLSOPP‡ and D. F. GIBBS
H. H. Wills Physics Laboratory, University of Bristol

[Received September 2, 1958]

ABSTRACT

Measurements in the form of oscillograms have been made of the electric field E, the electric displacement D, and the strain x, on both single crystal and ceramic barium titanate over a wide temperature range. Below the Curie point results depend strongly on the type of sample, and are given an interpretation in terms of domain change and piezoelectric mechanisms. Above the Curie temperature all specimens show electrostrictive behaviour with a coefficient Q_{33} which within experimental error is independent of specimen type, temperature, and applied field.

§ 1. INTRODUCTION

IT is well known that barium titanate exhibits strong electromechanical effects which may be classed with some difficulty as piezoelectric or electrostrictive. A general review has been given by Kay (1955), but there have been rather few experimental results published in which the strain has been measured directly, the work of Caspari and Merz (1950) and Schmidt (1956) being notable here. The investigations to be described in this paper have some affinity to those of Schmidt; the strain gauge used has already been described (Allsopp and Gibbs 1957).

Briefly, a single crystal or ceramic specimen, with coated electrodes, is mounted in a temperature controlled enclosure so that signals proportional to the field E, the electrical displacement D, and the strain x can be obtained and displayed on a cathode-ray tube, there being facilities for the absolute measurement of each variable. In general the calibration factors of the apparatus are known to a precision of better than $\pm 1\%$, but in many cases the overall accuracy is worse than this owing to greater uncertainty in the dimensions of the specimen and its electrodes, or in the case of very small strains, owing to a poor signal to noise ratio.

Any pair of variables can be selected to give X and Y deflections, thus giving three types of figure: D/E, x/E and x/D, and these can be photographed.

For most observations the voltage applied to the specimen had a frequency of 5 c/s, this low frequency being desirable mainly to avoid mechanical resonances in the strain measuring system.

The electrodes covered the whole of the large faces, and in preliminary experiments the crystal was supported under light spring tension between two metal balls of radius 1 mm which were mechanically connected to the strain gauge, so that a local, and not average, value of the strain was displayed. In contrast to this, the electric field was presumably uniform (apart from the effects of twinning), and the displacement signal proportional to integrated current, thus being a volume average over the crystal. The effect of the thrust of the supports on the crystal's behaviour was thought to have been obviated in later experiments, and some averaging of the strain obtained, by the use of soft leather pads as supports. The evidence for this is that the figures then remained nearly the same over a wide range of spring tensions, which was not the case with the metal ball supports.

---

† Communicated by the Authors.

‡ Now at Bernard Price Geophysical Institute, University of Witwatersrand, Johannesburg.

§ 2. RESULTS WITH SINGLE CRYSTALS

2.1. *Ideal Model*

In order to interpret the results, it is convenient first to recall what might be expected from the simplest ideal crystal. Here we consider a ' c-domain ' crystal in the form of a thin plate with the polarization vector everywhere normal to the large surfaces, and assume that the polarization suddenly reverses throughout the crystal when the applied field passes through the coercive value E_c. The D/E figure is the familiar idealized hysteresis loop of fig. 1 (*a*). Assuming that the crystal behaves in a simple piezoelectric manner and that the piezoelectric coefficient d_{33} reverses its apparent sign with domain reversal, it is clear that the x/E and x/D figures shown in figs. 1 (*b*) and 1 (*c*) would result.

Fig. 1

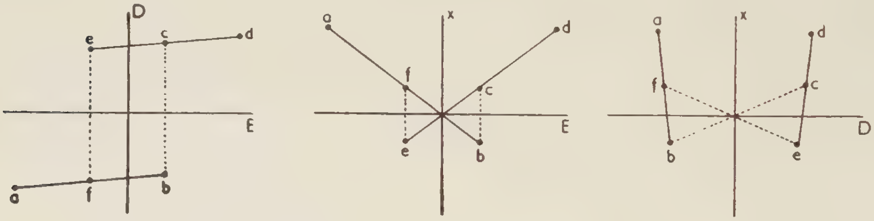

(*a*) (*b*) (*c*)

Ideal D/E, x/E and x/D figures for c-domain crystal. Paths during switching are shown dotted.

2.2. *Results at Room Temperature*

Crystals which, as grown, approached the ideal ' all c-domain ' configuration were selected by examination under polarized light. These will be referred to as ' group II ' crystals. A typical set of figures obtained with these is shown in fig. 2 (Pl. 47), in which the peak applied field increases progressively from (*a*) to (*e*).

The major qualitative deviations from the ideal of these group II crystals may be listed as follows:

(i) At low fields, where the peak value of E is less than the value of E_c obtained from a large field loop, there is often marked asymmetry in the figures, though the D/E figures do not resemble the straight lines expected of a single c-domain or a mixture of antiparallel c-domains.

(ii) Although the values of saturation polarization may be high (typically 20–24 μc/cm^2), hysteresis persists out to the tip of the D/E figures.

(iii) The cross over at the base of the x/D figures is not as clear-cut as in the ideal.

(iv) Even at the highest fields which it is possible to apply without breakdown, the tips of the x/E figures are still curved and have not turned into the straight lines expected of a simple single c-domain.

When crystals which optically show a greater degree of twinning (group I) are examined, these deviations become on the whole more marked, as typified in fig. 3 (Pl. 48). In addition:

(v) The strain obtained when the peak applied field is less than E_c is extremely small.

(vi) The x/D figures are more rounded at the base and less steep at the sides, though the sides remain approximately straight.

It thus seems that even the best available group II crystals, at least without special treatment, show marked qualitative deviation from the simple ideal of § 2.1. There are also quantitative deviations, and since these throw light on the performance of the crystals, we now consider three possible simplified mechanisms for which a rough value of the slopes of the x/D figures can be estimated.

2.3.

2.3.1. *Single domain piezoelectric model*

This is what has been assumed in the saturated regions of fig. 1. We have

$$\frac{\partial x}{\partial E}=d_{33}$$

by definition, and hence

$$\frac{\partial x}{\partial D}=d_{33}/\epsilon_3,$$

where ϵ_3 is the c-axis dielectric constant. These equations should thus give the slopes of the appropriate parts of the x/e and x/D figures if complete saturation is reached. A value of $2{\cdot}5\times10^{-6}$ e.s.u. for d_{33} may be deduced from the measurement of d_{31} by Caspari and Merz (1950) if, following these authors, we take $d_{33}/d_{31}=-2{\cdot}3$. Substituting $\epsilon_3=200$ (Merz 1953) we then have

$$\frac{\partial x}{\partial D}=1{\cdot}25\times10^{-8}\,\text{e.s.u.}$$

This process will be referred to as the p-mechanism.

2.3.2. 180° *rotation model*

This corresponds to the switching regions of fig. 1. Since d_{33} reverses sign under a field E_c, the resultant change in strain is $2d_{33}E_c$, and the corresponding polarization change is $2P_s$ or twice the saturation polarization. Since $D=4\pi P+E$, the slope of the x/D figure which corresponds to this mechanism is given by

$$\left(\frac{\Delta x}{\Delta D}\right)_{180}=\frac{d_{33}E_{\mathrm{C}}}{4\pi P_{\mathrm{S}}}.$$

The same result is obtained if a fraction m only of the crystal is assumed to be built from reversible c-domains, the rest being unchanged, provided that a 'natural' strain x of the (unclamped) c-domain component is assumed to result in an average strain mx of the whole crystal.

If we substitute $E_{\mathrm{C}}=3$ e.s.u. (typical of group II), d_{33} as before and $P_{\mathrm{S}}=7{\cdot}5\times10^4$ e.s.u. (Merz 1953), we obtain

$$\left(\frac{\Delta x}{\Delta D}\right)_{180}=8\times10^{-12}\text{ e.s.u.}$$

This process will be called the 180-mechanism.

2.3.3. 90° *rotation model*

When a domain initially polarized at right angles to the field direction (a-domain) turns into the field direction and thus becomes a c-domain, an elongation of approximately 1% results from the tetragonality of the unit cell, and an increment of polarization equal to the domain volume times P_{S} occurs. If the crude assumption is made that it is legitimate to make a simple volume average of these quantities over the whole crystal, it is clear that the slope of the x/D figure is given by

$$\left(\frac{\Delta x}{\Delta D}\right)_{90}=\frac{\text{Strain due to rotation}}{4\pi P_{\mathrm{S}}}=1{\cdot}1\times10^{-8}\text{ e.s.u.}$$

The increment of D will in general be greater than that stated owing to the increased dielectric constant of the a-domain, so that the slope is liable to be rather lower than the above figure, especially if the switching occurs at high fields.

This process will be called the 90-mechanism.

2.4. *Comparison of these Mechanisms with Experiment at Room Temperature*

It will be observed that the slopes of the x/D figures to be expected from the p- and 90-mechanisms are nearly the same, and about one thousand times greater than that to be expected from the 180-mechanism. Thus the p- and 90-mechanisms would be difficult to distinguish by examination of the x/D figures alone, but the rate of change of x with E is likely to be very different for the two mechanisms, being a simple straight line of slope d_{33} for the p-mechanism, and probably non-linear and hysteretic for the 90-mechanism. When the 90-mechanism is dominant in producing strain, we may therefore expect a large amount of hysteresis in the x/E figures, but little in the x/D figures. The 180-mechanism is likely to give hysteresis in both figures, and the p-mechanism in neither.

Values of $(\Delta x/\Delta D)_{180}$ calculated from the switching part of the x/D figures range from about 5×10^{-11} to 5×10^{-10} e.s.u. for group II crystals, i.e. from 5 to 50 times the value calculated in § 2.3.2. It therefore appears that even in the most ideal untreated crystal available, some 90-mechanism occurs, though the amount of a-domain necessary may be only about 0·5%.

Values of the apparent d_{33} calculated from the limiting slopes of the x/E figures of group II crystals also always gave results greater by a factor of between 5 and 10 than the value of Caspari and Merz. We conclude that the 90-mechanism persists even to the highest fields.

The average of $\partial x/\partial D$ over eight crystals in the high-D region was $1{\cdot}0 \times 10^{-8}$ e.s.u., in fair agreement with either p- or 90-mechanisms, and of these crystals only one gave a value exceeding the calculated $(\Delta x/\Delta D)_{90}$, though this high value was over twice the theoretical.

Some further evidence on these interpretations is given by the results on two special crystals shown in fig. 4 (Pl. 49). Here (*a*), (*b*) and (*c*) refer to a group II crystal, (*a*) shows the effect of initial application of a field, (*b*) shows the effect of maintaining the field for two hours (little further change is brought about by field alone) and (*c*) shows the result after having raised the temperature to near the Curie point and again having cooled to room temperature, the field being maintained throughout. This set of figures seems to indicate a close approximation to the ideal with only the p- and 180-mechanisms in operation, nevertheless a quantitative examination still indicates discrepancies. The saturation polarization measured from fig. 4 (*c*) is $24 \pm 2\,\mu$c/cm^2, in satisfactory agreement with the accepted value, but the ϵ_3 from the saturated part of the D/E figure exceeds 2000, compared with the low figure of 200 obtained by Merz. The value of d_{33} calculated from the tip of the x/E figure is $5{\cdot}2 \times 10^{-6}$ e.s.u., still over twice that obtained by Caspari and Merz, while that obtained from the switching region (if assumed to be 180-mechanism) is about 25×10^{-6} e.s.u. If the Caspari and Merz d_{33} value is accepted, we must conclude that the 90-mechanism is still not completely suppressed, though the residue of a-domain is only about one part in 1000. Probably one of the factors contributing to its greater suppression in the work of Caspari and Merz is the much slower rate of change of field employed by them.

Results on a crystal showing characteristics of the opposite extreme are shown in fig. 4 (*d*), (*e*), (*f*), (*g*) (Pl. 49). This group II crystal is probably highly atypical but is of interest because of the large degree of 90-mechanism displayed. It had been subjected to two heating cycles when these results were obtained, after subsequent cycles it reverted to a condition very similar to that which produced results in fig. 4 (*a*), (*b*), (*c*). The saturation polarization in fig. 4 (*g*) was $23 \pm 2\,\mu$c/cm^2, yet the mechanism of reversal is evidently very different from that in fig. 4 (*c*). The large pendant loops in the x/E figure of fig. 4 (*g*) are believed to correspond to the 90-mechanism, and may be compared with fig. 3 (*a*) of Kay (1955). About 7% of the crystal must be converted to a-domain to account for the observed strain.

In the x/D figure, the steeply sloping sides will be seen to be made up of two parts, a heavily exposed top part corresponding to near saturation, and a lightly exposed lower part corresponding to switching. The fact that these are nearly collinear provides some confirmation of the near equality of $\partial x/\partial D$ and $(\Delta x/\Delta D)_{90}$, though the confirmation is less striking than at first appears both on account of the steepness of the slope and because the upper region probably involves a mixture of *p*- and 90-mechanisms.

To account for the small amount of hysteresis in the *x*/*D* figure of fig. 4 (*g*), it seems necessary to assume that the 90-mechanism and 180-mechanism always operate at essentially different parts of the cycle. An idealized scheme which gives results resembling those obtained is shown in fig. 5. Here it is assumed that the crystal is wholly +c-domain from 'a' to 'd', and converts to 7% a-domain at 'e'. From 'e' to 'f' the slope is greater on the *D*/*E* figure but less on the *x*/*D* figure owing to the higher dielectric constant of the a-domain component. From 'f' to 'g' the c-domain component is assumed to reverse, while from 'h' to 'i' the a-domain component also converts to reversed c-domain. In practice the various transitions are not so sharply separated.

Fig. 5

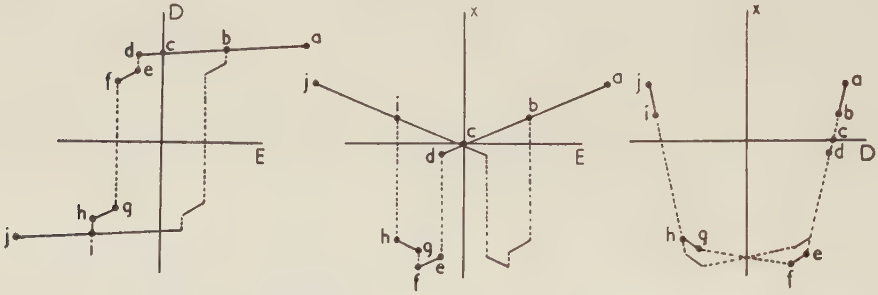

Ideal figures for crystal of fig. 4 (*d*), (*e*), (*f*), (*g*) (Pl. 49). Switching paths shown dotted.

As with other group II crystals, the strain is large even when fields less in peak value than E_c are supplied, as in fig. 4 (*d*). The crystal is here highly asymmetrical presumably being polarized mainly in the negative direction, the a-domains being formed when the field is in the positive direction.

In contrast, little strain is observed in group I crystals with fields lower than E_c, but apart from this feature, it appears that group I crystals can be understood as having the 90-mechanism dominant but spread over a wider range of field values.

2.5. *Experiments on Single Crystals at other Temperatures*

2.5.1. *Experiments below room temperature*

It has been shown by Merz (1949) that the apparent saturation polarization of a crystal suddenly decreases at each of the lower transition temperatures. The one group II crystal investigated here showed similar effects, but in contrast to Merz's results the saturation polarization also diminished continuously with decreasing temperature as shown in fig. 6. In the case of a group I crystal the decrease was continuous with no evident discontinuities, as also shown in fig. 6. It thus appears that the continuous decrease can be attributed at least in part to the gradual inhibition of domain switching mechanisms with decreasing temperature, and it is perhaps surprising that the continuous decrease was not found by Merz, whose crystal showed a room temperature P_S of 16 μc/cm^2, and must therefore have been twinned.

Fig. 6

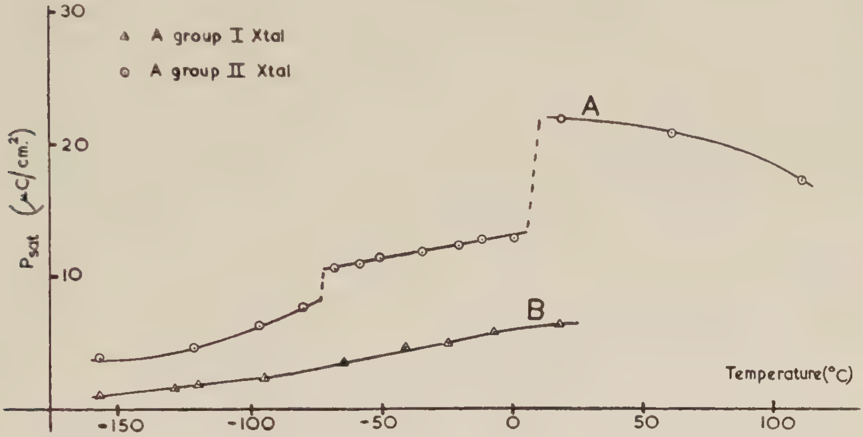

Saturation polarization of crystals as a function of temperature.

Observations of the x/E and x/D figures have also been made and these did not change greatly in shape down to a temperature of -40°c, though the attainable polarization and strain varied widely. In particular, there was little change in the slope of the steep part of the x/D loop, which seems odd in view of the change through 45° of the polarization vector at the 0°c transition, and the consequent necessary alteration of domain change mechanisms.

Below -40°c, x diminishes more rapidly than the apparent P_S, and below about -60°c the x/D figures no longer have their characteristic U shape. From -60°c to -150°c the total strain at 'saturation' polarization is about 10^{-4}, but the figures undergo complex changes which will not be pursued here as it may not be wise to generalize from the behaviour of one crystal.

2.5.2. *Experiments above room temperature*

The temperature range of greatest interest is that close to and on both sides of the Curie point, but observations in this region are sometimes made difficult either by excessive conductivity or breaking of the crystal. Results on a crystal of each group are shown in fig. 7 (Pl. 50). As would be expected, the x/E and x/D figures both become parabolic in the paraelectric region well above the Curie temperature, and a little above the Curie temperature 'double' D/E figures appear, where the crystal becomes ferroelectric only at high fields, as observed by Merz (1953). This field induced transition is more sudden in the group II crystals and is accompanied by a switching strain in the x/E figure bridging the parabolic (paraelectric) region and the more linear (ferroelectric) region.

The electrostrictive constant Q_{33} defined by $x_{33}=Q_{33}P_3{}^2$ was measured from the x/D figures above the Curie temperature and with one exception (a very thick crystal) found to be the same within experimental error for all crystals, and to be invariant with field and temperature in the range 130°–150°C. The weighted mean value was calculated as

$$Q_{33}=(6\cdot4\pm0\cdot3)\times10^{-13}\,\text{e.s.u.}$$

If it is assumed that Q_{33} varies slowly and continuously with temperature as the Curie point is traversed, and that it is not necessary to include higher order terms in the x/P relation even when ferroelectric polarization sets in, it is possible to relate the value of Q_{33} to the saturation polarization and lattice parameters (Merz 1949) and also to relate it to the piezoelectric constant d_{33} (Caspari and Merz 1950). Taking the lattice measurements of Kay and Vousden (1949) and a P_s of 18 μC/cm^2, we obtain in this way a Q_{33} of $1\cdot1\times10^{-12}$ e.s.u. just below the Curie point, in poor agreement with our directly determined value. We believe that the underlying assumptions rather than any of the measurements are at fault, most probably it is necessary to include higher order terms in the x/P relation. If this is so, calculations of d_{33} also become subject to considerable revision, quite apart from the higher value of P_s which has now become accepted.

In the region just above the Curie temperature where transitions between para- and ferroelectric phases can be field-induced, it is possible to make fairly good estimates of the switching strain Δx_c from the x/E and x/D figures of group II crystals, where the transition is sharp. Values of Δx_c of 2·2, 1·7, 1·3 and $1\cdot3\times10^{-3}$ were obtained in four experiments, which values may be compared with $3\cdot3\times10^{-3}$ calculated from the X-ray data of Kay and Vousden (1949). The apparent saturation polarization in this region has also been estimated by linear extrapolation of the extremes of the D/E figures to zero field. Values of P_s were also somewhat variable and lower than expected, being respectively 15, 11, 10 and 6 μC/cm^2. The discrepancies are thought to arise from the switching of only part of the crystal, the frequent shattering of crystals under such severe stress being understandable. Accurate temperature control is also difficult when such relatively large amounts of electrical energy are being dissipated in the crystal.

§ 3. RESULTS ON CERAMICS

A wide range of ceramic samples has been investigated, mostly in the form of discs about 1 cm in diameter and 1 mm thick. Some were as pure as possible, and others contained intentional additives. It is difficult to obtain accurate and reproducible results in many cases, partly because the behaviour of the specimens depends so much on previous history, partly because different specimens made as nearly as possible under the same conditions may differ considerably, and partly because of electrode difficulties. Preliminary experiments showed that many specimens do not undergo uniform strain when a field is applied, but may warp or 'dish' (as has been noted by Schmidt (1956)), hence the ball ended support was always used. The strain often varied by as much as 25% at different parts of the same specimen.

Owing to the high dielectric constants involved, minute gaps between the electrodes and the specimens have a very large effect. Electrodes of fired-on silver paste are generally satisfactory on dense ceramics, but in some cases the silver penetrates the body of the material appreciably, making the field non-uniform and uncertain. This difficulty was prominent with the more pure materials. Evaporated films of metal are initially good, but easily damaged. Further, their resistance is liable to become very high after heating; presumably they are broken up by relative movements of the grains when a phase change occurs. A technique of sputtering platinum, although producing good electrodes, was found to overheat and reduce the specimens.

A silver paste for cold application ('Elargol W4') was found generally satisfactory, but tended to separate from the ceramic below −60°C when strong fields were applied. A mixture of silicone grease and precipitated silver was found useful in this low temperature range, though inconvenient and of higher resistivity than the other electrodes.

3.1. *Results at Room Temperature*

Results on a number of different samples are shown in fig. 8 (Pl. 51). It will be seen that the x/D figures are roughly parabolic in form, but may differ from the ideal in that they may possess asymmetry (prepolarization), flattening of the vertex, and hysteresis. Values of Q_{33}' in the relation

$$x_3 = Q_{33}'P_3^2$$

were calculated from the parabola of best fit to the x/D figures, and ranged from $3{\cdot}0$ to $7{\cdot}9 \times 10^{-13}$ e.s.u., in rough agreement with the results of Schmidt (1956). Unlike the latter author, however, we find considerable variation with specimen material and considerable departures from the parabolic form, perhaps because larger fields (about 20 kv/cm) were often used by us. The flattening of the vertices has been illustrated in a previous paper (Allsopp 1957) and it is roughly true, as might be expected, that Q_{33}' is smaller in those specimens which show greater flattening.

The flattening is thought to be similar in mechanism to that suggested for group I crystals in 2·4, and this dominance of 180° changes at the vertex of the curve would also account for the hysteresis observed, the direction of traverse being invariably in accord with this principle.

Although giving a similar hysteresis, conductivity of the specimens does not seem to be the cause, both because of the high insulation resistance found and because of the insensitivity of the x/D figures to change over at least a 10 : 1 range of the frequency of the applied field.

The coefficient Q_{31}' has also been measured for two samples of pure barium titanate ceramic, by suitably modifying the mounting so that strain was measured in a direction at right angles to the applied field. The values obtained were $-0{\cdot}45 \times 10^{-13}$ and $-0{\cdot}51 \times 10^{-13}$ e.s.u., while the same specimens had Q_{33}' values of 3·6 and $3{\cdot}8 \times 10^{-13}$ e.s.u. respectively. The ratios Q_{31}' to Q_{33}' were thus $-0{\cdot}12$ and $-0{\cdot}13$, which may be compared with $-0{\cdot}38$ and $-0{\cdot}23$ calculated by Mason (1950) and Devonshire (1954). The low value of this ratio obtained by us may be the result of the rather high porosity of the samples.

3.2. *Prepolarization*

Results on a prepolarized ceramic containing 1·3% of cobalt oxide are shown in fig. 9 (Pl. 52), where the development of the quasi piezoelectric behaviour at small fields to the nearly parabolic behaviour at high fields may be traced. It must be remembered that the zero of neither D nor x can be established on these figures.

In such materials a large proportion of the domains are thought to be locked in the direction nearest to that of the prepolarizing field (we shall call these c-domains, and all others a-domains). Kay (1955) has suggested that the strain behaviour of a prepolarized ceramic might be accounted for by the linear piezoelectric effect on these locked c-domains. It appears to us that such a mechanism, although it must contribute, cannot account for the magnitude of the strains observed. In fig. 9 (*b*), for example, the applied field is 70 e.s.u. peak to peak, and the total strain $2{\cdot}1 \times 10^{-4}$, equivalent to a d_{33} value in a piezoelectric crystal of 3×10^{-6} e.s.u. This is a little greater even than the d_{33} value of a single c-domain crystal, which value could not be closely approached even by the most completely polarized ceramic. Against this argument it must be admitted that the field on the c-domains will be greater than that applied, owing to their relatively low dielectric constant, but it is difficult to see how the field and strain averaging could be done to produce such a big effect.

Although the problem is immensely complicated by the large internal stresses and fields which must exist when domain changes occur in the randomly oriented grains, and although the magnitude of the shear piezoelectric constant d_{15} is unknown, we suggest, in agreement with Mason (1950) that much of the strain in these prepolarized ceramics arises from 90° domain changes.

The prepolarized material contains then a preponderance of say +c-domains, with a proportion of a-domains and few −c-domains. Small fields in the apparently linear x/E region effect conversion only between +c- and a-domains, there being very little conversion to −c-domains. Thus under small fields the behaviour depends on the tendency of a reverse field to form or enlarge a-domains, while a forward field tends to remove them. The larger slope and greater hysteresis in the reverse field region of the D/E figure at moderate applied fields (such as in fig. 9 (*b*)), together with the reduced slope of the x/E and x/D figures in the same region, is thought to indicate the onset of 180° changes. An equivalent process would be the conversion of a-domains to −c-domains at a rate approaching that of conversion of +c- to a-domains.

The low-field asymmetry in the switching process, characteristic of prepolarization, is presumably produced by the internal field of the excess of c-domains, and it is perhaps surprising that asymmetry in the figures persists even when a large degree of switching to −c-domain must occur, as in fig. 9 (*e*). Possibly the preference for the +c direction is the result of partially compensating volume charges, formed by leakage or breakdown, on the polar ends of the original ' locked ' +c-domains. This may be one of the factors explaining the greater effectiveness of prepolarizing at a high temperature, where the conductivity is higher.

If the domain change mechanism is in fact the dominant one in producing strain, it would be expected that very strong fields would reduce the slope of the x/E figure owing to almost complete elimination of a-domains, as in the case of single crystals. There seems a slight tendency for this to happen, but it is not nearly so marked as with crystals. This is not surprising in view of the small distinction between c- and a-domains in many of the randomly oriented grains of the ceramic, and the consequent very intense field required to produce alignment.

3.3. *Temperature Effects with Ceramics*

Typical x/D figures for two different ceramics at various temperatures from −150°c to +135°c are shown in fig. 10 (Pl. 53). The following features are common to all observations made:

(i) The general form of the x/D figures is unchanged in the temperature range between −150°c and the Curie point. In particular, no changes are observed on passing through the two lower transition temperatures.

(ii) Above the Curie point the x/D figures are parabolic to within the limits of experimental error. The Q_{33}' coefficient in this range is also independent of temperature and specimen type (i.e. to small amounts of additives, small variations in BaO : TiO_2 ratio, and firing temperature and time). The mean value of Q_{33}' for five specimens each at several different temperatures is $(5{\cdot}8 \pm 0{\cdot}3) \times 10^{-13}$ e.s.u., and is thus the same (just within the estimated error) as Q_{33} for crystals.

(iii) Hysteresis in the x/D figures tends to increase below −100°c and above +100°c. The latter effect is usually attributable to conductivity, and varies widely from specimen to specimen.

(iv) In high purity material, there is a marked flattening of the vertex, especially just below the Curie point, where the decay-effect has a short time constant (cf. Allsopp 1957). The dip in Q_{33}' on traversing the Curie point, found by Schmidt (1956) may be of the same origin.

(v) It appears that the *extent* of the flattening increases with decreasing temperature, although the situation is confused by time effects.

Results on the variation of Q_{33}' with temperature tended to be erratic at very low temperatures, probably because of electrode difficulties, and the slowness of time effects. What appeared to be the most reliable results indicate a smooth fall of Q_{33}' with temperature, the coefficient changing by a factor of about two over the range +120°c to −150°c.

3.4. *Field-induced Transitions in Ceramics near the Curie Temperature*

The figures for a pure ceramic material as the temperature is raised through the Curie point are shown in fig. 11 (Pl. 54). It will be seen that ‘ double ’ hysteresis loops appear, the figures being comparable with those obtained with group I crystals. The paraelectric to ferroelectric transition here extends over a larger field range (i.e. a larger fraction of the cycle) than with single crystals. Less pure ceramic material failed to show these field-induced transitions, which do not appear to have been previously recorded in ceramics.

The strains in a direction at right angles to the applied field for the same material are shown in fig. 12 (Pl. 55). As would be expected, the x/E figures show transitions, just above the Curie point, between the parabola characteristic of the paraelectric phase and the pair of straight lines (approximately) of the ferroelectric phase. However, the remarkable feature is the sign of the strain, there being an *extension* in the transverse direction, as well as in the in-line direction, on conversion to the ferroelectric phase. The result may again be dependent on the comparative porosity of the pure material, and it has not been so far possible to check this, as the only samples of greater density were also of less purity, and did not show the effect.

ACKNOWLEDGMENTS

We are grateful to the Bell Telephone Laboratories for single crystals. to the Plessey Co., Towcester, for both single crystals and ceramics, to Mr. G. Grainger for technical assistance. and one of us (H. L. A.) is also indebted to the C.S.I.R. of South Africa for financial assistance.

REFERENCES

ALLSOPP, H. L., and GIBBS, D. F., 1957, *J. sci. Instrum.*, **34,** 308.
ALLSOPP, H. L., 1957, *Phil. Mag.*, **2,** 1100.
CASPARI, M. E., and MERZ, W. J., 1950, *Phys. Rev.*, **80,** 1082.
DEVONSHIRE, A. F., 1954, *Advanc. Phys.*, **3,** 85.
KAY, H. F., and VOUSDEN, P., 1949, *Phil. Mag.*, **11,** 1019.
KAY, H. F., 1955, *Rep. Progr. Phys.*, XVIII, 230
MASON, W. P., 1950, *Piezoelectric crystals and their application to Ultrasonics* (New York: van Nostrand).
MERZ, W. J., 1949, *Phys. Rev.*, **76,** 1221; 1953, *Ibid.*, **91,** 513.
SCHMIDT, G., 1956, *Z. Phys.*, **145,** 534.

The Thermoelectric Power of the Alkali Metals at Low Temperatures†

By J. M. Ziman
Cavendish Laboratory, University of Cambridge

[Received October 23, 1958]

Abstract

The effect of phonon drag is calculated, taking account of electron–phonon Umklapp processes, and anisotropy of the Fermi surface. For Na, the observations are perfectly fitted with a spherical surface. For K, Rb and Cs, the surfaces must bulge more than half way towards the faces of the Brillouin zone, whilst in Li it probably touches the zone boundary.

According to the conventional free-electron theory of a monovalent metal, the absolute thermopower, Q, at low temperatures should show the following features:

(*a*) It should be small in magnitude—perhaps 0·1 μv/degree at 10°K.

(*b*) It should be negative, in accord with the sign of the electronic charge.

(*c*) For all metals it should be approximately proportional to T.

The facts are quite otherwise (fig. 1 from the data of MacDonald *et al.* (1958)):

(*a*) Q is often several microvolts/degree.

(*b*) It may be positive or negative, or even change sign as the temperature varies.

(*c*) The temperature variation may show large oscillations, and is quite different for each metal.

That Q may be so large was explained by Hanna and Sondheimer (1957) in terms of 'phonon drag'. This effect, now well understood in the case of semiconductors (Herring 1954) enhances the heat current associated with a stream of electrons, and hence increases the thermopower. But, whilst (*a*) was explained, the other anomalies remain. Bailyn (private communication) has taken a further step, by noting that the sign of the phonon drag is not invariable in principle. Consider, for example, an electron–phonon 'Umklapprozesse'. (U-process.) An electron going from a state of wave-vector $\mathbf{k}$, to state $\mathbf{k}'$, with the emission of a phonon of wave-vector $\mathbf{q}$, loses crystal momentum of amount

---

† Communicated by the Author.

$$\mathbf{K}=\mathbf{k}-\mathbf{k}'=\mathbf{g}+\mathbf{q}, \qquad \qquad (1)$$

Fig. 1

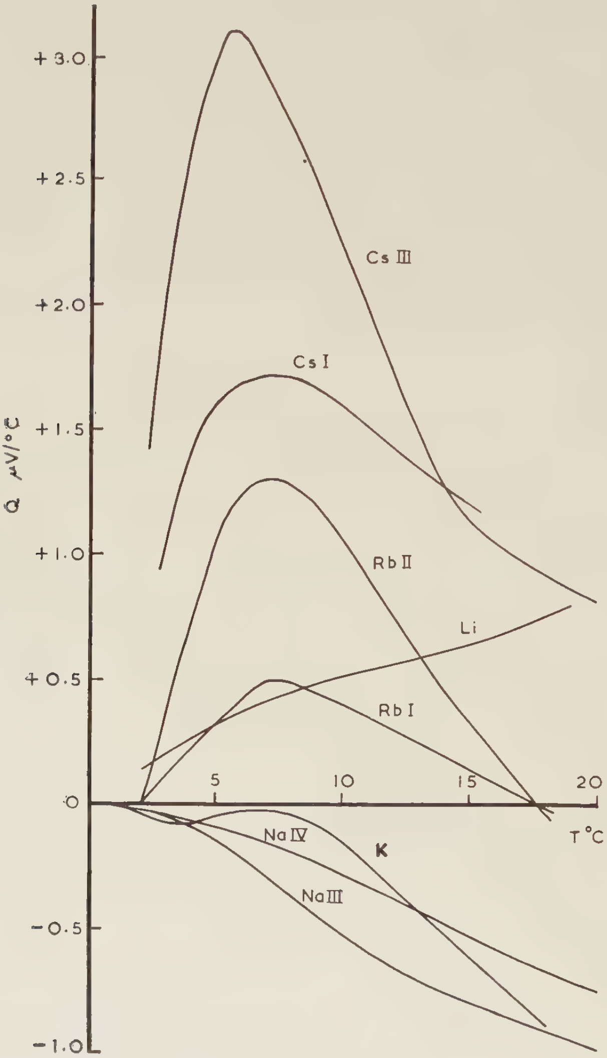

Absolute thermoelectric power of the alkali metals, from the data of MacDonald *et al.* (1958), who give details of the specimens.

where $\mathbf{g}$ is a reciprocal-lattice vector. It is quite easy, as we shall see, for $\mathbf{q}$ to be in the opposite direction to $\mathbf{K}$. As one might say, the phonon is emitted ‘backwards’ when the electron is scattered, and not necessarily, as in the normal ‘N-process’ in which $\mathbf{g}=0$, in the forward direction.

A phonon heat-current is thus created in the direction opposite to the main stream of electrons (fig. 2).

We still have to understand the temperature variation of Q, and the reason why it should differ from metal to metal In this paper some calculations are reported which seem to make this explicable, and which show that this phenomenon is a useful and sensitive index to the shape of the Fermi surface in the alkali metals. All that we do is to make a numerical calculation of the '*lattice thermopower*', Q_{L}, i.e. the contribution of phonon drag, taking account of both N-processes and U-processes using a typical form of the electron–phonon matrix element, and allowing for distortion of the Fermi surface towards the zone boundary.

Fig. 2

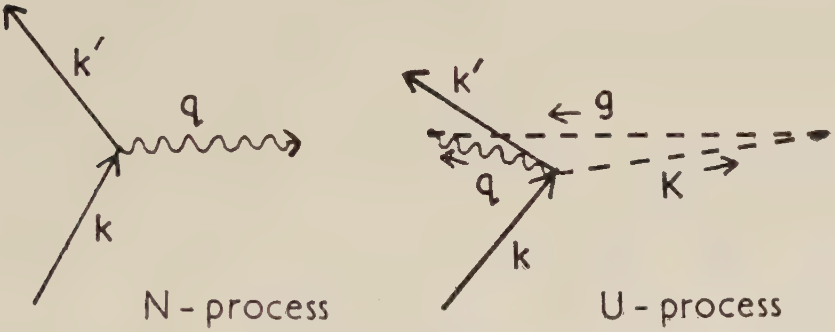

The derivation of a formula for Q_{L} will be published elsewhere (Ziman, *Electrons and Phonons*, Oxford University Press, § 9.13). From the variational principle (Ziman 1956)

$$Q_{\mathrm{L}} = -\frac{\mathrm{k}}{|\mathrm{e}|}\frac{1}{n_{\mathrm{a}}}\left(\frac{C_{\mathrm{L}}}{3N\mathrm{k}}\right)\frac{P_{1\mathrm{L}}}{P_{\mathrm{LL}}}, \qquad \text{. . . . . . .} \tag{2}$$

where n_{a} is the number of electrons per atom, and C_{L} is the lattice specific heat. The other symbols signify scattering integrals, viz.

$$P_{1\mathrm{L}} = \int\!\!\int\!\!\int (\Phi_{\mathbf{k}} - \Phi_{\mathbf{k}'})\Phi_{\mathbf{q}}\mathscr{P}_{\mathbf{k}}^{\mathbf{q}\mathbf{k}'}\,d\mathbf{k}\,d\mathbf{q}\,d\mathbf{k}', \qquad \text{. . . . .} \tag{3}$$

$$P_{\mathrm{LL}} = \int\!\!\int\!\!\int (\Phi_{\mathbf{q}})^2\mathscr{P}_{\mathbf{k}}^{\mathbf{q}\mathbf{k}'}\,d\mathbf{k}\,d\mathbf{q}\,d\mathbf{k}' + \text{other terms.} \qquad \text{. . . .} \tag{4}$$

Here $\Phi_{\mathbf{k}}$ is the steady state electron distribution, $\Phi_{\mathbf{q}}$ is the phonon distribution, and the integrals contain the probability of a process in which an electron is scattered from $\mathbf{k}$ to $\mathbf{k}'$, with the creation of a phonon. Only electron–phonon interactions are here dealt with explicitly, but there may be other terms in P_{LL}, arising from phonon–phonon interactions, scattering of phonons by impurities, etc.

To proceed, we must make an assumption about the various distribution functions. As usual, we put

$$\Phi_{\mathbf{k}} = \mathbf{k}\,.\,\mathbf{u}, \quad \Phi_{\mathbf{q}} = \mathbf{q}\,.\,\mathbf{u}, \qquad \text{. . . . .} \tag{5}$$

where **u** is a unit vector in the current direction. For the phonons, in particular, this is not very accurate (cf. the case of a semiconductor, where the long wave lattice waves go much further from equilibrium), but is not too bad when scattering by electrons is the main source of resistance to lattice conduction. With these assumptions, our formula can be expressed very simply, at low temperatures:

$$Q_{\mathrm{L}} = -\frac{\mathrm{k}}{|\mathrm{e}|}\frac{1}{n_{\mathrm{a}}}\frac{4\pi^4}{5}\left(\frac{T}{\Theta}\right)^3\frac{\langle \mathbf{K}\,.\,\mathbf{q}\rangle}{\langle q^2\rangle}. \quad . \quad . \quad . \quad . \quad . \quad . \qquad (6)$$

The brackets $\langle\ \rangle$ refer to averages over all electron–phonon scattering processes, at the rate at which they occur in the steady state.

If there are only N-processes, $\mathbf{g}=0$ in (1), making (3) and (4) equal. This is the case studied by Hanna and Sondheimer, who included in the denominator an empirical term as if the phonons were scattered by point impurities according to a Rayleigh law. By adjusting the amount of this scattering, they were able to fit the curve for Na up to quite high temperatures. There are many reasons, however, for supposing that U-processes are just as important. For example (Ziman 1954), in order to explain the lack of a minimum in the thermal conductivity of the alkali metals, we must replace the Bloch constant C^2 in the electron phonon scattering probability by a function $\mathscr{C}^2\ (K)$ which is not zero when the length of the scattering vector k exceeds the radius, $\mathfrak{Q}$ of the Debye sphere.

The problem of averaging for U-processes is geometrically complicated but it is not difficult to find a reasonable approximation (loc. cit., § 9.5). With the aid of (1) and the geometrical identity

$$\mathbf{K}\,.\,\mathbf{q} = \tfrac{1}{2}(K^2+q^2-g^2) \quad . \quad . \quad . \quad . \quad . \quad . \quad . \quad . \qquad (7)$$

it can be shown that

$$\langle \mathbf{K}\,.\,\mathbf{q}\rangle = \int_0^{\mathfrak{Q}} \frac{q^5\{\mathscr{C}^2(q)+\mathscr{C}^2{}_{QU}(q)\}\,dq}{(e^z-1)(1-e^{-z})}, \quad \langle q^2\rangle = \int_0^{\mathfrak{Q}} \frac{q^5\{\mathscr{C}^2(q)+\mathscr{C}^2{}_{WU}(q)\}\,dq}{(e^z-1)(1-e^{-z})}$$

(8), (9)

with $z=\hbar\nu/kT=q\Theta/\mathfrak{Q}T$. Here the terms in $\mathscr{C}^2(q)$ refer to N-processes; if $\mathscr{C}^2(q)$ were constant, as in the Bloch theory, each integral would be of the familiar type $(T/\Theta)^5\mathscr{J}_5(\Theta/T)$. The other terms in each integrand derive from U-processes, and are defined by

$$\mathscr{C}^2{}_{QU}(q) \equiv \frac{z'}{2gq^4}\int_{g-q}^{2\mathfrak{k}} \tfrac{1}{2}(K^2+q^2-g^2)K^2\mathscr{C}^2(K)\,dK; \quad . \quad . \qquad (10)$$

$$\mathscr{C}^2{}_{WU}(q) \equiv \frac{z'}{2gq^2}\int_{g-q}^{2\mathfrak{k}} K^2\mathscr{C}^2(K)\,dK. \quad . \quad . \quad . \quad . \quad . \quad . \quad . \quad . \qquad (11)$$

It is easy to recognize the average of (7) in the first of these. It is taken over that part of the Fermi sphere which can be reached by a phonon of wave-number q. The lower limit of K shows that it may not be less than $g-q$ (when g and q lie in a straight line). Nor can K exceed $2\mathfrak{k}$, the diameter of the Fermi sphere. For values of q less than

$$q_u = g-2\mathfrak{k} \quad . \quad . \quad . \quad . \quad . \quad . \quad . \quad . \quad . \qquad (12)$$

U-processes are impossible (see fig. 3), and the functions (10) and (11) are zero. The coordination number, z' of the reciprocal lattice, counts the number of places on the Fermi surface where this lower limit on q is approached.

Fig. 3

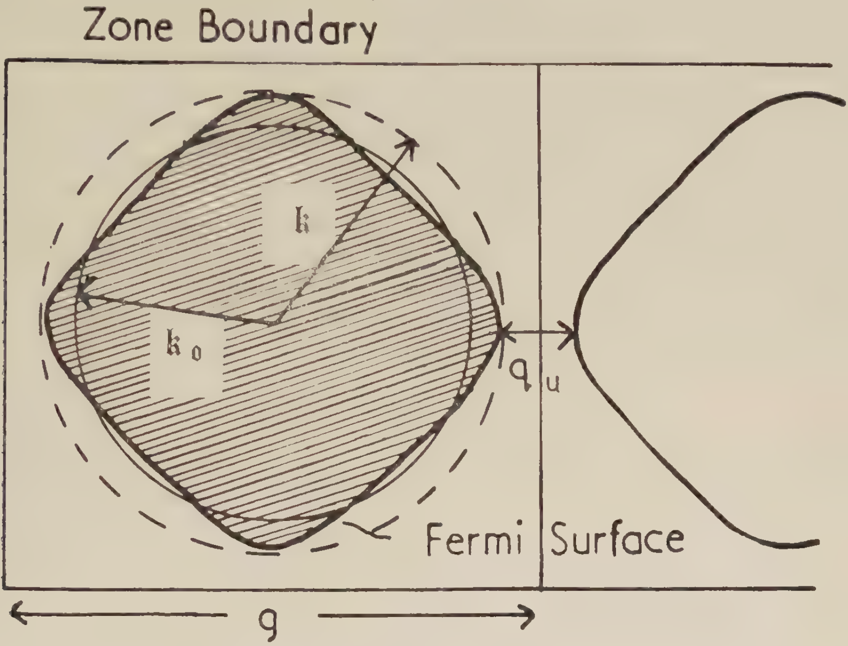

Geometry of the calculation for a non-spherical Fermi surface.

We see now that $\mathscr{C}^2_{QU}(q)$ tends to be negative. In (10), the term in $-g^2$ is much the largest. Because g is larger than $2\mathfrak{k}$, most contributions to $\langle \mathbf{K} \,.\, \mathbf{q} \rangle$ come from configurations where $\mathbf{K}$ and $\mathbf{q}$ are in opposite senses. Thus, N-processes and U-processes pull in opposite directions, and the sign of Q_L will depend on their balance. This, in turn, depends critically on the form of the electron–phonon interaction, and on the shape of the Fermi surface.

The best form of $\mathscr{C}^2(K)$ for describing the transport properties of the alkali metals is due to Bardeen (1937). For the sake of simplicity we shall use the main variable factor in this formula, i.e.

$$\mathscr{C}^2(K) = 9\{\sin (Kr_s) - (Kr_s) \cos (Kr_s)\}^2/(Kr_s)^6, \quad . \quad . \quad . \quad (13)$$

which arises, basically, from the overlap integral of two plane waves differing in wave vector by $\mathbf{K}$ in Wigner–Seitz cell of radius r_s, and which is characteristic of all theories which allow U-processes at all (Jones 1956). The other factors in the Bardeen formula arise from estimates of the deformation potential, and of the way it is screened by the free electrons. These factors are much less variable, and are not more significant in the calculation than the corrections for phonon dispersion, and polarization, which we have already neglected.

The formal analysis, up to now, is based on the assumption that the Fermi surface is nearly a sphere. Whilst this may be true topologically, we know that some distortion is probable in any real metal, and that an increase of only 14% in its radius would bring the surface into contact with the zone boundary. Even a small deviation in this direction can thus have an important effect on q_u, the lower limit of U-processes.

To allow for this possibility, we shall take $\mathfrak{k}$ in (10 and (11) to be an adjustable parameter, capable of assuming larger values than $\mathfrak{k}_0$, say, which is what would be for an exact sphere containing one electron per atom. That is, instead of deforming the Fermi surface, we simply swell it until it is the same minimum distance from the zone boundary as it would have been if it had been deformed without change of volume (fig. 3). It is just at those crucial points near the zone boundaries that we want to get q_u correct; precisely how the surface behaves in between does not much affect the calculation. We shall call

$$\epsilon=(\mathfrak{k}-\mathfrak{k}_0)/\mathfrak{k}_0 \qquad . \quad . \quad . \quad . \quad . \quad . \quad . \quad . \quad (14)$$

the measure of the anisotropy of the Fermi surface, that is, the amount by which it bulges, beyond its average radius, towards the faces of the Brillouin zone.

Equations (6)–(13) now define the computation. The integrations were done by simple trapezoidal sums on a desk calculator, and no great accuracy is claimed for them. Curves showing Q_{L} as a function of the reduced temperature, T/Θ, are plotted in fig. 4, for various values of ϵ. For comparison, the experimental data of fig. 1 are plotted on the same scale. The reduction of the temperature requires some choice of values of Θ. I have used the following: Li, 430°; Na, 160°; K, 100°; Rb, 68°; Cs, 54°, which seem representative 'specific heat' values of this fickle constant. This at least gets the scale of C_{L} correct, even if it is not the best value to put into the scattering integrals P_{IL} and P_{LL}. Where there is a very big impurity effect, curves for different specimens are shown for some of the metals.

The first point to be noted is the very precise fit, below $\Theta/10$, between the experimental results for Na, and the theoretical curve for a spherical Fermi surface. There are no adjustable parameters in this, which surely shows that the theory is on the right lines. It is true that, at higher temperatures, the thermopower is not as large, in magnitude, as our formula predicts. Here the calculations of Hanna and Sondheimer would apply; that is, the denominator of (2) is increased by the scattering of phonons from impurities. The case of specimen IV, a dilute alloy of K in Na, where the thermopower is not nearly so large, confirms this.

The curious curve for K also follows extremely closely the shape calculated for $\epsilon=7\%$. The difference could well be the standard electronic thermopower, $\pi^2k^2T/e\zeta_0$, which would just prevent Q from changing

Fig. 4

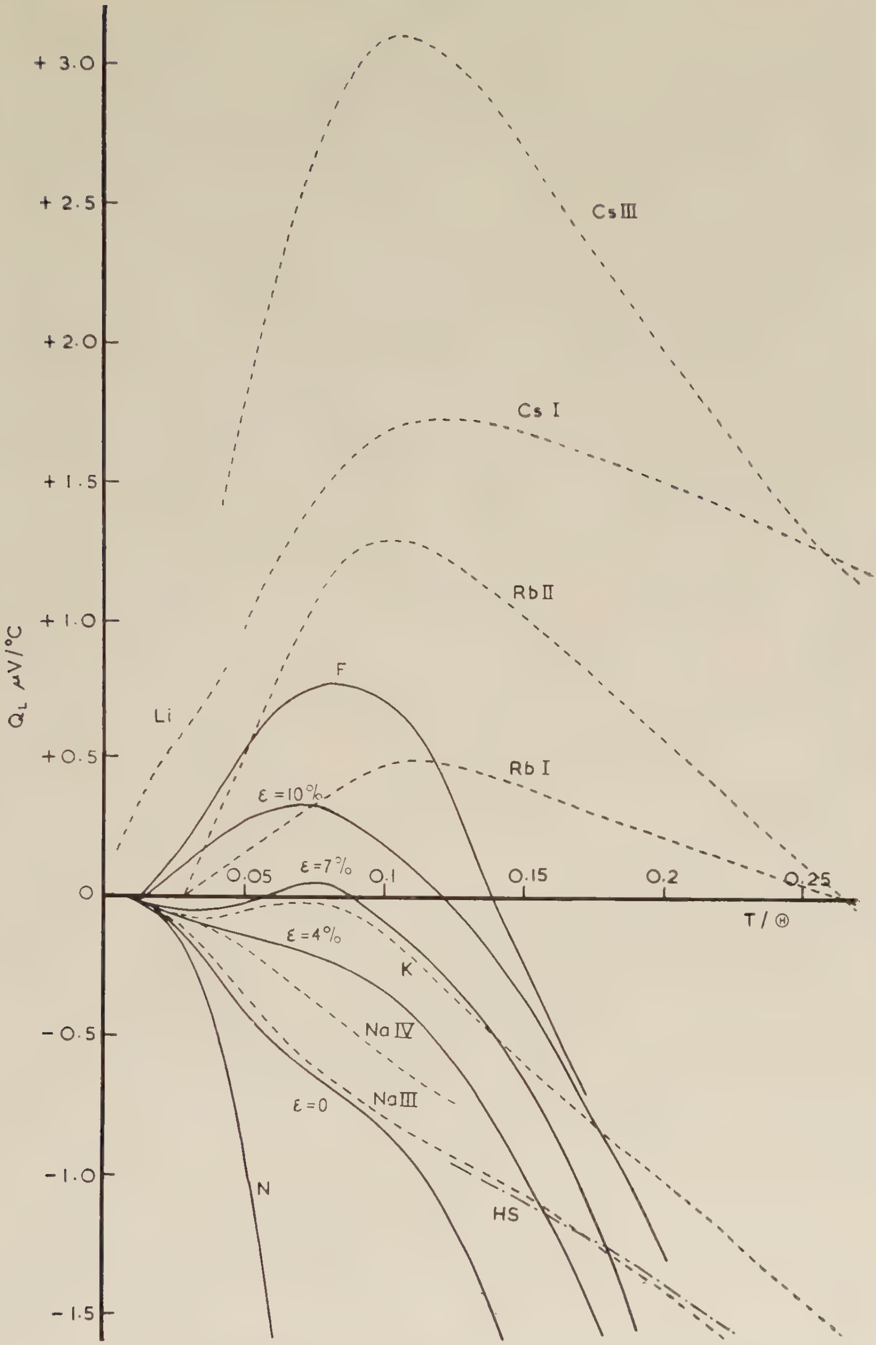

Absolute thermoelectric power as a function of reduced temperature.

———— $\epsilon=4\%$ lattice thermopower calculated for various degrees of anisotropy of the Fermi surface.

———— N calculated for N-processes alone.

———— F calculated for an arbitrary form of electron–phonon interaction.

— · — · — HS calculated by Hanna and Sondheimer (1957).

— — — — Na experimental data from fig. 1.

sign, as observed. The cause of the wiggle is clear. As the temperature falls, the term $\mathscr{C}_{QU}^2$ in (8) becomes dominant over $\mathscr{C}^2$, and Q_L becomes positive. This is because the typical phonon is only a bit above q_u in wave number, and $\mathbf{K}$ and $\mathbf{q}$ are rather rigorously aligned into opposition. But then, at lower temperatures, these U-processes are frozen out, and the lattice thermopower reverts to its negative value, under the influence of N-processes alone. In principle, it should tend to the curve N, which is just the limiting form of (6) when both averages are equal.

The heavy alkali metals, Rb and Cs, are not so well fitted. Qualitatively their thermopowers follow the pattern of the curve for $\epsilon = 10\%$, i.e. rise to a high positive peak, and then fall, perhaps to zero and negative values, at the lowest temperatures. It is not difficult to fabricate a form of electron–phonon interaction which would show such behaviour. For example, the curve labelled F (for Fudged) indicates what happens if we keep $\epsilon = 10\%$, but arbitrarily double $\mathscr{C}^2(K)$ at large values of K. There is no mathematical reason why the peak should not be raised as high as we want by a suitable choice of $\mathscr{C}^2(K)$. For Rb we note that the curves cut the axis, just as if U-processes were being frozen out at some value of q_u corresponding to ϵ lying between 7 and 10%. The same may be true for Cs but the extrapolation is not reliable. In these elements it is interesting to note the effect of impurities. In Rb, an increase in the resistivity by a factor 9 divides the thermopower by about 2·5. Presumably this is due to an extra term in the denominator of (6), from the scattering of phonons by these impurities.

Finally consider Li. Here the thermopower is decisively positive, and shows no sign of falling below the axis. Is this because, in Li, the Fermi surface touches the zone boundary? The calculation is not really adapted to this case, and the data are meagre, but it certainly seems so.

To clinch the argument of this paper, we need independent evidence on the shape of the Fermi surface in the alkali metals. This has been discussed in detail by Cohen and Heine (1958) and Garcia-Moliner (1958). In each metal the exact amount of anisotropy is not yet certain, but there is a general pattern, into which the present results fit perfectly. Indeed, the lattice thermopower is probably one of the properties most sensitive to any anisotropy of the Fermi surface, and one of the best indices of its shape.

It also seems as if one could deduce fresh information about the form of the electron–phonon interaction. If, as in Rb, one can roughly fix the shape of the Fermi surface, one may then play with the form of $\mathscr{C}^2(K)$ to make theory and experiment agree. It is not difficult to see how it could be improved in the right direction. Then, in turn, one could compute the other transport properties, and look for complete consistency. Until we have a sound derivation of the electron–phonon scattering at large angles, this is a promising empirical approach to this difficult problem.

ACKNOWLEDGMENTS

This work was stimulated by the long range field of influence of Dr. D. K. C. MacDonald at the National Research Council, Ottawa. I am grateful to him, and to Drs. Cohen, Heine, and Garcia-Moliner, for showing me their work before publication.

REFERENCES

BARDEEN, J., 1937, *Phys. Rev.*, **52,** 688.
COHEN, M. H., and HEINE, V., 1958, *Advanc. Phys.*, **7,** 395.
GARCIA-MOLINER, F., 1958, *Proc. phys. Soc. Lond.* (in the press).
HANNA, I. I., and SONDHEIMER, E. H., 1957, *Proc. roy. Soc.* A, **239,** 247.
HERRING, C., 1954, *Phys. Rev.*, **96,** 1163.
JONES, H., 1956, *Handb. der Phys.*, XIX, 227.
MACDONALD, D. K. C., PEARSON, W. B., and TEMPLETON, I. M., 1958, *Proc. roy. Soc.* A, **248,** 107 ; *Phil. Mag.*, **3,** 917.
ZIMAN, J. M., 1954, *Proc. roy. Soc.*, A, **226,** 436; 1956, *Canad. J. Phys.*, **34,** 1256.

CORRESPONDENCE

Measurements of Thermoelectricity below 1°K—III

By D. K. C. MacDonald, W. B. Pearson and I. M. Templeton
Division of Pure Physics, National Research Council, Ottawa, Canada

[Received November 21, 1958]

In two earlier letters to this Journal (MacDonald *et al.* 1958 a, b) we have summarized some results of note which we have obtained on the Group IB and alkali metals in the temperature range below 1°K. We wish here to mention some further results of interest on the heavier alkali metals and on various transition metals. We deal first with the latter.

In our first note we reported that the IB metals, and gold in particular, showed remarkably large thermoelectric powers—greatly in excess of current theoretical predictions—and consequently we wished to examine other metals of neighbouring groups. Part of our interest stems from the fact that a metal with a *sufficiently* large thermoelectric power might enable thermoelectric refrigeration to be realized at low temperatures (cf. MacDonald *et al.* 1959). We have now made measurements on specimens of nickel, palladium, iron, cobalt and platinum; in general these metals show much lower absolute thermoelectric powers, S, than gold. Platinum of high purity, however, with $S \simeq -1\,\mu\text{V}/^\circ\text{C}$ at about 1°K approaches gold most nearly in magnitude of thermoelectric power; it is also notable that in platinum S is remarkably *constant* below say 1·5°K down to as low as about 0·3°K. An interesting feature is the dependence in sign and magnitude of thermoelectric power on impurity found in some of these metals even at these very low temperatures. Figure 1 illustrates this behaviour for two samples of nickel and some results for palladium and iron are also summarized in table 1. It will be seen that in these

Table 1

Metal specimen	Approximate residual resistance ratio ($R_{4\cdot2^\circ\text{K}}/R_{\sim295^\circ\text{K}}$)	Absolute thermoelectric force, E, at about $1{\cdot}2_5$°K (volts)
Ni I	16×10^{-3}	$+6\ \times10^{-9}$
Ni II	$6{\cdot}4\times10^{-3}$	$-2{\cdot}9\times10^{-8}$
Pd I	43×10^{-3}	$\sim+6\ \times10^{-9}$
Pd II	36×10^{-3}	$-3{\cdot}5\times10^{-8}$
Fe I	17×10^{-3}	$+3\ \times10^{-9}$
Fe II	$9{\cdot}4\times10^{-3}$	$-2{\cdot}2\times10^{-8}$
Pt I	2×10^{-3}	$-1{\cdot}2\times10^{-6}$
Pt II	49×10^{-3}	$-3{\cdot}3\times10^{-7}$
Co I	10×10^{-3}	$-2{\cdot}5\times10^{-8}$

three metals the transition to the purer sample of metal leads to a change of sign of thermoelectric force from positive to negative together with a quite considerable increase in magnitude. Further experiments are planned to examine this process in more detail and to investigate the influence of specific impurities.

Fig. 1

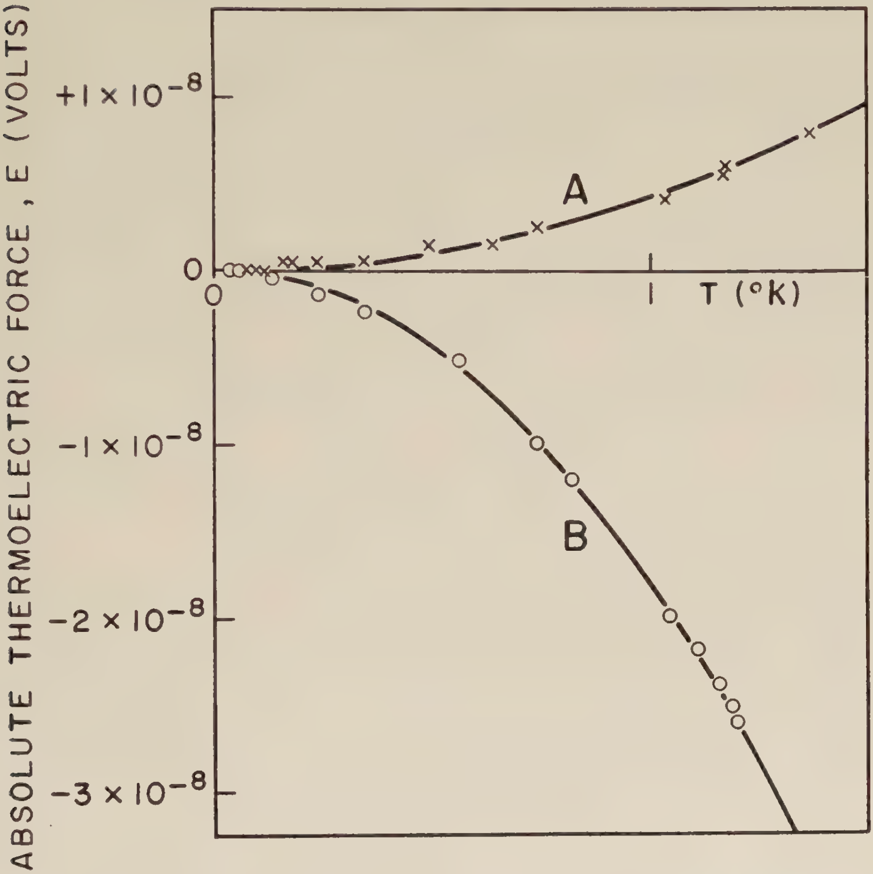

Absolute thermoelectric force observed on two specimens of nickel.

A. Specimen Ni I (see table 1); the full line represents the equation $E = +4{\cdot}2_5 \times 10^{-9}\, T^2$ (volts), and thus $S = +8{\cdot}5 \times 10^{-9}\, T$ (v/°c).

B. Specimen Ni II (see table 1); the full line represents the equation $E = -1{\cdot}8_3 \times 10^{-8}\, T^2$ (volts), and thus $S = -3{\cdot}6_6 \times 10^{-8}\, T$ (v/°c).

A suggestion of Dr. C. V. Heer (Ohio State University) that the high entropy contribution found in cobalt below 1 °K (Heer and Erickson 1957) might perhaps lead one to look for a large thermoelectric power, was followed up. A sample of cobalt was measured, but a quite normal thermoelectric force was observed as indicated in table 1.

Table 2

Metal specimen	Approximate residual resistance ratio $(R_{4\cdot2^\circ\mathrm{K}}/R_{\sim295^\circ\mathrm{K}})$	Absolute thermoelectric force, E, at about $1{\cdot}2_5$°K (volts)
Rb I	30×10^{-3}	$+1{\cdot}3\times10^{-8}$
Rb II	$3{\cdot}5\times10^{-3}$	$-3\quad\times10^{-9}$
Cs I	$6{\cdot}5\times10^{-3}$	$+4\quad\times10^{-8}$
Cs II	$1{\cdot}4\times10^{-3}$	$+4\quad\times10^{-8}$

Fig. 2

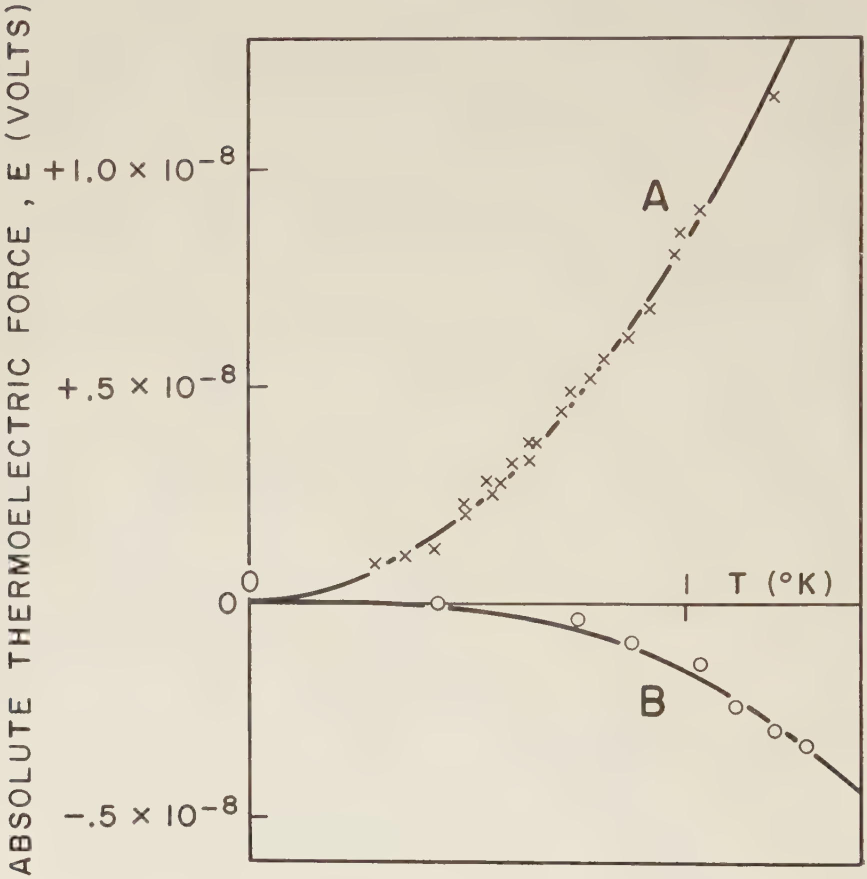

Absolute thermoelectric force observed on two specimens of rubidium.
A. Specimen Rb I (see table 2); the full line represents the equation $E=+8{\cdot}4\times10^{-9}\,T^2$ (volts), and thus $S=+16{\cdot}8\times10^{-9}\,T$ (v/°c).
B. Specimen Rb II (see table 2); the full line represents the equation $E=-1{\cdot}6\times10^{-9}\,T^3$ (volts), and thus $S=-4{\cdot}8\times10^{-9}\,T^2$ (v/°c).

The sensitive dependence on purity of the metals discussed above is also found in rubidium and the behaviour of two samples is shown in fig. 2 (see also table 2). It is interesting to notice again that in the purer sample the thermoelectric power, S, becomes negative and also that S then appears to become proportional to T^2 (rather than to T) at the lowest temperatures (cf. also MacDonald *et al.* 1958 b). In caesium, however (see table 2), the thermoelectric power appears to remain positive even in very pure samples.

REFERENCES

HEER, C. V., and ERICKSON, R. A., 1957, *Phys. Rev.*, **108,** 896.
MACDONALD, D. K. C., MOOSER, E., PEARSON, W. B., TEMPLETON, I. M., and WOODS, S. B., 1959, *Phil. Mag.* (in the press).
MACDONALD, D. K. C., PEARSON, W. B., and TEMPLETON, I. M., 1958 a, *Phil. Mag.*, **3,** 657 ; 1958 b, *Ibid.*, **3,** 917.

Observation by X-ray Diffraction of Dislocations in a Diamond

By F. C. FRANK
H. H. Wills Physics Laboratory, University of Bristol

and A. R. LANG
Division of Engineering and Applied Physics, Harvard University,
Cambridge 38, Massachusetts, U.S.A.†

[Received January 2, 1959]

IN a recent paper Frank *et al.* (1958) present evidence in support of the idea that most 'trigons' on natural octahedral faces of diamond are etch-pits. They suggest also that the trigons may be centred on dislocations. The diamond they examined, a good quality Type I 'blue-white' octahedral stone, showed clusters of trigons on each face. There was also a centre of strain inside the diamond which could be detected by its birefringence. The strain nodulus was located approximately at the intersection of perpendiculars from the trigon clusters on each face. Hence it appeared likely that there were dislocations radiating from the strain nodulus outward to the trigons. An x-ray examination of the diamond has been undertaken to test the validity of this proposed dislocation distribution.

It has been shown that individual dislocations in crystals may be detected by x-ray diffraction (Lang 1958). A general survey of the dislocation content of a nearly perfect crystal can be made using the 'projection topograph' technique (Lang 1959). A pair of projection topographs, derived from Bragg reflection in a given plane and its inverse, provide a stereo-pair which enables the three-dimensional distribution of dislocations to be seen. Such a stereo-pair is reproduced in fig. 1 (*a*) and (*b*) (Pl. 56). The glancing angle for the 111 reflections used was small (eight degrees for Ag $K\alpha$ radiation) so that the octahedron appears nearly as a parallelogram in projection. Both individual dislocations and close bundles of dislocations can be seen radiating from the strained inner region outwards towards the faces. Elastic strain and the high dislocation density prevent resolution of individuals close to this centre. Surface damage, especially along the edges of the crystal, accounts for specks of enhanced diffracted intensity. About one-half of all dislocations present should be visible in this stereo-pair of photographs assuming that the various Burgers vectors occur with equal frequency. The hypothesis of Frank *et al.* concerning the general distribution of dislocations is thus strikingly confirmed. It is planned to perform a detailed X-ray diffraction study of this crystal to establish the direction of Burgers vectors of the dislocations and to correlate their outcrop with individual surface features.

---

† On leave at H. H. Wills Physics Laboratory, University of Bristol.

ACKNOWLEDGMENTS

One of the authors (A. R. L.) wishes to thank the U.S. Office of Naval Research for support. The experiments were carried out on diffraction instruments constructed under Contract Nonr-1866(39) and with an X-ray source kindly provided by Dr. J. W. Mitchell, H. H. Wills Physics Laboratory. Thanks are also due to Messrs. Industrial Distributors Limited for the loan of the diamond.

REFERENCES

FRANK, F. C., PUTTICK, K. E., and WILKS, E. M., 1958, *Phil. Mag.*, **3**, 1262.
LANG, A. R., 1958, *J. appl. Phys.*, **29**, 597 ; 1959, *Acta Cryst.* (in the press).

Probability Density of Electron Separation in a Uniform Electron Gas

By N. H. MARCH and W. H. YOUNG
Department of Physics, The University, Sheffield

[Received November 7, 1958]

WE briefly report here a new method of approach to the correlation problem in a uniform electron gas, within the framework of density matrix theory. The earlier important paper of Mayer (1955) using this method has been shown independently by Tredgold (1957) and Koppe (1957) to lead to a variational scheme which is not complete, due to difficulties associated with subsidiary conditions. We propose here a uniform method of describing the electron correlations throughout the entire density range, and show that our method does indeed lead to accurate results in the high and low density limits. We hope to report detailed calculations for intermediate densities later, but at least we show in this note how a reasonably accurate picture of the correlation effects may be obtained over a wide density range.

Following Mayer (1955), we introduce the probability density $F_2(\xi_{12})$ of separation ξ_{12} between electrons; this being essentially the diagonal element of the second order density matrix. We use the variable $\boldsymbol{\xi}$, rather than $\mathbf{r}$, defined by

$$r_s\boldsymbol{\xi}=\left(\frac{3}{4\pi}\right)^{1/3}\mathbf{r} \quad . \quad . \quad . \quad . \quad . \quad . \quad . \quad . \quad . \quad . \quad (1)$$

where r_s is the radius of a sphere containing one electron. Then, as Mayer has shown, the potential energy per particle V may be written

$$V=-\frac{1}{2}\left(\frac{3}{4\pi}\right)^{1/3}\cdot\frac{1}{r_s}\int_0^\infty 4\pi\xi\{1-F_2(\xi,r_s)\}d\xi \quad . \quad . \quad . \quad (2)$$

and to emphasize the importance of F_2 we first prove a new result; that the total energy per particle E may be written exactly in terms of F_2. This may be achieved by using the many-body virial theorem for this problem in the form given recently by one of us (March 1958). Re-writing this theorem as a differential equation for the energy $E(r_s)$, given $V(r_s)$ from (2), it may be shown that

$$E=\frac{3}{10}\left(\frac{9\pi}{4}\right)^{2/3}\cdot\frac{1}{r_s^2}+\frac{1}{r_s^2}\int_0^{r_s} r_sV\,dr_s, \quad . \quad . \quad . \quad . \quad (3)$$

the constant of integration being simply the Fermi energy.

Thus we focus attention on the calculation of F_2, and for simplicity of presentation we shall at first neglect spin. With N particles, let $\Psi(\mathbf{r}_1, \mathbf{r}_2 \ldots \mathbf{r}_N)$ be any antisymmetric wave function such that it is normalized to unity. We now define corresponding density matrices (see for example Löwdin 1955)

$$\gamma(\mathbf{r}_1'|\mathbf{r}_1)=N\int\Psi^*(\mathbf{r}_1', \mathbf{r}_2\ldots\mathbf{r}_N)\Psi(\mathbf{r}_1, \mathbf{r}_2\ldots\mathbf{r}_N)d\mathbf{r}_2\ldots d\mathbf{r}_N, \quad . \quad (4)$$

$$\Gamma(\mathbf{r}_1'\mathbf{r}_2'|\mathbf{r}_1\mathbf{r}_2)=\frac{N(N-1)}{2}\int\Psi^*(\mathbf{r}_1', \mathbf{r}_2', \mathbf{r}_3\ldots\mathbf{r}_N)\Psi(\mathbf{r}_1, \mathbf{r}_2, \mathbf{r}_3\ldots\mathbf{r}_N)d\mathbf{r}_3\ldots d\mathbf{r}_N. \quad . \quad . \quad . \quad (5)$$

Then considering the function Φ defined by

$$\Phi(\mathbf{r}_1, \mathbf{r}_2\ldots\mathbf{r}_N)=\sqrt{\left(\frac{N}{\gamma(\mathbf{r}_1|\mathbf{r}_1)}\right)}\Psi(\mathbf{r}_1, \mathbf{r}_2\ldots\mathbf{r}_N) \quad . \quad . \quad . \quad (6)$$

it is easily shown that

$$\int\Phi^*(\mathbf{r}_1, \mathbf{r}_2\ldots\mathbf{r}_N)\Phi(\mathbf{r}_1, \mathbf{r}_2\ldots\mathbf{r}_N)\,d\mathbf{r}_2\ldots d\mathbf{r}_N=1. \quad . \quad . \quad . \quad (7)$$

Furthermore Φ is antisymmetrical in $\mathbf{r}_2, \mathbf{r}_3\ldots\mathbf{r}_N$, and can therefore be used to construct density matrices of various orders for $N-1$ particles, in coordinates $\mathbf{r}_2\ldots\mathbf{r}_N$. In particular

$$\frac{2}{\gamma(\mathbf{r}_1|\mathbf{r}_1)}\Gamma(\mathbf{r}_1\mathbf{r}_2'|\mathbf{r}_1\mathbf{r}_2)$$

is a first order density matrix for $N-1$ particles, for any arbitrary fixed $\mathbf{r}_1$.

We now apply the above general result to the electron gas problem. Here $\gamma(\mathbf{r}_1|\mathbf{r}_1)$, the mean electron density, is a constant, γ say, and the 'particle density' for $N-1$ particles is

$$\frac{2}{\gamma}\Gamma(\mathbf{r}_1\mathbf{r}_2|\mathbf{r}_1\mathbf{r}_2)\equiv\frac{2}{\gamma}\Gamma(\mathbf{r}_1\mathbf{r}_2)$$

for fixed $\mathbf{r}_1$. We may write in this case

$$\frac{2}{\gamma}\Gamma(\mathbf{r}_1\mathbf{r}_2)=f(\mathbf{r}_{12})\,;\quad \mathbf{r}_{12}=\mathbf{r}_2-\mathbf{r}_1 \quad . \quad . \quad . \quad . \quad . \quad (8)$$

and it is sufficient to investigate $(2/\gamma)\Gamma(0\;\mathbf{r}_2)=f(\mathbf{r}_2)$, where we can think of axes as fixed at electron 1. Clearly to assume any first order density matrix for $N-1$ particles is not sufficient, for the antisymmetry property requires that

$$f(0)=0 \quad . \quad . \quad . \quad . \quad . \quad . \quad . \quad . \quad . \quad (9)$$

for particles of like spin. Then $f(\mathbf{r})$ is intimately related to $F_2(\xi)$, the latter representing an angular average of $f(\mathbf{r})$.

Having seen how the second order density matrix may be re-expressed in a form related to a first order matrix for $N-1$ particles we shall now attempt to set up a model in keeping with the requirements put forward here. We restrict ourselves to a first order density matrix of the simplest kind, constructed from a set of orthonormal single particle functions $\psi_i(\mathbf{r})$, as

$$\sum_{1}^{N-1}\psi_i^*(\mathbf{r}')\psi_i(\mathbf{r}).$$

We were essentially helped in our considerations by seeking a unified treatment which includes both the Hartree–Fock solution, known to be correct in the high density limit, and the low density case (Wigner 1938). Wigner's low density calculation assumed that the potential energy was minimized when the electrons went on to the sites of a body-centred cubic lattice. Now, of course, this can only be interpreted as a lattice relative to a given electron we have singled out, as no real set of lattice points can occur preferentially in a uniform gas. Thus the lattice can be thought of as describing the configuration of all the other electrons, once axes are fixed on one particle. Of course, even then, all orientations of this lattice are equally probable, and so eventually we must average over angles to obtain physically significant results. Wigner finds that orbitals centred on the lattice sites can be represented by harmonic oscillator functions

$$\psi=\left(\frac{\alpha}{\pi}\right)^{3/4}\exp\left(\frac{-\alpha r^2}{2}\right)\,;\quad \alpha=\frac{1}{r_s{}^{3/2}}, \quad . \quad . \quad . \quad . \quad (10)$$

for which ψ^2 tends to the delta function in the low density limit. If the density is very small, the functions (10) can be treated as orthogonal (effectively zero outside their own sphere) and hence are a valid set from which to form a first order density matrix of the kind we require. However, with N particles, we have N harmonic oscillator functions, and to obtain a suitable first order density for $N-1$ particles we must remove the density contributed by one of the orbitals; the one centred on the origin. We can then build up an acceptable function F_2 by averaging over angles. The result thus obtained for $r_s = 100$ is shown in curve 1 of the figure, and for such a low density the present method should provide a truly accurate representation of the real situation. We see that the probability density F_2 is violently oscillatory and of a highly complex functional form. In order to follow the change in F_2 as r_s is reduced, we have plotted in curve 2 the case $r_s = 4$. We should emphasize that extrapolation to such a density is not justified fundamentally, as the orbitals are now no longer orthogonal, and also do not make $f(0)$ zero for particles of like spin. Various estimates of the range of validity of the low density argument of Wigner give $r_s > \sim 10$–20. Nevertheless, whichever value we assume for the lower limit of approximate validity, it is clear that F_2 is still oscillatory about the line $F_2 = 1$, to a significant degree, and any acceptable probability density must contain such behaviour.

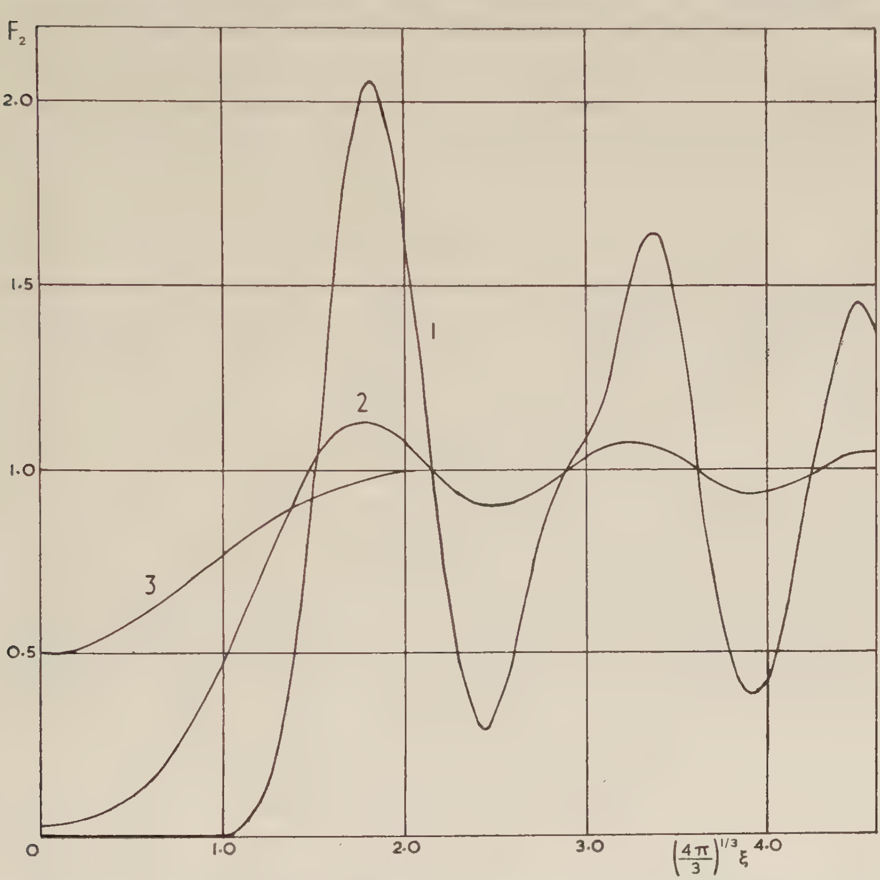

Probability density $F_2(\xi)$ as function of electron separation ξ. Curve 1. Low density form for $r_s = 100$. Curve 2. Extrapolated low density form for $r_s = 4$. Curve 3. Fermi hole, correct in the limit $r_s \to 0$.

We see then that Wigner's arguments can be fitted into the present scheme, and give a good deal of information about the form of F_2. However, we wish to see how the high density form can be obtained from the present method. One thing which suggests itself is to extrapolate the low density F_2 into $r_s=0$, but doing this we find no Fermi hole, due essentially to the failure of the Gaussian orbitals to (*a*) satisfy orthogonality requirements and (*b*) have nodes at the positions of like spin electrons. The question then arises as to what the localized functions centred on lattice sites must be in this limit. It seemed clear to us that since plane waves provide the correct solution in the high density limit, free-electron Wannier functions must be intimately related to this case. We conclude by showing that this is indeed so, and we demonstrate that for a one-dimensional Fermi gas, the exact solution may be obtained in this way.

If we consider a lattice spacing π/k_0, then the free electron Wannier functions may be written

$$\psi_m(x)=\frac{1}{(\pi k_0)^{1/2}}\frac{\sin k_0(x-m\pi/k_0)}{(x-m\pi/k_0)}=\frac{(-1)^m\sin k_0x}{(\pi k_0)^{1/2}(x-m\pi/k_0)}. \qquad (11)$$

Summing over the sites of an infinite lattice we can write

$$\sum_{-\infty}^{\infty}\psi_m{}^*(x')\psi_m(x)\simeq\frac{1}{\pi k_0}\int_{-\infty}^{\infty}\frac{\sin k_0(x'-m\pi/k_0)}{(x'-m\pi/k_0)}\frac{\sin k_0(x-m\pi/k_0)}{(x-m\pi/k_0)}\,dm$$

$$=\frac{k_0}{\pi}\frac{\sin k_0(x'-x)}{k_0(x'-x)}. \qquad (12)$$

Hence, in particular

$$\sum_{-\infty}^{\infty}\psi_m{}^2(x)=k_0/\pi. \qquad (13)$$

This latter result may be obtained by direct summation and is exact.

Now, according to our model, we form the density for $(N-1)$ particles by removing the density contributed by the localized orbital centred on the origin, in order to make $f(0)=0$, and ensure normalization to $(N-1)$. Then we find

$$\sum_{-\infty}^{\infty}\psi_n{}^2(x)-\psi_0{}^2(x)=\frac{k_0}{\pi}\left[1-\frac{\sin^2 k_0x}{(k_0x)^2}\right]. \qquad (14)$$

In this case the exact second order density matrix can be written down from a two-by-two determinant (see for example Löwdin 1955) involving the first order matrix

$$\frac{k_0}{\pi}\frac{\sin k_0(x'-x)}{k_0(x'-x)},$$

the result being

$$\frac{1}{2}\begin{vmatrix}\dfrac{k_0}{\pi} & \dfrac{\sin k_0(x'-x)}{\pi(x'-x)}\\ \dfrac{\sin k_0(x'-x)}{\pi(x'-x)} & \dfrac{k_0}{\pi}\end{vmatrix}=\frac{1}{2}\left(\frac{k_0}{\pi}\right)^2\left[1-\left\{\frac{\sin k_0(x'-x)}{k_0(x'-x)}\right\}^2\right]. \qquad (15)$$

From (8), we must multiply (14) by $\gamma/2 = k_0/2\pi$ in order to compare with (15). The equivalence then evident proves that we obtain an exact description of the Fermi hole in this case, using localized orbitals on a lattice; the orbitals being free electron Wannier functions.

So far, we have not seen how to extend our high density arguments exactly to the real three-dimensional gas, with two spin directions. However, the following model will lead, at least, to a fairly accurate representation of the Fermi hole. In this high density limit we think of Wigner's body-centred-cubic lattice as two interpenetrating simple cubic lattices, and we centre on each lattice site a free electron Wannier function for a simple cubic lattice, the functions on one lattice being multiplied by a spin function α, those on the other lattice by a spin function β. Then we can again form a first order matrix for $N-1$ particles, and the probability density we obtain may be written

$$1-\frac{1}{2}\left[\frac{\sin c\xi_x}{c\xi_x}\,\frac{\sin c\xi_y}{c\xi_y}\,\frac{\sin c\xi_z}{c\xi_z}\right]^2; \quad c=2^{-1/3}\pi. \quad . \quad . \quad . \quad (16)$$

To obtain $F_2(\xi)$ we must average this over angles, and we have not yet achieved any closed result. However, we shall obtain a fair approximation to the Fermi hole, as the following argument shows. If we go back to the basic form for the simple cubic Wannier functions,

$$\psi(\mathbf{r})=\frac{1}{8(\pi k_0)^{3/2}}\int_{\text{unit cell}} \exp(i\mathbf{k}\,.\,\mathbf{r})dk_x\,dk_y\,dk_z \quad . \quad . \quad (17)$$

and replace the cube of volume $8k_0^3$ in $\mathbf{k}$ space by an equal volume sphere before performing the integration, then we obtain the exact Fermi hole.

Further work is now in progress to determine an acceptable form of localized orbital $\psi(\mathbf{r})$ in the intermediate density range, which goes into the Gaussian function (10) at low densities, and into functions at least intimately related to the Wannier functions we have described in the high density limit.

ACKNOWLEDGMENT

One of us (W. H. Y.) wishes to acknowledge the award of a Town Trustees Fellowship by the University of Sheffield.

REFERENCES

KOPPE, H., 1957, *Z. Phys.*, **148,** 135.
LÖWDIN, P. O., 1955, *Phys. Rev.*, **97,** 1474.
MARCH, N. H., 1958, *Phys. Rev.*, **110,** 604.
MAYER, J. E., 1955, *Phys. Rev.*, **100,** 1579.
TREDGOLD, R. H., 1957, *Phys. Rev.*, **105,** 1421.
WIGNER, E. P., 1938, *Trans. Faraday Soc.*, **34,** 678.

REVIEWS OF BOOKS

Solid State Physical Electronics. By ALDERT VAN DER ZIEL. (London: Macmillan, 1958.) [Pp. 604.] 37*s.* 6*d.*

AMONG the rapidly growing number of text-books on solid state electronics this book occupies a unique place for several reasons. In the first place, the value for money is outstanding by present standards, there being just over 600 pages. The emphasis throughout is on the physical principles involved in the working of various solid state devices, rather than on the more academic theory of the solid state or on the more engineering details such as circuit design. The range of topics is wider than might be expected from the title, and includes such things as thermionics, field, secondary and photo-electric emission in as much detail as might be expected in a book on vacuum electronics.

With such a wide range, the treatment is necessarily somewhat condensed, but most of the important mathematics is worked through in detail and one's feeling after reading a chapter is that the subject has been given a credible outline and the minimum necessary has been taken on trust. The number of references has been kept down by including among them a large proportion of text-books and review articles, but in spite of this the book seems well abreast of the times. A number of problems is included, many of a numerical nature with values quoted which are typical of current practice.

Altogether the book is well produced, very readable, and can be strongly recommended. D. K. G.

Low Temperature Physics and Chemistry. Editor: J. R. DILLINGER. (The University of Wisconsin Press, 1958.) [Pp. 676.] $6.00.

DURING one week in August 1957, 225 papers were presented to 440 delegates attending a conference on Low Temperature Physics and Chemistry at Madison, Wisconsin. The detailed report now published provides a pretty complete picture, albeit somewhat pointillistic, of the situation in almost every branch of cryogenic research at the time of the conference. The editor has performed his task very thoroughly and produced a volume which will be of value to workers in this field for some time to come. It is perhaps a pity we have had to wait over a year for it, but that is the price one must pay for elegance of production. The monetary price seems very reasonable by modern standards.

A. B. P.

Expansion Machines for Low Temperature Processes. By S. C. COLLINS and R. L. CANNADAY. (Oxford: Clarendon Press, 1958.) [Pp. 115.] 12*s.* 6*d.*

THIS short, moderately priced book brings together a large mass of information on the design and use of expansion machines. The evolution of the reciprocating expansion engine is traced historically from the air expansion machines used for refrigerating ships in the latter part of the nineteenth century to the first applications to air liquefaction in Claude's machine. The further development of these engines for the liquefaction of hydrogen and helium is then described in more detail. This section contains much interesting information about Professor Collins' own important contributions to machine design, and might well have been expanded further at the expense of some of the earlier chapters of the book. In particular, information about the modifications which have been introduced into commercial helium liquefiers and their effect on efficiency and maintenance would have been very valuable.

The latter part of the book deals with the design and performance of various turbine expansion machines used in large scale air liquefaction, and contains a useful comparison of the advantages of different types. If the book is intended primarily for low temperature engineers, this section might profitably have included a discussion of the changes in the rest of the plant which have to be made when a turbine is used instead of a high pressure reciprocating machine. The book is well illustrated and has a useful bibliography.

Principles of Modern Physics. By A. P. French. (New York and London: John Wiley & Sons.) [Pp. 355.] 54*s*.

Modern physics spreads its net so wide that it can mean whatever an author wants it to mean, and especially the field in which he is himself active. By the same token it involves so many trees that it is very easy to get lost among them, wandering on with a catalogue of detail. Dr. French knows the subject, and the dangers, very well and sets out to carve a clear path from one landmark to another. For him modern physics is the discovery of the individual atom and the exploration of its structure, by the classical, quantum theoretical and finally wave mechanical methods. He is concerned to trace the development of the essential physical concepts, rather than to impart a lot of information, with the advanced undergraduate or early postgraduate student in mind. The jacket (not the Preface) speaks of the 'thorough examination of a limited number of topics'. On the contrary, the text is much more a concise introduction to the whole range of subject matter of modern atomic and nuclear physics. As the Preface says, 'collateral reading' is expected, and a considerable amount of it (supplemented by seminar discussions) will certainly be needed from the average student. The book has the clarity of Oldenberg's *Introduction to Atomic Physics* at the level of treatment of Born's *Atomic Physics*, to which it is a worthy successor. More one cannot expect at the length and the price.

V. E. C.

Elektronenbeugung. By Ernst Bauer. (Munich: Verlag Moderne Industrie.) [Pp. 240, with 120 figures.] DM 32.

Electron diffraction has long since reached the stage of being accepted as a research tool with a field of application all its own. Techniques are well established and a great number of applications are to be found in the literature, but there has been a conspicuous lack of a practical handbook explaining the experimental procedures in a way that a non-specialist can understand. It is this need which the author sets out to meet, with a considerable degree of success. The book is divided into three parts: theoretical (56 pp.), description of apparatus and methods (95 pp.) and an outline of applications (47 pp.). He deliberately excludes proofs, quoting only the essential relations, and hence is able to cover the geometric theory (Bragg) in 15 pp., the kinematic theory (Laue) in 9 pp. and the dynamic theory in 16 pp. The treatment of practical topics is similarly compressed, and it is doubtful whether a beginner will gain sufficient grasp of the subject unless he follows up the suggestions given for further reading. These are, however, very full, and 550 references are quoted in all. The survey of applications ranges over the chemical, electrical and optical industries, as well as metallurgy. The book is likely to find a welcome where it is particularly addressed: the industrial scientist who wants to know how to use a new technique and is more concerned about the how than the why of it. He will especially appreciate the list of suppliers of various types of equipment on the last page.

V. E. C.

Handbook of Physics. Edited by E. U. Condon and H. Odishaw. (New York: McGraw-Hill Book Company, Inc., 1958.) [Pp. 1473.] 194*s*.

This massive volume with short articles by experts on every subject from arithmetic to nuclear fission could be very useful to anyone planning an honours course in physics, a series of text books or wanting to know the salient factor on some field of research outside his speciality. Some of the articles are very up to date with references to papers as recent as 1957. N. F. M.

Progress in Crystal Physics, Vol. 1. By R. S. Krishnan. (Madras: S. Viswanathan, 1958.) [Pp. 198.] Rs 20 or 30*s*.

This book is both a review of experimental and theoretical work in certain selected fields of Crystal Physics and also a compilation of the available data concerning these properties. After a short introduction which refers to geometrical crystallography and to crystal growth, there are seven chapters dealing respectively with Thermal Expansion, Thermal Conductivity, Elastic Constants, Photoelastic Effect, Thermo-optic Behaviour, Faraday Effect in diamagnetic crystals and dielectric properties of ionic crystals. Each chapter has been written by two or three members of the Department of Physics of the Indian Institute of Science, and altogether there are seven contributors. Professor R. S. Krishnan has contributed to four chapters himself and is to be congratulated as general editor on the coherence and readability of the work. The summaries of the experimental methods used in the measurements of the physical properties and the theories by which they can be interpreted are clearly described. In many cases the reader is referred to a full review or book and little is given here. A valuable feature of the articles is that each author has done original work in the subject on which he has written. The reviews cover the literature and give a fair account of conflicting theories and experimental results.

The difficulty of finding adequate tables of data on the physical properties of crystals is well known. The present book is therefore sure to be welcomed for the full, clear, and detailed tables provided at the end of each chapter. The collections of references to original papers and books will also greatly facilitate the study of the subject by research workers.

The choice of symbols for representing the many physical quantities discussed in such a book presents many problems to the author as well as to the reader. Only in one chapter is there a glossary of symbols. In any future edition it would be helpful if a general index of symbols were provided. The early appearance of succeeding volumes will be much appreciated by all those who study the physical properties of crystals. W. A. W.

[*The Editors do not hold themselves responsible for the views expressed by their correspondents.*]

Fig. 2

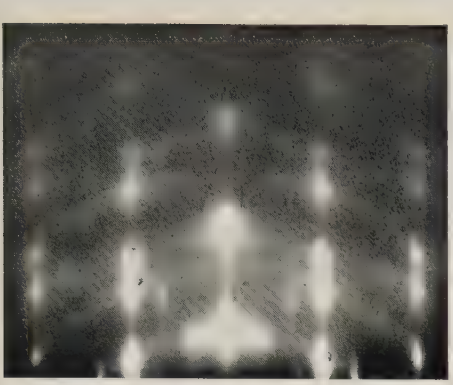

A 1000 Å layer of silver deposited at a substrate temperature of 40°c. Mica [010] azimuth.

Fig. 3

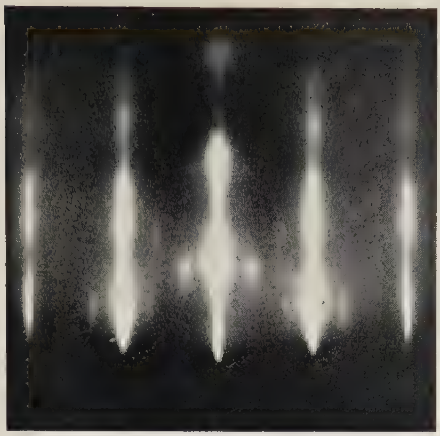

A 1000 Å layer of silver deposited at a substrate temperature of 75°c. Mica [010] azimuth.

Fig. 4

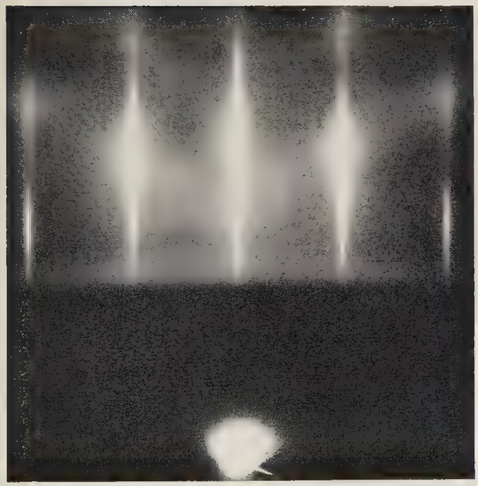

A 1000 Å layer of silver deposited at a substrate temperature of 275°c. Mica [010] azimuth. The elongation of the diffraction spots arises from lack of electron penetration into the smooth (111) surface.

Fig. 6

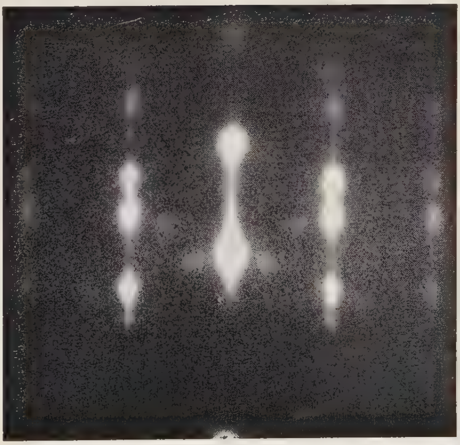

A 50 Å layer of silver deposited at a substrate temperature of 275°c. Mica [010] azimuth.

Fig. 7

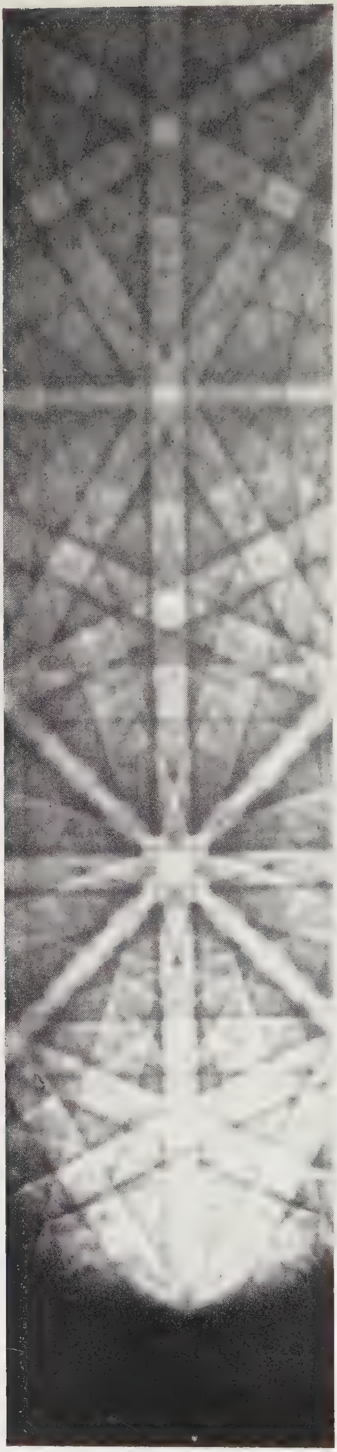

A high-angle Kikuchi pattern from a 1000 Å layer of silver deposited at a substrate temperature of 270°c. Glancing angle of incidence approximately ten degrees. Mica [100] azimuth.

Fig. 1

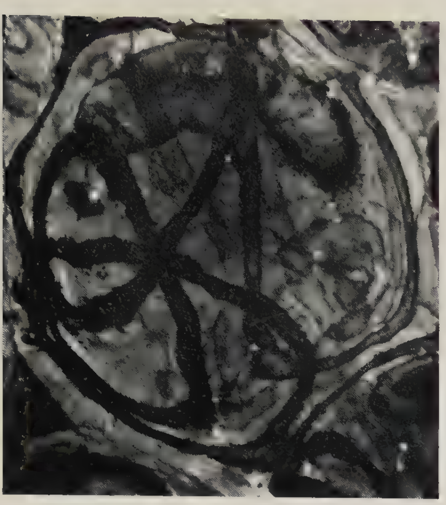

Prominent extinction contours attributed to the occurrence of 'dimpled regions' in the film (see fig. 2 (*b*)). (×57 000.)

Fig. 4

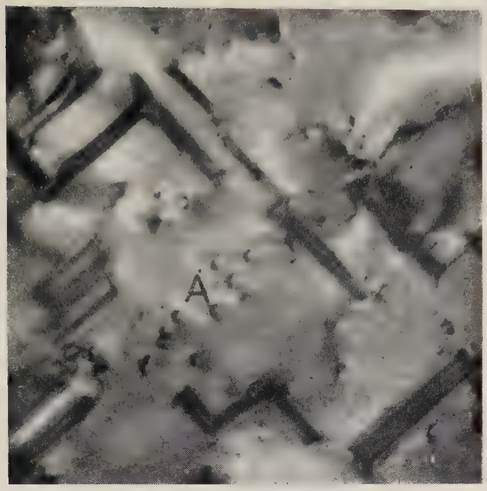

A (100) film of gold showing stacking faults and individual dislocations, such as at A. (×140 000.)

Fig. 5

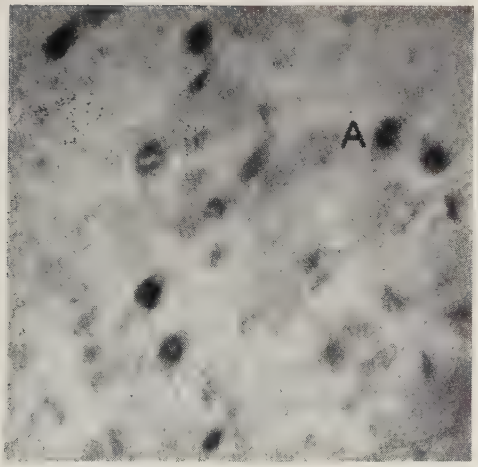

Dislocation loops in a (111) gold film. (×340 000.)

Fig. 6

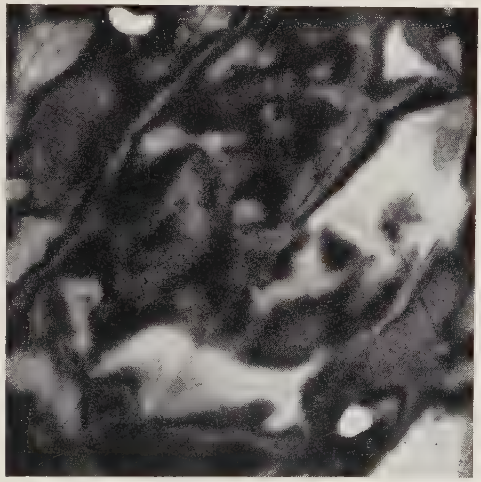

The appearance of stacking faults during the electron bombardment of the specimen. (×120 000.)

Fig. 8

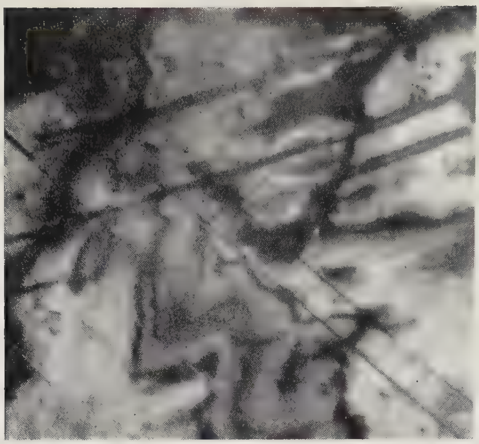

Stacking faults in a (111) film as seen with the electron beam inclined to the plane of the film. (×180 000.)

Fig. 9

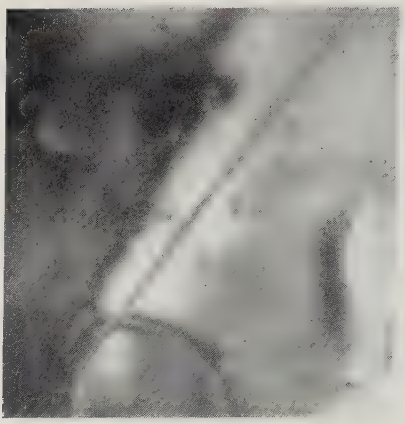

A stacking fault in a (111) film showing fringes with a twisted appearance. (×180 000.)

Fig. 10

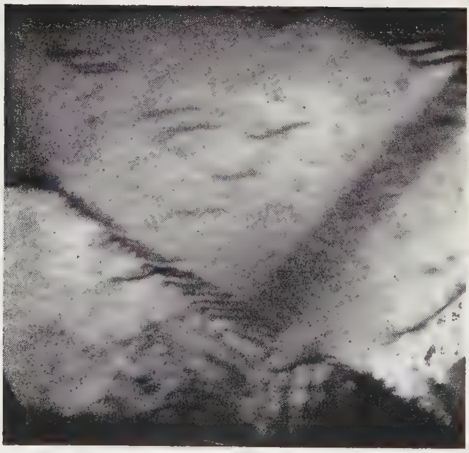

A low angle boundary in an annealed gold film. (×71 000.)

Fig. 11

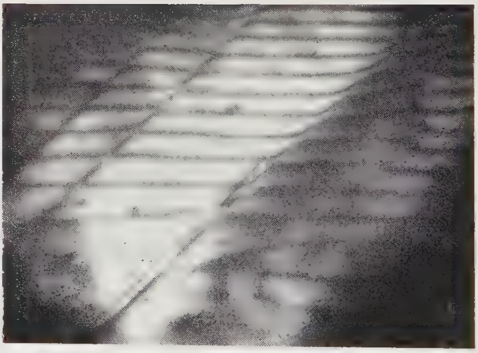

A regular dislocation array in an annealed gold film. (×71 000.)

Fig. 2

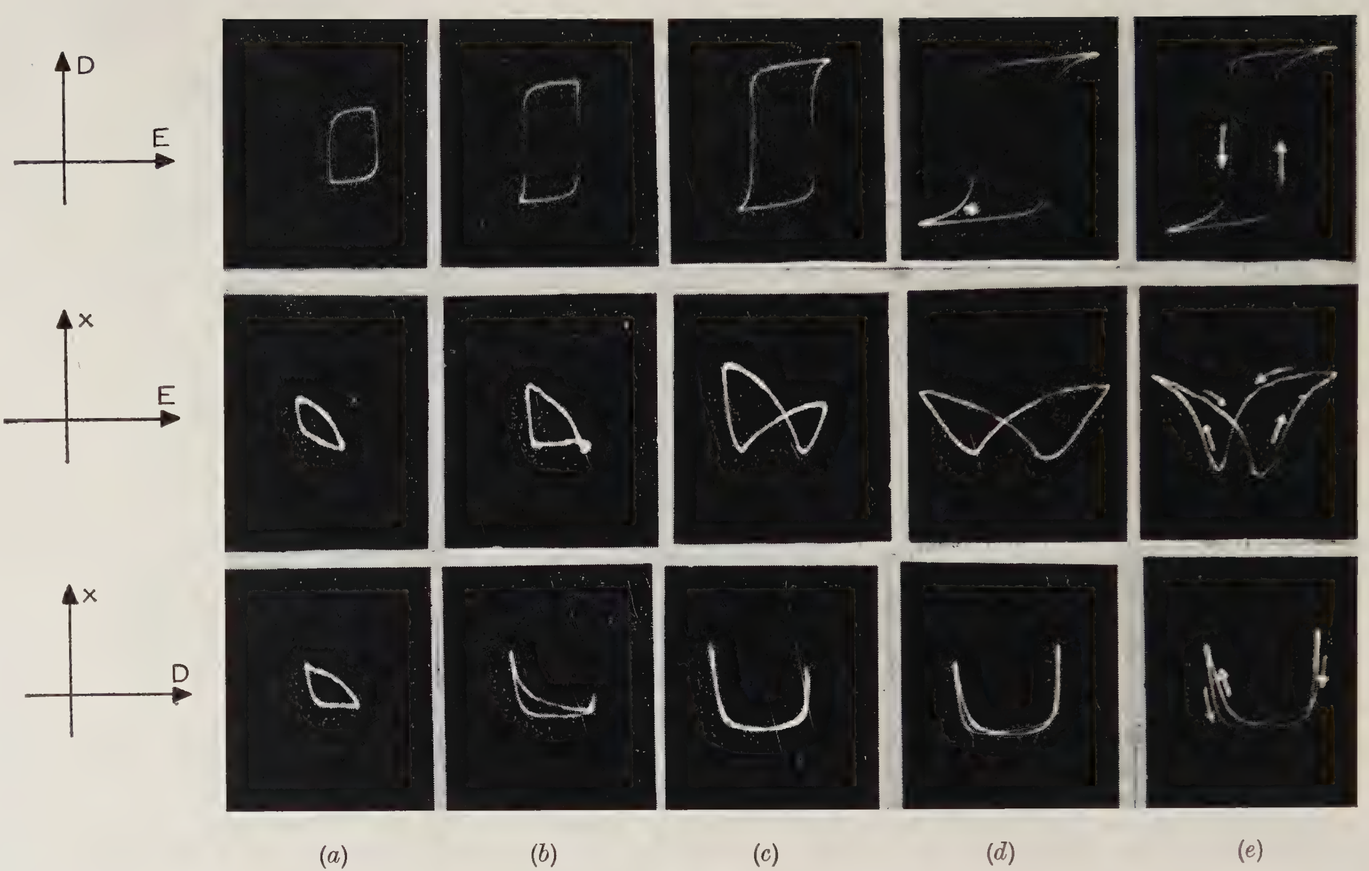

Experimental figures from group II (relatively untwinned) crystal, applied field progressively increasing from (*a*) to (*e*)

Fig. 3

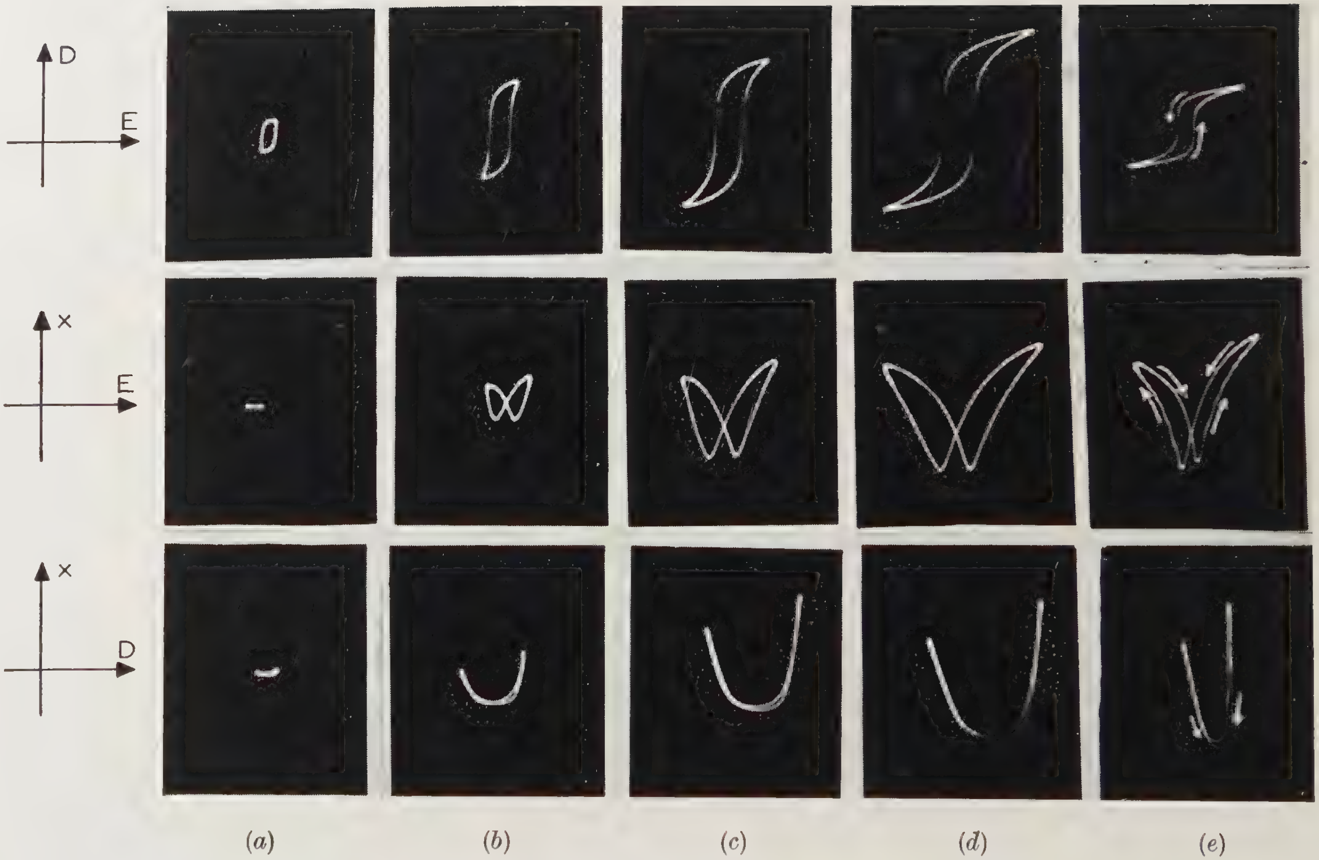

Experimental results from group I (twinned) crystal, applied field progressively increasing from (*a*) to (*e*).

Fig. 4

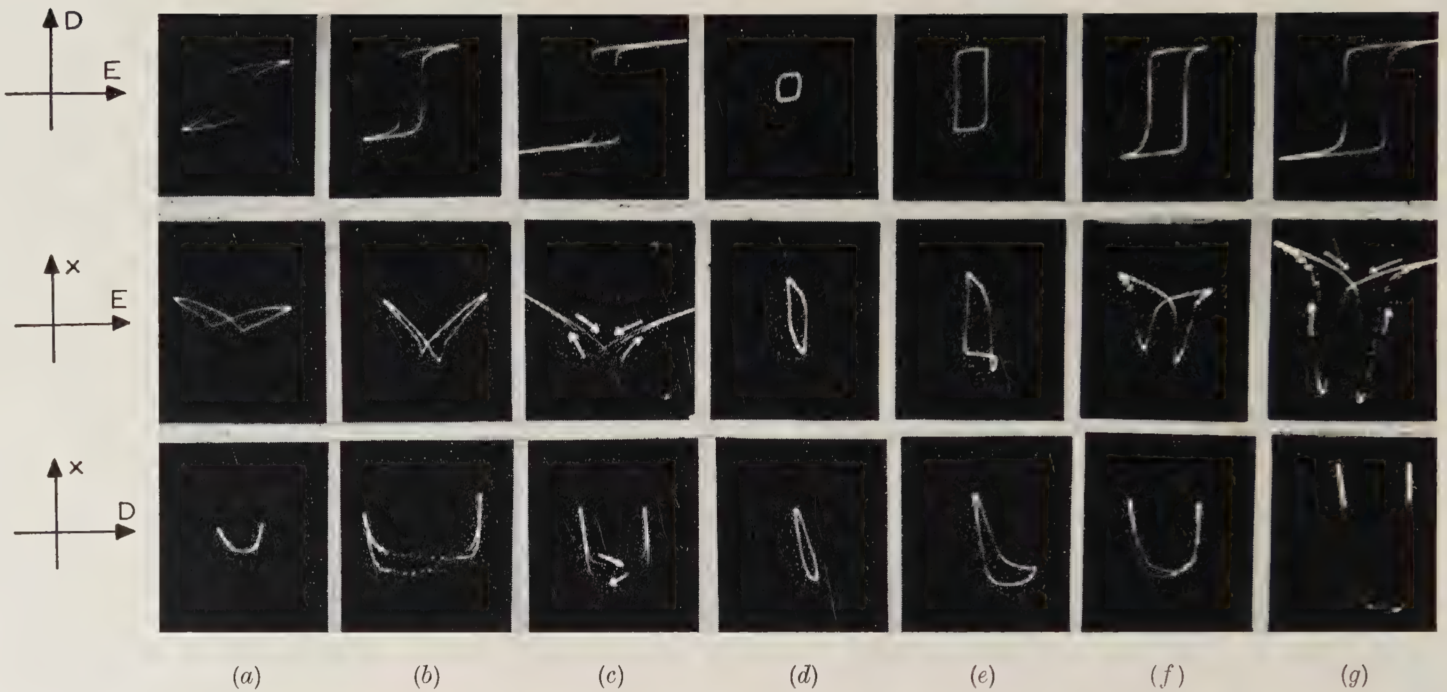

(a) (b) (c) (d) (e) (f) (g)

Experimental results on group II crystals.

(*a*) Initial application of field. (*b*) After 2 hours. (*c*) After temperature cycling. (*d*), (*e*), (*f*), (*g*) Different crystal showing unusual amount of 90-mechanism. Progressively increasing fields.

Fig. 7

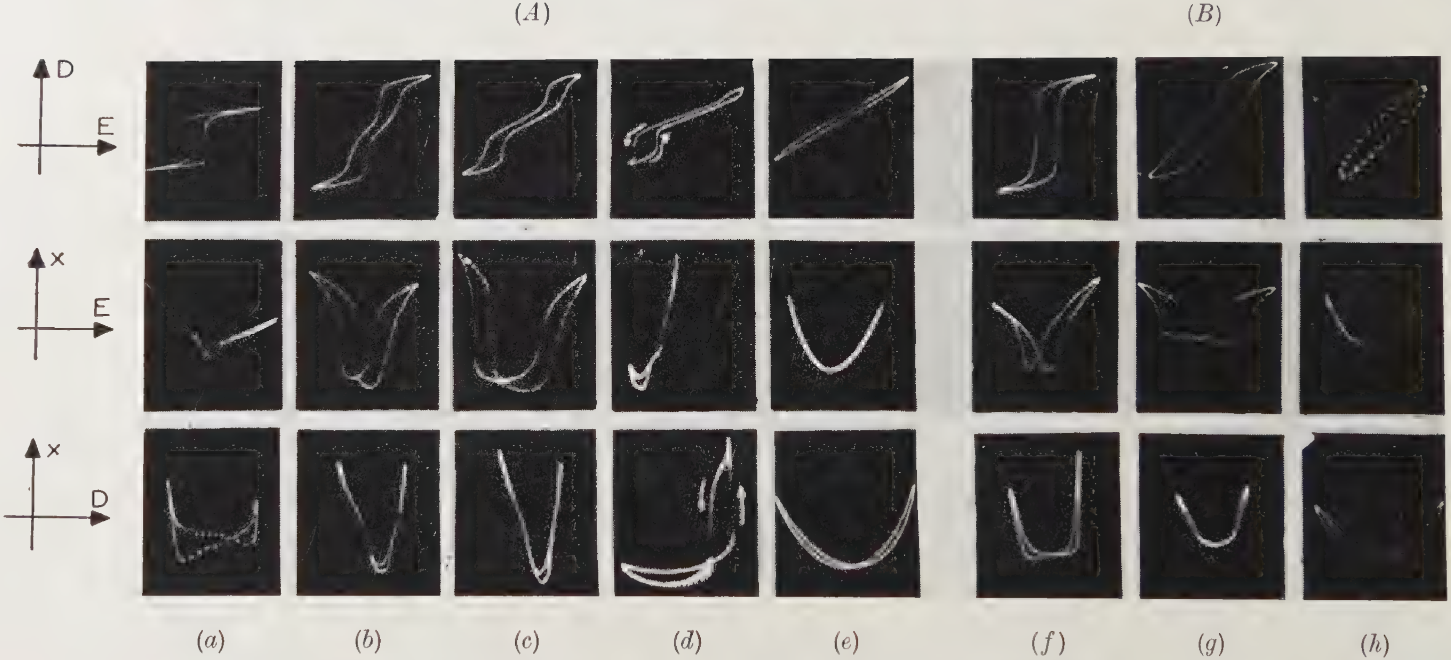

Experimental results on group II crystal (*a–e*) and group I crystal (*f–h*).
(*a*) 85°c, (*b*) 116°c, (*c*) 120°c, (*d*) 124°c, (*e*) 131°c, (*f*) 87°c, (*g*) 114°c, (*h*) 125°c.

Fig. 8

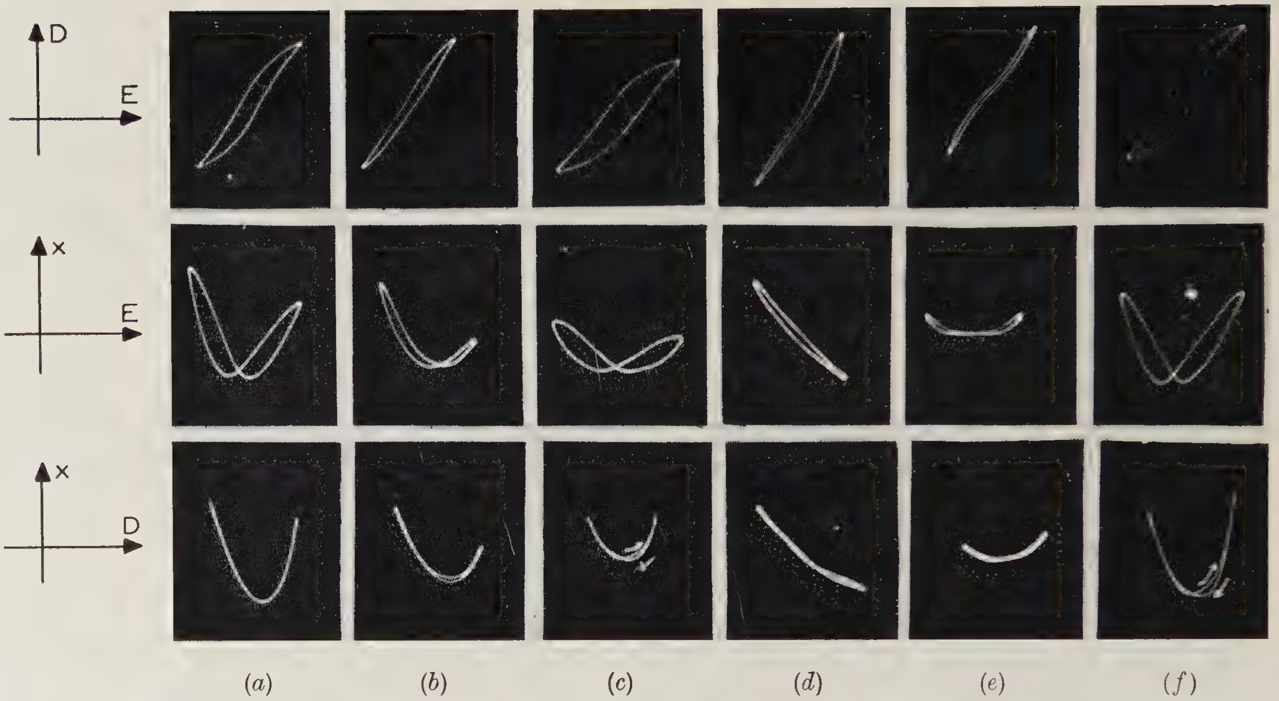

Experimental results (room temperature) on a range of ceramics. Peak applied field 20 kv/cm.
Additives as follows:
(*a*) 0·1% Y_2O_3, (*b*) 0·5% MnO, (*c*) 0·05% MnO, (*d*) 1·3% CoO, (*e*) 0·51% MgO, (*f*) Pure $BaTiO_3$.

Fig. 9

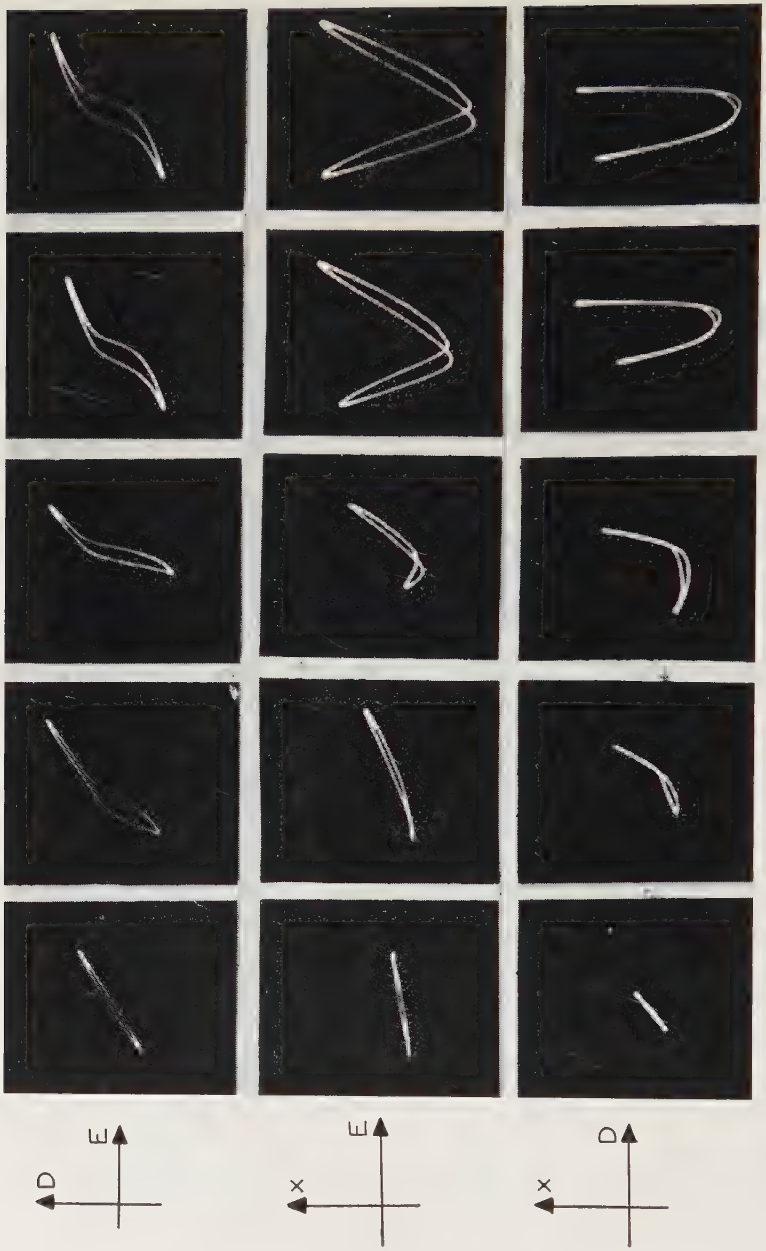

(a) (b) (c) (d) (e)

Prepolarized ceramic containing 1·3% CoO. Progressively increasing field.

Fig. 10

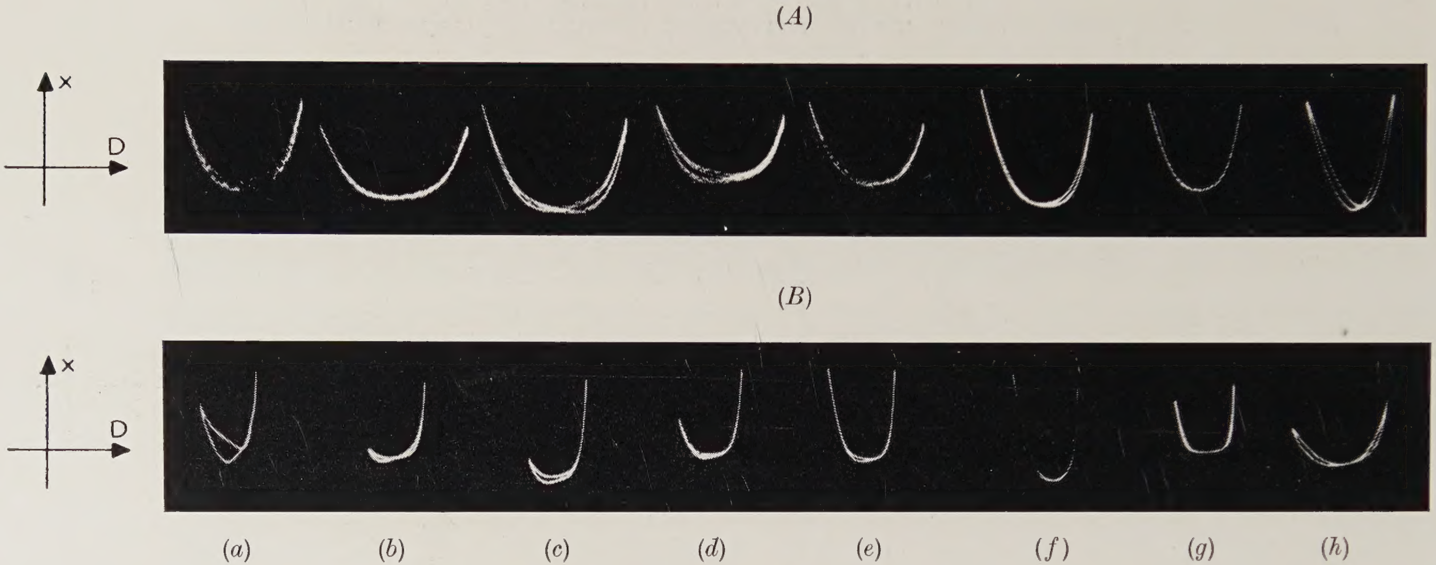

x/D figures for ceramics over a wide temperature range.

(*A*) With 0·05% MnO, (*B*) Pure $BaTiO_3$. Temperatures in °c as follows:

(*A*) (*a*) −150, (*b*) −86, (*c*) −51, (*d*) −11, (*e*) +18, (*f*) +59, (*g*) +100, (*h*) +135.
(*B*) (*a*) −148, (*b*) −97, (*c*) −62, (*d*) − 7, (*e*) +18, (*f*) +60, (*g*) +122, (*h*) +132.

Fig. 11

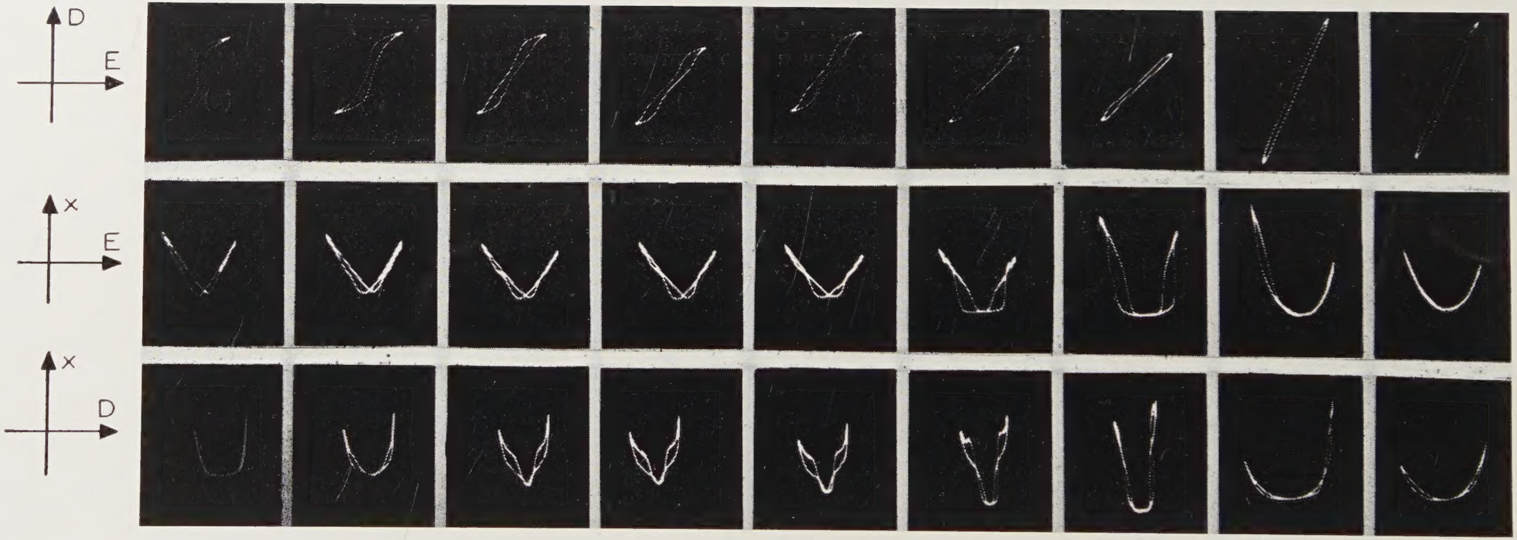

(*a*) (*b*) (*c*) (*d*) (*e*) (*f*) (*g*) (*h*) (*i*)

Results on pure $BaTiO_3$ ceramic near the Curie temperature. Strain measured in line with field. Temperatures (*a*) 122°c, (*h*) 129°c, (*i*) 135°c. Intermediate temperatures not measured.

Fig. 12

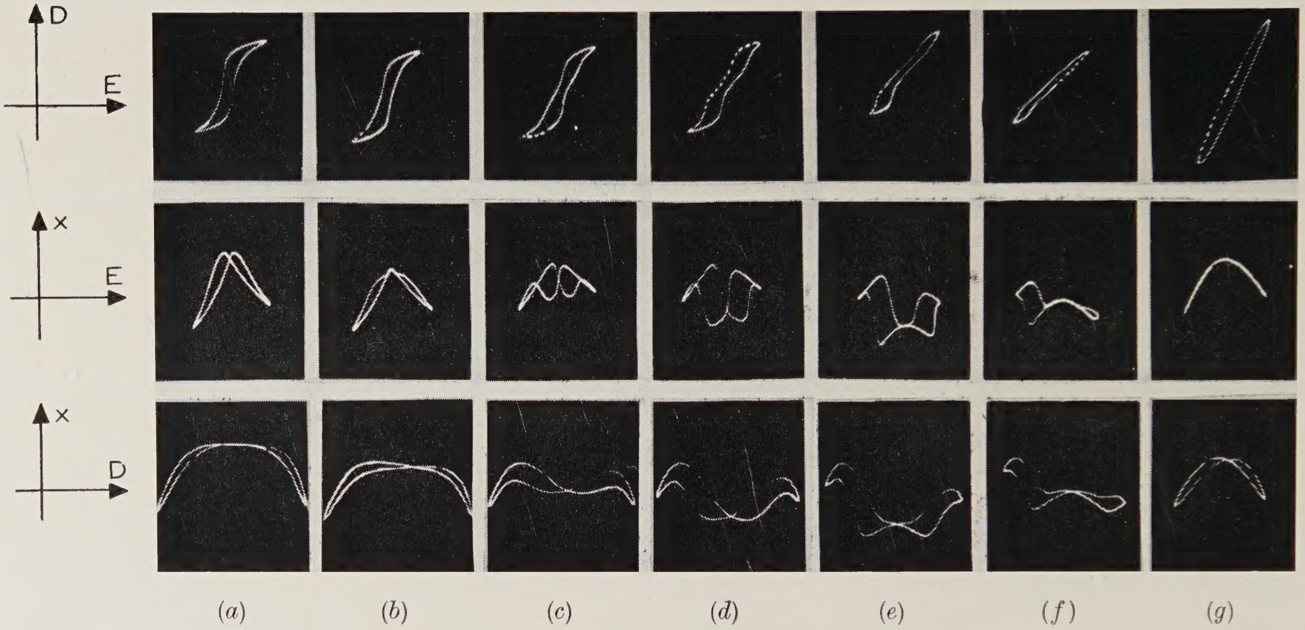

Results on pure $BaTiO_3$ ceramic near the Curie temperature. Strain measured at right angles to field. Temperatures 127–131°c, intermediate values not measured.

Fig. 1

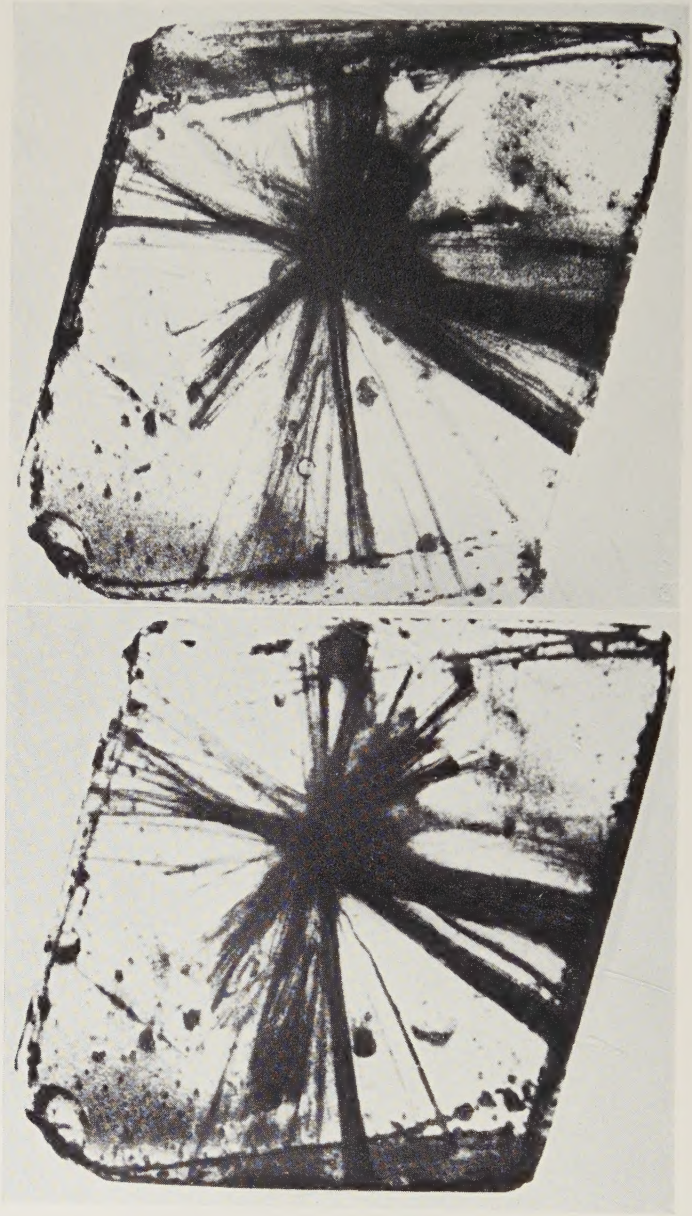

(*a*) (*b*)

Stereo-pair of projection x-ray topographs of diamond showing radiating dislocation structure.